Università della Calabria

Facoltà di Scienze Matematiche, Fisiche e Naturali

Hydrogen Physisorption Processes on Porous Solids

Tesi di Dottorato di Ricerca in Fisica, Ciclo XXII

di

Georgios Kalantzopoulos

Supervisori:

Prof. R. G. Agostino   Dr. Enrico Maccallini

Coordinatore del corso di Dottorato:
Prof. G. Falcone

Arcavacata di Rende, Cosenza
December 2009

Index

Introduction

Environmental pollution has arrived at a critical level and the need for clean energy is more imminent than ever. Additionally fossil fuels tend to become extinct and combined with the environmental issue we have to turn to novel and pollutant-free energy. On this perspective, hydrogen molecule (H_2) is one of the best candidates to handle those problems because it exhibits the highest heating value per mass of all chemical fuels[1] . However, it should be emphasized that the H_2 function in novel energy source is as energy carrier in fuel cells, internal combustion engines and space applications. Although research in extracting electric power from hydrogen has arrived in a sufficient level[2] , a lot of work needs to be done in hydrogen storage.

In principle hydrogen can be stored in six different methods: (1) high-pressure gas cylindrical containers[2] , (2) liquid in cryogenic tanks[3] , (3) chemically bonded in covalent and ionic compounds[4] , (4) absorbed in interstitial sites in a host metal[1] , (5) through oxidation of reactive metals and water[5] and (6) adsorbed on porous materials with large specific surface area[6] . The first two methods employ sophisticated materials and density of stored hydrogen varies between $(36 - 72)$ kg/m^3 [1,7] . Furthermore, their weight does not make them versatile for mobile applications i.e. hydrogen powered automobiles. Moreover they present safety problems because H_2 is highly explosive. Hydrogen can be dissociated and get chemically bonded in covalent and ionic compounds or to get absorbed in metals forming metal hydrides. In this case energy needs to be spent to retrieve hydrogen from the host material since the covalent bond needs high amount of energy to brake. Metals like Li, Na, Al or Zn can react with water and can extract hydrogen through the formation of a hydroxide[5] . Lastly, the adsorption of hydrogen on porous solids with high surface area is governed by van der Waals forces and demonstrates reversible storage but small storage capacity in ambient temperature[6,8,9] .

In order to guide and assist research centers and industry, the Department of Energy (DOE) of the United States and European Union have set a target of 6% gravimetric

storage capacity for 2010 and 9% for 2015[10] . This number corresponds to the system's efficiency comprising the adsorbing material, the tank walls and the gas input/output regulator. Hence the adsorbing material should exhibit much higher performance. In regard to this threshold we need to develop and study the sorption properties of new materials. The key step for designing suitable, novel materials will be to understand and analyze the nature of molecular hydrogen binding in adsorption/desorption mechanisms. The porous materials are a keystone which can fulfill the DOE and EU requirements.

In fact they possess low skeleton density and high specific surface area. Specific surface area (SSA) is the area of the material that is accessible to the adsorbate and in a porous material apart from the external surface includes the surface of all the pores, cavities and capillarities. Up to date work shows a linear connection between maximum gravimetric density and surface area[11] . In addition the porous materials can be tailored with light constituents which are important for achieving higher percentage in the H_2 storage capacity. Apart from these it is also important to enhance the interactions between adsorbate and adsorbent's surface. Surface functionalization through the existence of sp^2 orbitals, effect of point charge, creation of surface dipoles and complexes are routes that can improve the surface's interaction with hydrogen[12] . In principle there are three types of interactions that govern the interaction between hydrogen and host materials and can be categorized depending on their nature: 1) dispersion (van der Waals), 2) electrostatic and 3) orbital interactions. On the other hand, regarding the structure of the adsorbent crystallinity, pore size distribution and the obtaining of a as close to real value for specific surface area are parameters that should be put together and be correlated how they affect the sorption properties[13,14,15,16] .

The most well known techniques for measuring gas phase hydrogen sorption in porous solids are the volumetric[17] and the gravimetric methods and thermal desorption spectroscopy (TDS)[18] . Our main probe tool will be the volumetric technique which although has some issues that need to be resolved and standardized, has become the most common one. Using volumetric technique for the assessment of hydrogen storage capacity there are particular issues that need to raised and resolved.

All starts from the real gas law

$$PV = Z(P,T)nRT \qquad\qquad\qquad (0.1)$$

where Z(P,T) is the compressibility of the gas.

Moles n are what it is required in order to calculate the H_2 storage capacity. However its value is calculated indirectly through the measurement of P and T and the knowledge of V and gas's compressibility Z. Therefore error propagation needs to be calculated in order to define the amount of error that a system produces in the evaluation of the H_2 adsorbed moles. Moreover issues like system calibration, temperature control and monitoring in system and on the sample, pressure reading, gas purity and compressibility, sample pretreatment and history, sample's degassing, system to sample volume ratio and approach to the pressure gas equilibrium have to be specified and well defined for every laboratory[19,20].

On this scheme, it will be described the development of a novel volumetric apparatus (Sievert-type apparatus)[21] built by considering all the existing guidelines and instructions in the literature in order to have an overall understanding of the experimental results[19]. In particular, the purpose of this work is to shed light into the interaction of H_2 molecules in gas phase with the porous surface of Periodic Nanoporous Organosilicas (PNOs)[22]. This kind of material can be synthesized with tailored adsorption properties by tuning either the crystallinity, or the pore size or the SSA or the chemical constituents or introducing appropriate functionalization. The analysis of the experimental data in static and dynamic conditions will be addressed to the understanding of the mechanisms occurring during interaction of the PNOs with hydrogen in low and high pressures. The second of the work presented here will be study of modified and unmodified zeolites by the novel volumetric apparatus in low and high pressures and by thermal desorption spectroscopy and the results will be interpreted for gas solubility and mobility applications.[23]

Bibliography

(1) Zuttel, A. *Naturwissenschaften*, **2004**, *91*, 157-172.
(2) Andreas Züttel, Andreas Borgshulte, Louis Shlapbach *Hydrogen as a Future Energy Carrier*, 1rst ed., Wiley-VCH Verlag GmbH & Co. KGaA, Weinheim, **2008**. p.344.
(3) Zhou, L. *Renew. Sust. Energ. Rev.*, **2005**, *9*, 395-408.
(4) Fichtner, M. *Advanced Engineering Materials*, **2005**, *7*, 443-455.
(5) Steinfeld, A. *Int. J. Hydrog. Energy*, **2002**, *27*, 611-619.
(6) Xiao, B.; Yuan, Q. C. *Particuology*, **2009**, *7*, 129-140.
(7) Schlapbach, L.; Zuttel, A. *Nature*, **2001**, *414*, 353-358.
(8) Svec, F.; Germain, J.; Frechet, J. M. J. *Small*, **2009**, *5*, 1098-1111.
(9) Thomas, K. M. *Dalton Trans.*, **2009**, 1487-1505.
(10) **DOE Targets for On-Board Hydrogen Storage Systems for Light-Duty Vehicles** http://www1.eere.energy.gov/hydrogenandfuelcells/storage/pdfs/targets_onboard_hydro_storage.pdf, **Feb. 2009**
(11) Panella, B., Hones, K., Muller, U. *et al. Angewandte Chemie-International Edition*, **2008**, *47*, 2138-2142.
(12) Lochan, R. C.; Head-Gordon, M. *Physical Chemistry Chemical Physics*, **2006**, *8*, 1357-1370.
(13) Gogotsi, Y., Portet, C., Osswald, S. *et al. Int. J. Hydrog. Energy*, **2009**, *34*, 6314-6319.
(14) Kolotilov, S. V.; Pavlishchuk, V. V. *Theor. Exp. Chem.*, **2009**, *45*, 75-97.
(15) Cabria, I.; Lopez, M. J.; Alonso, J. A. *Carbon*, **2007**, *45*, 2649-2658.
(16) Yushin, G., Dash, R., Jagiello, J. *et al. Advanced Functional Materials*, **2006**, *16*, 2288-2293.
(17) Sieverts, A.Z. *Physical Chemistry*, **1907**, *60*, 129.
(18) Panella, B.; Hirscher, M.; Ludescher, B. *Microporous and Mesoporous Materials*, **2007**, *103*, 230-234.
(19) Broom, D. P. *Int. J. Hydrog. Energy*, **2007**, *32*, 4871-4888.
(20) Karl J. Gross, K. Russel Carrigton "Recommended Best Practices for the Characterization of Storage Properties of Hydrogen Storage Porous Materials," **2008**,
(21) Maccallini, E., Policicchio, A., Kalantzopoulos, G. *et al. in preparation*, **2009**.
(22) Inagaki, S., Guan, S., Ohsuna, T. *et al. Nature*, **2002**, *416*, 304-307.
(23) Maccallini, E.; Kalantzopoulos, G.; Policicchio, A.; Krkljus, I.; Golemme, G.; Buonomenna, M.G.; Hirscher, M.; Agostino, R.G. *In preparation*, **2009**.

1   Fundamentals: Physisorption and Diffusion Models

1.1   Hydrogen molecules absorption: Chemisorption and Physisorption mechanisms

Hydrogen molecules (H_2) can be absorbed from solid state sample either as a dissociated atom and therefore be chemically attached by covalent bond or as a molecule and in this way be physically attached by van der Waals-like forces.[1] In the case of chemical absorption the interaction between H_2 and the sample can occur either in the bulk or on the surface and the absorption mechanism is called chemisorption, while physical absorption of hydrogen takes place on the surface sample and is named physisorption. In order to quantify the energy involved in the chemisorption and physisorption of hydrogen molecules, the enthalpy of formation (ΔH) is considered as reference parameter. In particular in the case of chemisorption ΔH is particularly high and lies in the range of (10 – 100) kJ/mol, while the physisorption involves enthalpy in the range of (1 – 10) kJ/mol. Usually the chemisorption needs energy by thermal annealing ranging between room temperature[2] and 900 K[3] , in order to remove the chemisorbed hydrogen. In several cases, the chemisorption mechanism results in an irreversible process, while the physisorption is a reversible one [4,5] .

Considering the different bonds' energy and the surface barrier, the kinetics of the hydrogen molecules go from fast to slow diffusion in the physisorption and chemisorption respectively. In figure 1.1 the energy bonds diagram level versus hydrogen-surface sample distance is depicted in order to compare the two considered absorption mechanisms.
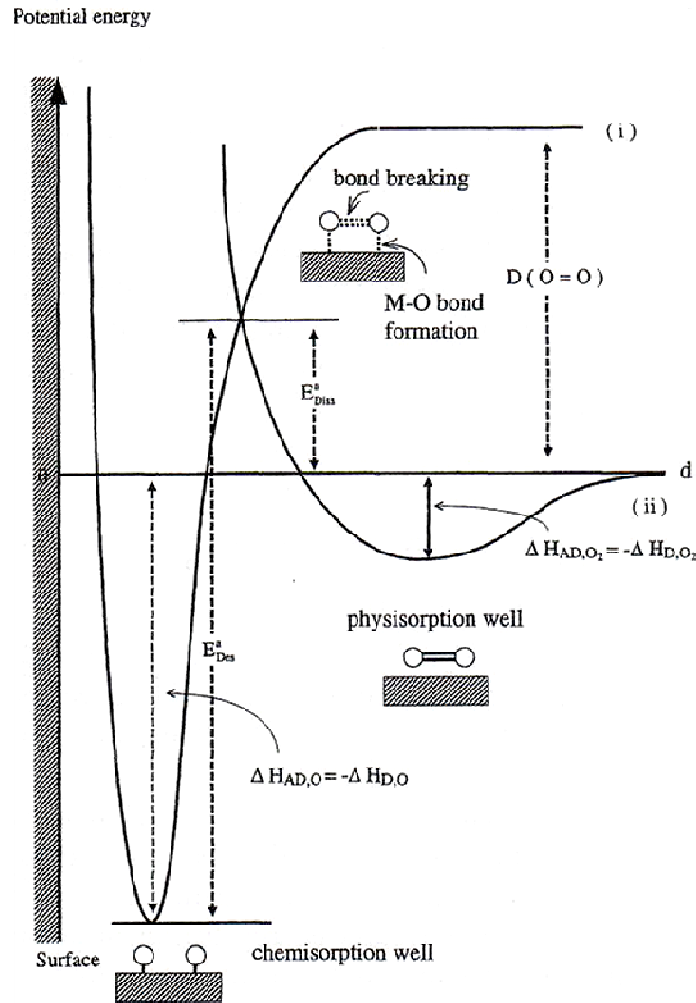
Figure 1.1: *Potential energy curve as a function of hydrogen-surface distance.*

The metal hydrides represent one of the most important cases in the hydrogen chemisorption. On that material the hydrogen absorption is related to sample phase transition from metal to metal hydride (MH) complexes[6,7]. The metallic bond (LaNi$_5$, TiFe, MgNi,..) forms metal hydrides through chemical hydrogenation and hydrogen can get released by a dehydrogenation procedure of the hydride by heating treatment. Depending on dehydrogenation process, the MH are characterized as hydrides of high or low temperature[8] : hydrides based on La are low temperature MH (desorption temperature of 300 K)[9] with main disadvantage to have low storage capacity (<2% gravimetrically) whereas high temperature MH (desorption temperature of 463 K) based on Mg can achieve a gravimetric capacity of 7%[10]. On

the other hand, these last materials possess low kinetics of hydrogenation/dehydrogenation while releasing hydrogen.[7] Furthermore their high weight and high cost consist these materials not a feasible method for on-board hydrogen storage applications.[11]

In the case of physisorption, the adsorption mechanism requires smaller temperature in order to reactivate the adsorbent material removing the adsorbed hydrogen molecules from the sample surface[2] . The interactions that govern physisorption are attributed to resonant fluctuations of the charge distributions producing dispersive (van der Waals) interactions[2] . In that interaction, the adsorbent-adsorbate interaction is governed from the formula

$$U(r) = 4\varepsilon \left[\left(\frac{\sigma}{r} \right)^{12} - \left(\frac{\sigma}{r} \right)^{6} \right]$$ (1.1)

where r is the distance surface adsorbent − adsorbate, while σ and ε are the potential parameters which characterize the H_2 − H_2 and surface sample − H_2 interactions respectively. This interaction consists of an attractive and a repulsive term that decrease with r^{-6} and r^{-12} respectively.[8] The optimum distance from the sample surface, where physisorption takes place, is coincident with adsorbate radius.

However an additional parameter that can be tuned in order to increase the storage capacity is the number of the available adsorption sites, which can be accomplished by high specific surface area (SSA). The SSA is the adsorbent's surface accessible to the adsorbate per mass unit of the adsorbent. Depending on the material, the SSA ranges between 30 m^2/g (graphite) and 4200 m^2/g (covalent organic frameworks, COF).[12] Samples at high SSA are called porous materials and depending on the pore size can be divided in either nano- or meso-porous materials.

Additional parameters which can be varied in the porous material at high SSA in order to increase the storage capacity are the pore size[13,14,15] and the surface chemical constituent[16,17] .

Pore size is important because gas molecules have a dynamical radius during adsorption processes and therefore first of all they have to enter into the pore. In addition if the pore size is in particular values[13] different mechanisms of adsorption

like capillarity can be activated which enhance the storage capacity of the porous material.

The variation of the surface chemical constituent into the porous materials could enhance the physical interaction between adsorbent surface − adsorbate by introducing light metals (Li$^+$, Mg$^+$) or by inserting aromatic rings in the structure of the porous material.[16,18,19]

The typical curves utilized to investigate the samples storage capacity are the isotherm plots (see figure 2.2) which can be obtained by either volumetric or gravimetric apparata.
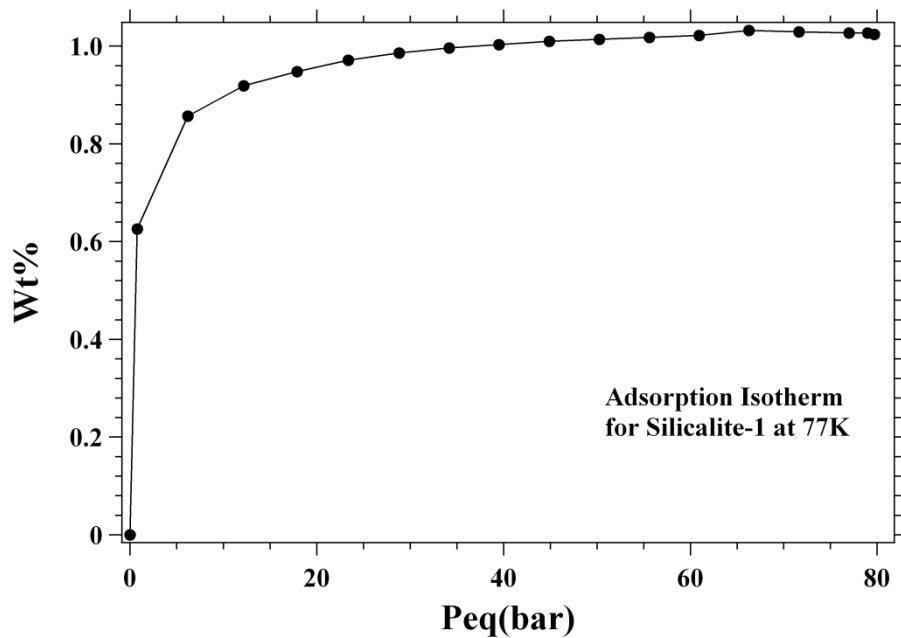
Figure 2: *Typical isotherm curve for Silicalite-1 obtained at 77K by volumetric apparatus.*

The investigated quantity depicted on the isotherm curves is relating the adsorbed gas moles n^a into the surface sample per sample mass (m^s) by the relation

$$\frac{n^a}{m^s} = f(p, T, system) \tag{1.1}$$

where *p* and *T* are the adsorbate, adsorbent and apparatus equilibrium pressure and temperature respectively, while *system* represents the additional parameters of the acquiring apparatus (system void volumes, gas purity, …) which will be discussed into the chapter 2.

For a specific adsorbate gas on a particular system under a fixed temperature the expression (1.1) is simplified to

$$\frac{n^a}{m^s} = f(p)_T \tag{1.2}$$

The formula (1.2) describes the adsorption isotherm relating, at constant temperature, the amount of the adsorbed gas and the system pressure[20] , considering also the system contribution. All types of adsorption isotherms ever recorded in the literature in porous materials can be grouped in six classes as IUPAC recommends (see figure 1.3).[21]

Physisorption in microporous materials generally reproduces a Type I adsorption isotherm (Langmuir-type isotherm). This typology demonstrates a quick increase in adsorption in low pressures and then an asymptotic behavior giving out the saturation of the adsorbent's surface. The variation depicted at relatively low pressures is connected with the strength and nature of interaction between adsorbate and adsorbent. The grade of adsorption is determined from the surface coverage coefficient ϑ:

$$\theta = \frac{number\ of\ sites\ occupied\ by\ the\ adsorbate\ (N_S)}{total\ number\ of\ sites\ available\ on\ the\ adsorbent\ (N)} \tag{1.3}$$

which is directly related to n^a.
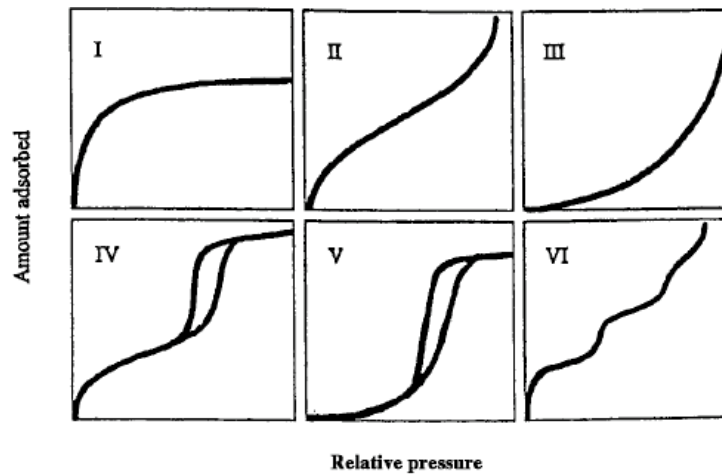
Figure 1.3: *Classification of adsorption isotherms in porous materials by IUPAC.*[21]

Apart from providing information about the maximum storage capacity of a particular gas into the investigated samples, the isotherm curves line-shape analysis can estimate either the energy bonds involved into the adsorption mechanism or some additional material porous properties by using selected theoretical models. In fact from its curvature can be extracted information concerning the enthalpy of adsorption and the porosity of the sample. The parts where derivative takes the maximum and minimum value that for a Type I isotherm are the low and high pressure regions of the isotherm, can give insight on the heterogeneity of the sample (see section 1.2.2).

The theoretical models exploited in this experimental work are the Langmuir and Tóth models.[22,23]

1.2   Theoretical Model Approaches

1.2.1   The Langmuir Model

The adsorption isotherms of porous solids with high SSA can be interpreted, at first approach, by making use of the Langmuir model[22] which considers the following approximations:

- Adsorbent's surface is considered uniform and all the adsorption sites are equivalent. In the best case, one monolayer of the adsorbate molecules can be formed.

- At constant temperature, there is a dynamical equilibrium between adsorbate and adsorbent during the adsorption and desorption processes.

- The adsorbate molecules interact and create either physical or chemical bond with the adsorbent surface during their approach to an unoccupied site, meanwhile they stay neutral when they come across an occupied site avoiding the formation of second monolayer.

- Temporally, the enthalpy of adsorption per site remains constant and independent from the surface coverage since the adsorbate's molecules are considered localized on the surface.

Supposing that the amount of the adsorbed gas molecules depends on the number of unoccupied adsorption sites and from the gas pressure, the expression describing the time-rate of adsorbed molecules is:

$$g_a = k_a P(1 - \theta) \tag{1.4}$$

On the other hand, desorption time-rate depends, in first approach, on either the probability of the gas molecules to occupy an adsorption site (Boltzmann's law) or the number of occupied sites by the formula:

$$g_d = \theta k_d \quad where \quad k_d = \beta e^{-\frac{\Delta H}{kT}} \tag{1.5}$$

where k_a and k_d stand for the constants of adsorption and desorption respectively. Assuming dynamical equilibrium between adsorbed and desorbed gas molecules, the mechanism involved in the Langmuir model can be described in the following way:

$$M_{c(g)} + cS \xrightarrow{k_a, k_d} c(M - S) \tag{1.6}$$

where c is equal to either 1 or 2 in the case of physisorption and chemisorption respectively.

Finally, in the Langmuir model, the rate of adsorbed molecules into the sample surface can be expressed as the following:

$$\frac{dN}{dt} = k_a(1 - \theta)P^c - k_d\theta P^c \tag{1.7}$$

At the equilibrium, there is no variation in the number of molecules adsorbed and desorbed on the surface sample, then:

$$k_aP(1 - \theta)^c = k_d\theta^c \tag{1.8}$$

Taking into account the (1.3), it is possible to determine the grade of adsorption like:

$$\theta = \frac{N_S}{N} = \frac{(KP)^{1/c}}{1 + (KP)^{1/c}} \tag{1.9}$$

where the concentration in weight of the adsorbed molecules per percentage of mass unit (wt%) is expressed:

$$wt\% = A\frac{(KP)^{1/c}}{1 + (KP)^{1/c}} \tag{1.10}$$

In (1.10) A is the maximum storage capacity of the adsorbent, K represents the ratio between adsorption and desorption constants. Values of K higher than 1 indicate strong interaction between the surface and the adsorbed molecules. In the case of physisorption into the porous material c=1.
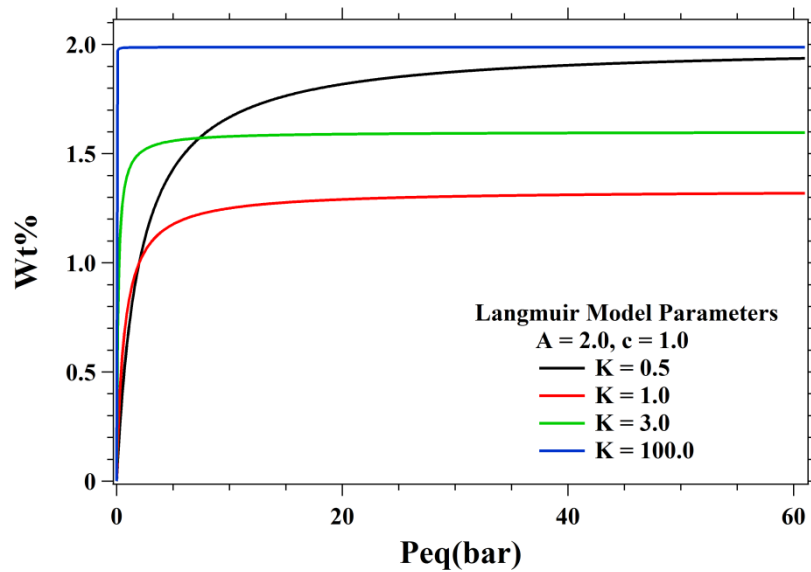
Figure 1.4: *Langmuir Equation shape different K-values. A- and c-values are fixed.*

The enhancement of the *K*-value increases the adsorption in low pressures (figure 1.4). Following this, maximum storage capacity (*A*-value) is reached in high pressures. On the other hand, maximum storage capacity is reached in significantly lower pressure for small values of *K*-value.

1.2.2   The Tóth Model

In most of the porous samples with high SSA and considering real experimental conditions, the Langmuir model's approximations are inapplicable. That model is mainly considering equivalent adsorption sites which require structurally and energetically homogenous properties at the sample surface. Additionally, Langmuir model can be applicable precisely only in the pressure range of (0 – 1) bar, while over this limit the compressibility alters gas's behavior and we are no longer in the zone where Henry's law is applied. For this reason, the relations (1.5) and (1.6) are not anymore appropriate. To keep up with, in the Langmuir model each adsorption site can host one adsorbate's molecule while in relatively high pressures more than one adsorbate's molecules can be found at each adsorption site[24].

In order to describe adsorption at relatively high pressures and heterogeneous materials,[a] József Tóth[23,25,26,27,28,29,30] proposed in 1962 a new model. He started from the experimental evidence that among samples of the same SSA, the one with heterogeneous properties adsorbs more gas molecules. In fact heterogeneity introduces energy competition between the adsorption sites resulting in a faster occupation of the most energetically favorable sites. However there should not be any difference in the samples' maximum storage capacities since both samples possess the same SSA. Keeping this in mind, in order to have higher grade of adsorption ϑ, Tóth introduced the relation

$$\theta^t > \theta \tag{1.11}$$

with $\quad 0 < t < 1$.

Considering the same dynamical equilibrium of the Langmuir model between adsorbed and desorbed hydrogen molecules, the equation that Tóth proposed will have the form:

$$wt\% = A \frac{KP}{(1+(KP)^t)^{\frac{1}{t}}} \tag{1.12}$$

where A is the maximum theoretical storage of the material, K the equilibrium constant

$$K = \frac{K_{ads}}{K_{des}} \; , \; K_{des} = e^{\left(\frac{-\Delta H}{kT}\right)}$$

as described in the Langmuir model.

The t-coefficient describes the heterogeneity as inserted by Tóth: when it is closer to the unity, more homogeneous are the structural characteristics of the sample and

---

[a] With heterogeneous properties, he considered samples with different pore size distribution and different surface morphology.

the energetic characteristics of its surface. For $t=1$ (1.12) takes the form of Langmuir equation and describes surface samples with homogeneous properties (equivalent sites). In order to understand the Tóth model, the relation (1.12) has been plotted at different K- and t-values (see figures 1.5 and 1.6).
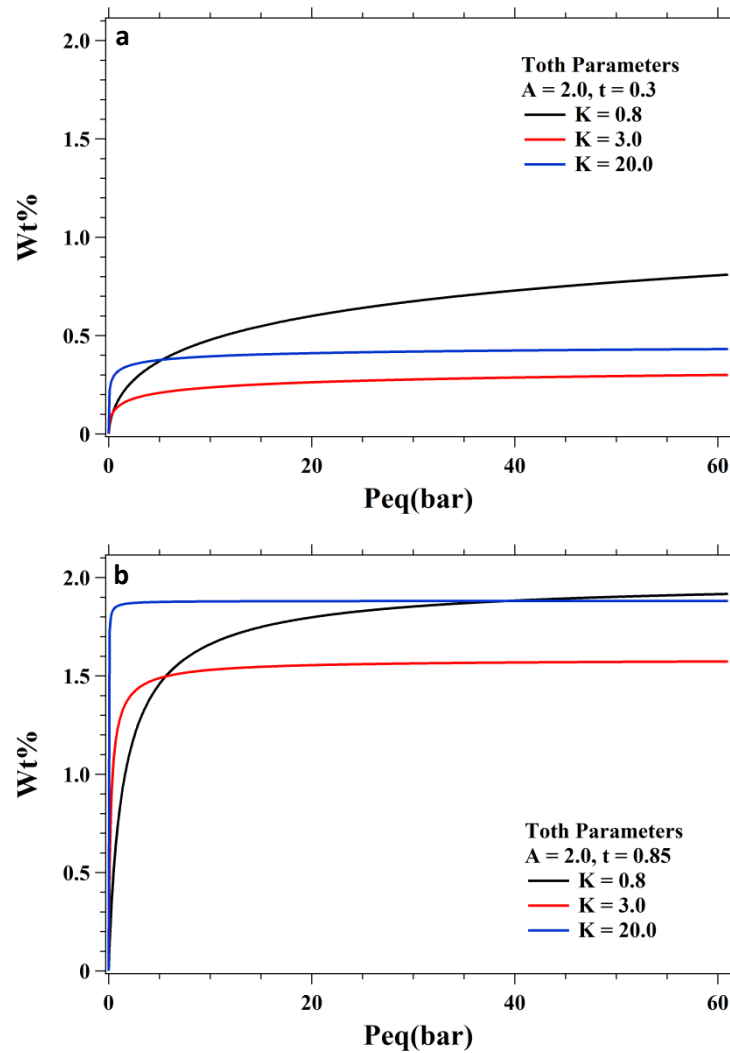
Figure 1.5: *Tóth Equation shape for low t-value (a) and high t-value (b). Three different values are assigned to K-value in each case.*

In particular, for fixed storage capacity and low heterogeneity (fixed t-value), surface is composed of several equivalent adsorption sites which results in a quicker saturation of adsorption sites. From the other side, low t-value describes a surface with non-equivalent adsorption sites that possess high diversity. In the latter case, in order to reach the fixed maximum storage capacity, it requires higher pressure values because of the less favorable adsorption sites. This can be due to broad pore distribution since different pore sizes mean different surface's affinity to hydrogen.

Low K-value means weaker interaction of adsorbate with the surface and the adsorption sites being occupied gradually by increasing the pressure (figure 1.5). This reflects on the isotherm curvature on a slower increasing of the curve at relatively lower pressure, as expected. On the other hand, high K-value demonstrates stronger interaction between adsorbate and surface and adsorption sites are occupied in relatively low pressures (figure 1.5). In terms of energy, high K-value means high ΔH, therefore higher bonding energy between the adsorbent and the adsorbate. Low t-value indicates slow surface coverage whereas for high t-values maximum storage capacity is reached in comparatively lower pressure. In the latter case, the situation is close to the Langmuir model (figure 1.4) because the t-values are similar (0.85 and 1).
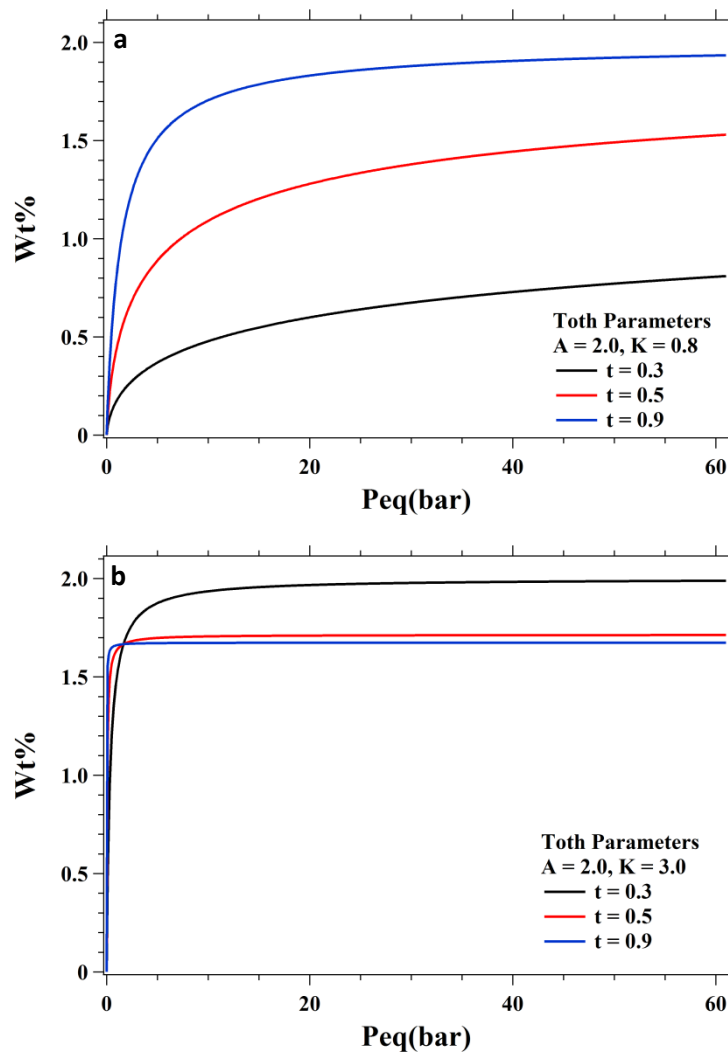
Figure 1.6: *Tóth Equation shape for different values of t for a low K-value (a) and high K-value (b).*

When storage capacity is fixed, K-value possesses a low fixed value and t-value varies, the shape corresponds to the shape of Figure 1.6a panel. Interaction between adsorbent and adsorbate is weak and equivalent sites are occupied quickly while the inhomogeneous surfaces (low t-value) will be saturated in relatively high pressures. From the other side, on Figure 1.6b, for fixed high K-value equivalent adsorption sites are occupied quicker than above and in their case maximum storage capacity is achieved in relatively very high pressures. For low t-value, maximum storage capacity is approached in relatively lower pressure.

1.3   Layered hydrogen adsorption: Number of molecules per nm^2

One of the most important samples properties in the sorption measurements is the SSA. The SSA takes into account the active sites which are involved in gas adsorption therefore sample with higher SSA are expected to give the bigger storage capacity in gas adsorption experiments. Hirscher et al[31] investigated the hydrogen storage capacity of the porous material as a function of SSA verifying a linear dependence of the two parameters. However the ability of the samples to store the molecular species does not depend only on the SSA value but can be also due to the possibility to adsorb more than one mono layer. In the hydrogen storage capacity, the enhancement of the SSA is not the only route to get the DOE target of 6%. In fact these results could be obtained in samples with lower SSA but with an enhanced physical interaction of hydrogen-porous material.[32] The evaluation of the adsorbed molecules per nm^2 (molec/nm^2) could indicate the efficacy of the sample to create more than one mono layer by the following formula

$$N_{mol}/nm^2 = N_a \cdot wt\% / (PM_{gas} \cdot SSA \cdot 10^{20}) \tag{1.13}$$

where N_a is the Avogadro's number, PM_{gas} is the molecular weight of the adsorbed gas, wt% the adsorbed gas weight percent, and SSA is the BET specific surface area of

the sample in m^2/g (the factor takes into account the unit conversion). For Silicalite-1 and MCM-41, has been obtained the figure 1.7 (see below) where it is clear the asymptotic value of 8 N_{mol}/nm^2. This value is close to the expected one which is in the (6.95 ÷ 8.55) N_{mol}/nm^2 range in the formation of one monolayer of adsorbed hydrogen molecules. In fact, the area occupied by H_2 molecule is 0.117 nm^2 in the solid phase and 0.144 nm^2 in the liquid phase. While being adsorbed and forms a monolayer, hydrogen can be considered as a bi-dimensional liquid where hydrogen's binding to surface is not directional but permits molecules mobility into the adsorbed phase.
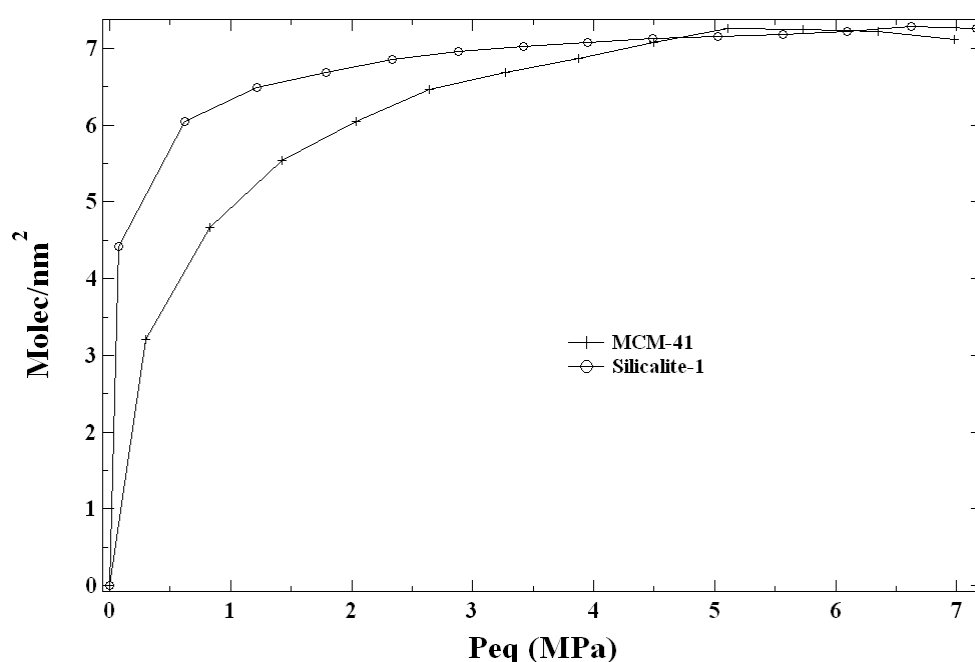
Figure 1.7: *Molecules per nm^2 adsorbed on the silicalite-1 and MCM-41 at LN_2 temperature.*

As a consequence, great care should be taken into account into the SSA determination. Actually, the most recognized techniques to estimate the SSA is the BET measurement by nitrogen molecules. To check the reliability of the BET SSA evaluation we utilized the method proposed from Tóth[33] which determines the SSA by BET measurements with different gas (in our case hydrogen). Most of the time the two methods are in agreement for several samples while for some measurements, the SSA obtained with H_2 is overestimated. The calculation of SSA by Tóth method[33] is obtained from the knowledge of the maximum mole adsorbed

from the sample. This value can be due to the formation of single or double layer of adsorbed gas which, in principle, can be formed also in the N_2 BET measurements. Therefore in this case the techniques are not reliable for the determination of SSA in porous material because the BET technique is based on the creation of one mono layer of adsorbed molecular specie. The difference in the SSA determination by N_2 and H_2 BET measurements can be also due to different molecular size. In fact, being smaller the hydrogen molecules size, we could expect the probing of even smaller porous channel by H_2 which are not accessible to N_2 molecules.

1.4 Adsorption properties in dynamical conditions: Diffusion coefficient

Beside the isotherm curves, the volumetric apparatus can give indication on the dynamical adsorption properties of the sample as well. To keep track of the transient events, pressure versus time graphs are acquired during the measurements. The typical pressure decrease subsequently to the expansion from the calibrated reservoir to the sample holder volume containing the silicalite-1 powders is depicted in figure 1.8.
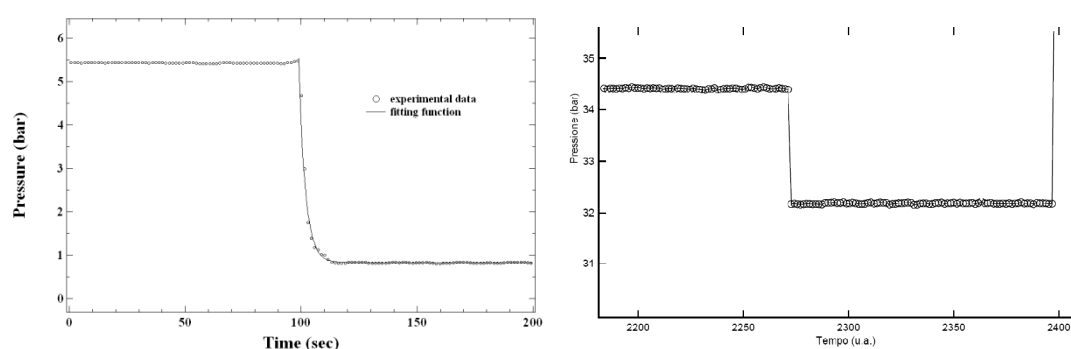
Figure 1.8: *Exponential decay of the pressure when the valve between the reservoir and the sample holder volumes is open (left panel). The continuous line represents the fitting results obtained by exponential function. As an example, the same measurements are reported when the sample holder void volume is empty (right panel).*

After a sudden pressure decrease from P_0 (starting pressure) to $P_0{}'$ (in figure 1.8, the $P_0{}'$ value is represented from the cross), mainly due to the rapid diffusion of the gas molecules in the free volume, it is present a slower decrease of the H_2 pressure down to P_1 mainly imputable to the diffusion/adsorption process inside the zeolite pores. While the first step is directly valuable by knowing the involved volumes, the second slope is a peculiar feature of the gas/adsorber system at the measured pressure and temperature conditions. At a first glance, the latter behaviour can be described with an exponential decay with time constant τ and amplitude $\Delta P = P_0{}' - P_1$. As long as gas diffusion in microporous and mesoporous samples is concerned, this is a rough simplification of a complex phenomenon involving pore diffusion, viscous flow, surface diffusion and heat transfer.

In order to improve the evaluation of the gas kinetic into the pores, the Fick's second law is considered[34,35] which is represented, in one dimension, from the formula:

$$\frac{\partial C}{\partial t} = D \frac{\partial^2 C}{\partial x^2}$$

(1.14)

where D is the diffusion coefficient of the gas into the considered material and C is the gas concentration diffusing into the material pores.

The Fick's law describes, temporally, the tendency of substances to naturally diffuse into the empty spaces in order to remove the spatial gradients of its concentration. The fluid equilibrium state will be reached with typical diffusion time τ which depends on the gas itself and the investigated material.

In general the diffusion coefficient is related to the pressure and gas concentration by the relation:

$$D = D_0 \frac{\partial \ln P}{\partial \ln C}$$

(1.15)

The Fick's law can be easily resolved considering three assumptions:[34,35]

- Constant diffusion coefficient

- The shape of the diffusing material

- The boundary condition

The first condition is fulfilled over a small change in the adsorbed phase concentration arising D=D_0 in the relation (1.14).[35,36] In fact either in liquid or vapour or adsorbate phase at low concentration, Henry's law is satisfied and the pressure is directly proportional to the concentration and under these conditions

$$\frac{\partial lnP}{\partial lnC} \sim 1$$

The second requirement is fulfilled by taking into account different shapes for the absorbing as sphere, cylinder, slab and cube.[35]

The last assumption depends on the concentration boundary conditions during the diffusion mechanism.[35] In fact the diffusion can occur with constant or variable concentration at the surface of the material. The former case describes the diffusion of gas in stationary conditions, excluding in this way the gas adsorption into the pores materials. The latter considers the variation of the gas concentration at the sample surface due to different mechanisms (gas adsorption, sample surface barrier, etc…) taking into account constant volume experiments. In Figure 1.9 the typical moles per unit volume versus Time graph is represented.
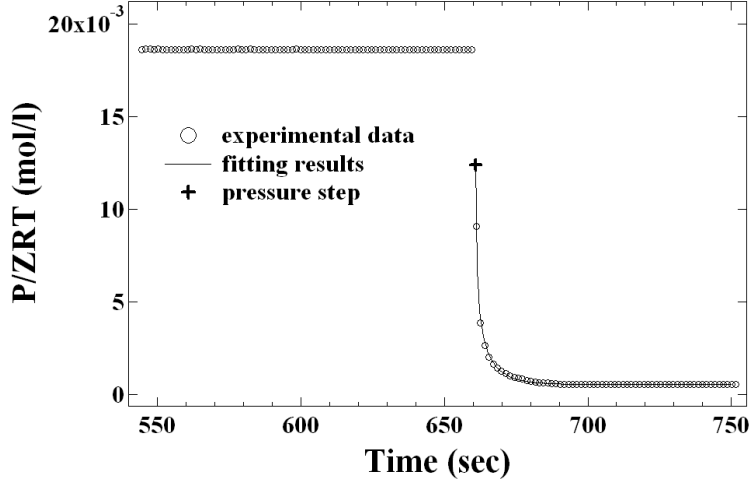
Figure 1.9: *PcT experimental data fitted by decaying function versus of hydrogen time diffusion/adsorption. The continuous line represents the fitting results by using the formula (1.16) (see below). The cross represents the sudden pressure decrease after the valve opening between the reservoir and the sample holder volumes.*

According to the theory presented previously concerning to the gas molecules diffusion, the results of the fit procedure have been obtained by using the formula:[a]

$$m_t = (m_0 - m_\infty) \cdot 6 \cdot \sum_{n=1}^{\infty} \frac{\exp(-Dp_n^2 t / r^2)}{9\Lambda/(1-\Lambda) + (1-\Lambda)p_n^2} + m_\infty \qquad (1.16)$$

where D is the diffusion coefficient, r is the channel length where the hydrogen molecules diffuse, m_0 and m_∞ are the moles for volume unit after the opening of the valve between the reservoir and the sample holder volumes and at the equilibrium pressure respectively. The m_0 value has been calculated considering the expansion of the gas only on the sample holder volume removing, on its value, the contribution of the sample volume. The D_0/a^2 values extrapolated at lower pressure are 0.0046 sec^{-1} and 0.0106 sec^{-1} (the error is the 5%) for silicalite-1 and MCM-41 respectively.

Taking into account the relation (1.15) and the fitting results of D_0, we obtain the curves of figure 1.10.

---

[a] Spherical shape has been utilized to resolve the Fick's law for silicalite-1 and MCM-41
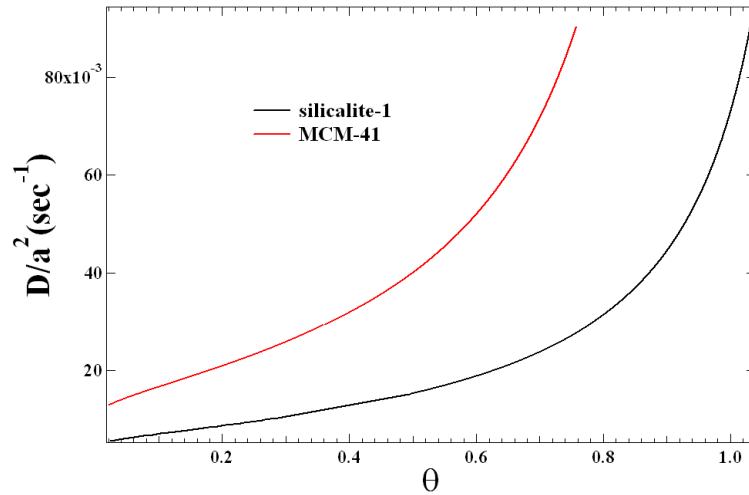
Figure 1.10: *Diffusion coefficient normalized to a² for silicalite-1 and MCM-41 versus hydrogen coverage ϑ.*

The data in figure 1.10 have to be multiplied for the average a-value which is ~100 nm and 18μm for MCM-41 and silicalite-1 respectively.

Therefore, considering the data of figure 1.10, the silicalite-1 presents slower kinetics.

The analysis of the dynamics in adsorption is an important aspect of hydrogen energy in view of application as it was pointed out from DOE recently.[37]

Bibliography Chapter 2

(1) Fr. Rouquerol, J. Rouquerol & K. Sing *Adsorption by Powders and Porous Solids*, 1rst ed., Academic Press, Marseille, **1999**. p.10.
(2) Zuttel, A. *Naturwissenschaften*, **2004**, *91*, 157-172.
(3) Chiarello, G., Maccallini, E., Agostino, R. G. *et al. Physical Review B*, **2004**, *69*.
(4) Zhou, L. *Renew. Sust. Energ. Rev.*, **2005**, *9*, 395-408.
(5) Fichtner, M. *Advanced Engineering Materials*, **2005**, *7*, 443-455.
(6) Grochala, W.; Edwards, P. P. *Chem. Rev.*, **2004**, *104*, 1283-1315.
(7) Sakintuna, B.; Lamari-Darkrim, F.; Hirscher, M. *Int. J. Hydrog. Energy*, **2007**, *32*, 1121-1140.
(8) Andreas Züttel, Andreas Borgshulte, Louis Shlapbach *Hydrogen as a Future Energy Carrier*, 1rst ed., Wiley-VCH Verlag GmbH & Co. KGaA, Weinheim, **2008**. p.173-175.
(9) Liang, G., Boily, S., Huot, J. *et al. Journal of Alloys and Compounds*, **1998**, *268*, 302-307.
(10) Leng, H. Y., Ichikawa, T., Hino, S. *et al. J. Phys. Chem. B*, **2004**, *108*, 8763-8765.
(11) Schlapbach, L.; Zuttel, A. *Nature*, **2001**, *414*, 353-358.
(12) Han, S. S.; Mendoza-Cortes, J. L.; Goddard, W. A. *Chemical Society Reviews*, **2009**, *38*, 1460-1476.
(13) Bhatia, S. K.; Myers, A. L. *Langmuir*, **2006**, *22*, 1688-1700.
(14) Gogotsi, Y., Portet, C., Osswald, S. *et al. Int. J. Hydrog. Energy*, **2009**, *34*, 6314-6319.
(15) Yushin, G., Dash, R., Jagiello, J. *et al. Advanced Functional Materials*, **2006**, *16*, 2288-2293.
(16) Klontzas, E., Mavrandonakis, A., Tylianakis, E. *et al. Nano Lett.*, **2008**, *8*, 1572-1576.
(17) Mavrandonakis, A., Klontzas, E., Tylianakis, E. *et al. Journal of the American Chemical Society*, **2009**, *131*, 13410-13414.
(18) Mavrandonakis, A., Tylianakis, E., Stubos, A. K. *et al. J. Phys. Chem. C*, **2008**, *112*, 7290-7294.
(19) Mpourmpakis, G., Tylianakis, E., Papanikolaou, D. *et al. J. Nanosci. Nanotechnol.*, **2006**, *6*, 3731-3735.
(20) S.J. Gregg, K.S.W. Sing *Adsorption, Surface Area and Porosity*, Second ed., Academic Press, Harcourt Brace & Company, Publishers, London, **1982**.
(21) IUPAC *Pure & Applied Chemistry*, **1985**, *57*, 603.
(22) Langmuir, Irving *Physical Review*, **1916**, *8*, 149.
(23) Toth, J. *Journal of Acta Chimica Academiae Scientiarum Hungaricae*, **1962**, *32*, 39.
(24) Kalantzopoulos, G.; Maccallini, E.; Agostino, R.G. *in preparation*, **2009**.
(25) Toth, J. *Advances in Colloid and Interface Science*, **1995**, *55*, 1-239.
(26) Toth, J. *Adsorption. Theory, Modelling and Analysis*, ed., Dekker, New York, **2002**. p.1.
(27) Terzyk, A. P., Chatlas, J., Gauden, P. A. *et al. Journal of Colloid and Interface Science*, **2003**, *266*, 473-476.
(28) Toth, J. *Journal of Acta Chimica Academiae Scientiarum Hungaricae*, **1971**, *69*, 311.
(29) Toth, J. *Journal of Colloid and Interface Science*, **1994**, *163*, 299-302.
(30) Toth, J. *Journal of Colloid and Interface Science*, **1997**, *185*, 228-235.
(31) Hirscher, M.; Panella, B. *Scripta Materialia*, **2007**, *56*, 809-812.
(32) Kalantzopoulos, G.; Maccallini, E.; Agostino, R.G. *in preparation*, **2009**.
(33) Toth, J.; Berger, F.; Dekany, I. *Journal of Colloid and Interface Science*, **1999**, *212*, 402-410.
(34) Crank, J. *The matematics of diffusion*, ed., Oxford University Press, New York, **1975**.
(35) Karger, J; Ruthven, D.M. *Diffusion in zeolites and other microporous solids*, ed., John Wiley & Sons, **1992**.
(36) Sircar, S. *Aiche Journal*, **2001**, *47*, 1169-1176.
(37) Gross, K.J.; Russell, K.; DOE, U. S., Ed., 2008.

2   Experimental Techniques

2.1   Sievert's Apparatus

2.1.1   Experimental apparatus

The volumetric gas storage apparatus (also known as a Sieverts' apparatus) consists of a gas manifold with a series of tubes and valves connecting the sample holder void volume to the gas reservoirs void volume and pressure transducers (figure 2.1).

The achievement of reliable results on the gas storage isotherms, (also known as *Pressure concentration Temperature (PcT) curves),* with high accuracy up to 8 MPa, has been obtained by novel apparatus (*f*-PcT - DeltaE S.r.l) replacing and optimizing different part of similar apparata described in the literature (dotted line in figure 2.1).
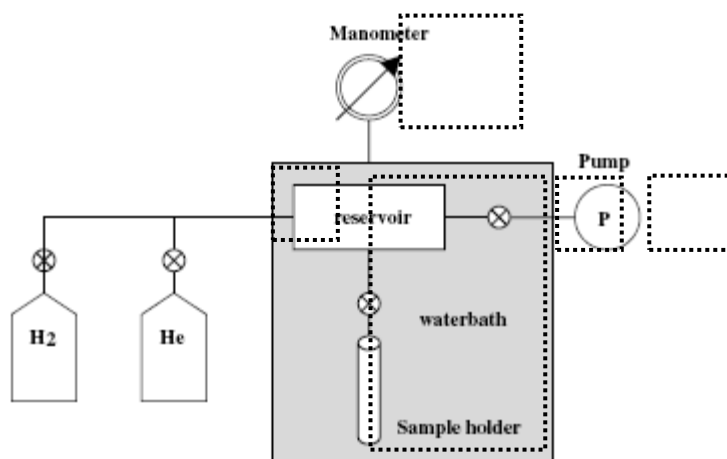
Figure 2.1: *Schematic representation of the Sieverts' apparatus.*[1]

The apparatus allows the admittance of different species from a gas manifold into a calibrated reservoir (CR) and the subsequent expansion of that gas in the sample holder volume (SH) hold at a fixed temperature. The missing moles after the gas expansion, calculated considering the gas pressure and temperature, are adsorbed into the sample. The gas expansion is repeated at increasing pressures allowing the evaluation of the sorption isotherm in terms of sorbed moles versus equilibrium

pressure. Desorption curve is measured by letting the gas contained in the SH volume expands into the previously evacuated CR. In this case, the desorbed moles contribute to the measured pressure as an excess value.

2.1.1 Apparatus brief description

A mass flow controller (MFC) is inserted to control the admittance gas in the reservoir. Two pressure transducers with end scale of 0.1 MPa (P1) and 10 MPa (P100) are mounted in the reservoir volume to measure the lower and higher pressures ranges respectively. Errors of 0.001 kPa and 0.001 MPa are made in the pressure measurements respectively. The principal system void volumes are divided by electrovalves.

The sample holder is thermalized with a specific bath at different temperature (liquid nitrogen temperature LN_2, liquid argon) and heated in the range $300 - 800$ K. The temperature of the reservoir is measured by a probe (A) with a precision of ca. 0.015 K (figure 2.5), while the SH temperature is measured by k-type thermocouple which takes in account the A probe measurements as reference temperature. The temperatures of the reservoir and SH is monitored at different points checking his uniformity within the error of 0.1%.

The vacuum has been obtained by pumping system consisting of membrane and turbo molecular pump achieving pressures less than 1.3×10^{-3} mbar. The system volumes have been chosen according to the evaluation of the volume/mass relationship of Wang and Suda.[2]

All the equipment (pressure and temperature measurements, valves, pumping system, time settings, LN_2 level and data acquisition and analysis) is controlled by home made software which manages the apparatus by an acquisition card.

The system has been tested by measuring the PcT isotherms of Silicalite-1 (ZSM-like sample with MFI topology) and MCM-41.[3]

However, before the discussion of the experimental results, we present all the experimental details underlying the PcT apparatus. As reference, the review-article of Broom is taken into account which exposes all the experimental problems

concerning the hydrogen adsorption measurements.[4] Broom defines some simple but fundamental concepts: repeatability, reproducibility and accuracy of measurements. Repeatability is the closeness of the agreement between the results of successive measurements carried out under the same conditions. The reproducibility is the closeness of the agreement between the results of measurements carried out under changed conditions. To conclude the accuracy of the instruments and measurements is the ability to provide experimental data close to the expected results. To fulfil those requirements great care has to be taken into account on the measurements procedure, observer, experimental conditions and location.

Keeping in mind all the experimental considerations of Broom, we focused carefully on the PcT experimental setup showing all the solutions.

First of all, the PcT measurements require the knowledge of hydrogen adsorbed moles into the sample which are obtained taking into account the real gas law (see formula 0.1 at Introduction).

Therefore great care has to be considered in the acquisition and processing of pressure and temperature values and system void volumes calibration. In this way the experimental setup requires hardware (H) and software (S) solutions in order to minimize all the error sources. The equation (0.1) can be utilized only for pure gases, since high gas purity is required. To summarize the following experimental details has to be considered and discussed critically:

1. Gas Purity

Two main sources can contaminate the adsorbed gas: intrinsic gas purity (H) and oil from low vacuum pumps (H). The first problem is due to the nominal purity of the gas set from the vendor company. For instance hydrogen 5.0 means H_2 with purity of 99,999%. If the reservoir void volume V_0 is filled with H_2 at P_0 pressure and the H_2 moles are n_0, the contaminations moles are 10^{-5} times n_0. Because of the adsorbed moles into the samples pores range in between ~10^{-3} - 10^{-4}, the error made in the adsorbed hydrogen moles evaluation can range between 1-10% which is an enormous value compared to the error made in the P, V and T measurements (see

section 2.2.6 in the propagation error evaluation). The second one could be related to the use of classical rotary pumps.

2. Thermal gradients

The equation (0.1) can be utilized in gas thermal equilibrium. Therefore all the system thermal gradients have to be removed. The thermal gradients can be divided in intrinsic (S) and extrinsic (H). The former are produced from the electrovalves which warm up during their opening. The latter can appear when the measurements are not carried out in stable conditions (i.e. at room temperature).

3. Pressure measurements

The accuracy in pressure measurements does not depend only on the pressure manometer nominal error, but evaluation on the manometers calibration and analogical signal acquisition has to be spent.

4. System void volumes calibration

The calibration of system void volumes (H and S) is not a trivial task to deal. The normal procedure utilized in the literature is the gas expansions into the sample holder void volume filled with a specific solid material with well know density. Usually to obtain error less than 1% in the estimation of the adsorbed moles, error of 0.1-0.5 % should be obtained in the void volumes evaluation (see section 2.2.6, error evaluation).

5. Sample Properties

In order to obtain the adsorbed moles, several sample properties has to be known: sample skeleton density (H and S), adsorbed gas density (S) and surface specific area (SSA) (H). In addition the PcT apparatus provides also the analysis of the typical gas diffusion time into the sample (H).

All that experimental problems will be faced on the next paragraph taking into account the adopted solutions in the literature.

2.1.2   Experimental Considerations

2.1.2.1 Gas purity

Usually the gas used for adsorption experiments can have intrinsic impurity. An additional problem derives from oil impurities of low vacuum pumps. To solve these problems we adopt some solutions. The apparatus presents a void volume close to the gases-in filled with zeolites (zeolite trap, ZT) which is merged in liquid nitrogen (LN_2) bath during the measurements in order to absorb the gas contaminations (water, carbon monoxide, etc…) guarantying in this way the gas purity during the experiments. Previously, the ZT is heated and evacuated to remove the contaminations physisorbed and chemisorbed in the zeolites. To exclude contaminations coming from pumping system we decided to use oil free pump. In this way we can be sure that in the worst condition of gas return or vacuum system failure, the gas into the system void volumes will not contaminated from oil returned of rotary pump.

2.1.2.2 Pressure measurements

The accuracy in pressure measurements is one of the most important parameter in gas adsorption experiment. The precise knowledge of gas pressure is fundamental in order to be accurate about the quantity of gas adsorbed on the storing materials. However accurate pressure value does not depend only on the pressure manometer nominal error, but evaluation on the manometers calibration and analogical signal acquisition has to be spent.

The calibration of our apparata to get the best adsorption measurement needs some considerations. First of all, because of adsorption isotherms from 0 up to 8 MPa will be acquired, we need the best accuracy over the entire pressure range. To get this result, we decided to use pressure manometer with the similar nominal error. The former works in the range (0-0.1) MPa, usually used for small pressure adsorption measurements, and the latter in the range (0-10) MPa to reach higher pressure.

In order to obtain great accuracy in pressure data acquisition, the manometers calibration has been verified. In particular the manometers must measure 0.1 MPa when the system is evacuated. In addition, possible pressure offset has been measured and removed. However the offset are not very crucial because the utilized pressure values in formula (2.6) in order to calculate the adsorbed moles (see below) considers pressure difference.

2.1.2.3 Real gas law and compressibility

At high pressure measurement the representation of the real gas law by compressibility factor Z is very important for the meaning of the data. If the compressibility is neglected significant error can be done in the calculation of the wt% adsorbed (see figure 2.2).

The equation considered during the experiments is the real gas law in the formulation taking into account the compressibility factor Z(P,T) (see formula (2.1)).

In order to obtain an accurate evaluation of gas adsorbed moles (n_{ads}), small errors in the measurements of temperatures, pressure and volumes are required. An accurate evaluation of the compressibility factor is of great importance in the determination of n_{ads}, too. However the compressibility of the gases presents different behaviour by changing the temperature and the pressure. In figures 2.3a and b are reported the compressibility factor of H_2 at liquid nitrogen temperature (LN_2) and room temperature respectively. In the second case because of the temperature value can range in (288 − 298) K, three different curves are taken into account.
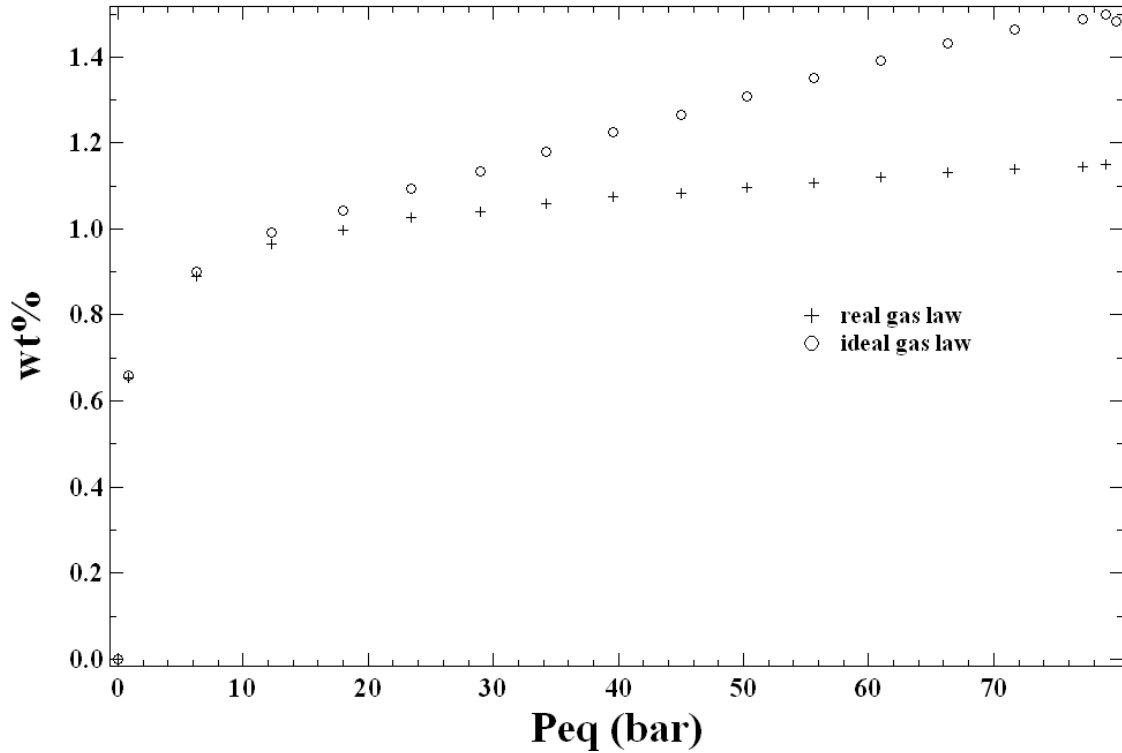
Figure 2.2: *Adsorbed H$_2$ (wt%) in ZSM-like zeolite taking into account the real and ideal gas laws.*
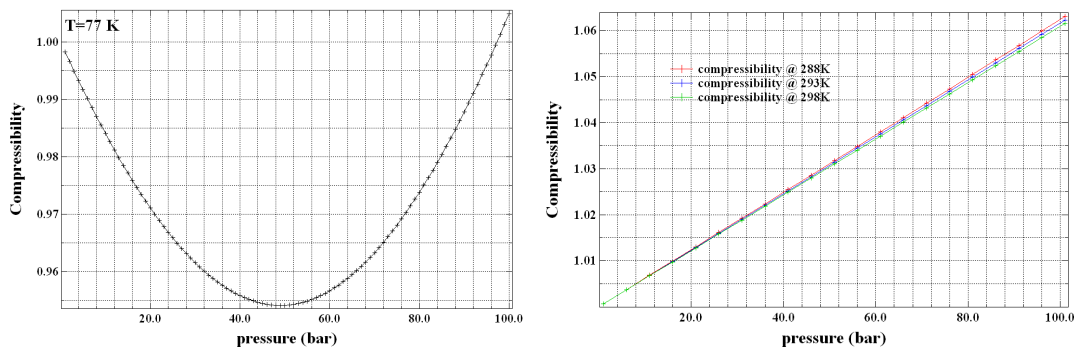
Figure 2.3: *Compressibility factor of H$_2$ a) at 77 K and b) at 288 K, 293 K and 298 K.*

As an example, in figure 2.2 the wt% of H$_2$ adsorbed from ZSM-like powder is represented taking into account the real and ideal gas laws.

If the contribution of the compressibility is removed, the curve of the wt% is overestimated. In fact, at high pressure and low temperatures, the real hydrogen gas

is denser into the respect to the ideal case. For the same gas at low pressure (< 0.1 MPa), the ideal and real gas laws are practically identical, as expected.

In the case of methane adsorption measurements, the compressibility factor evaluation is more complex. In fact in our case, the normal procedure considers PcT isotherms at different temperature ranging in (283 − 323) K. In this way the compressibility factor of methane consists of a complex dependence in pressure and temperature which can be well reproduced by non trivial two dimensional fitting results.

Many works outlined the importance of this correction[4,5,6] and to be more accurate we compared the data sheet of NIST[7] and Perry's handbook data[8] resulting in a fair agreement. The contribution of the compressibility has been considered also in the system void volumes calibration and sample density evaluation, depending on the gas and the pressure range utilized.

2.1.2.4 Temperature measurements and thermal gradients

The right knowledge of the gas temperature is an important task to resolve. Considering relation (0.1), if gas temperature is under- or over-estimated, the adsorbed gas moles will be over- or underestimated. In the literature several experimental works deal with the temperature measurements[9,10,11,12,13] but only few of them discuss about the thermal gradient between the reservoir and the SH.[2,4,5,6]

The gas presence in the apparatus at high pressures should facilitate the achievement of equilibrium temperature. In fact, the thermal conductivity of helium and hydrogen are ranging, at room temperature and in the pressure range (0 − 10) MPa, between (0,156 − 0,162) W/(m K) and (0,186 − 0,194) W/(m K) respectively, while at LN_2 temperature and 0 − 10 MPa pressure range it changes between (0,062 − 0,076) W/(m K) and (0,054 − 0,092) W/m K respectively.[7] If the average speed of the two gases are, at 273 K and 0.1 MPa, 1200 m s^{-1} and 1700 m s^{-1} respectively,[14]

the gas expansion will be very fast and its thermalization optimized according to the relation

$$k = \frac{n \overline{v} \lambda c_v}{3 N_A}$$

(2.1)

where k is the thermal conductivity, n the molecules per unit volumes, $\overline{v}$ the mean molecules speed, λ the mean free path, c_v the molar heat capacity and N_A the Avogadro's number.

Keeping in mind those values, the thermal transpiration effect can be neglected if helium and hydrogen gases are utilized.[15]

In order to stabilize efficiently its temperature, the calibrated reservoir is enclosed in a box where the temperature is measured with an accuracy of ca. 0.005 K (figure 2.4). This section of the gas line is fixed in thermal equilibrium with the room temperature and monitored during the experiments.

However, we believe the main problem derived from the management of the thermal gradient between the RT section and the controlled temperature one. This thermal gradient has to involve a small part of the gas line volume in order to minimize the uncertainty of the temperature determination and thus of the gas moles in the gas line. Rouquerol et al.[15] pointed out how this problem has important consequences in the calibration of the volumes with different temperatures.

To efficiently reduce this problem, we let the temperature gradient involve a short section of a 1/8" steel pipe. In the worst condition, where the two sections are kept at RT and LN_2, we estimated that a gradient temperature region extended for 5 mm will result in a 0.1% error in the evaluation of the adsorbed moles.

To keep a more stable temperature profile when very low temperatures are concerned, we use a control on the cooling liquid level with a feed-back system that maintain it at a fixed position with respect to the gas line. Using LN_2 as coolant, desorption rate was estimated to be 0.2 mm/min and therefore a very slow adaptation of the position was necessary.

A further source of temperature gradients is due to the use of electromagnetic valves (see the paragraph concerning the volumes). In fact, the solenoid and the internal ferromagnetic cylinder are heated in proportion to the electric power absorption and the time of use. We minimized this effect, which was not discussed in the literature,[9] by both hardware (increase of the heat exchange area) and software (reduction of the "power on" time) solutions.

All the described work on the temperature control allowed us to obtain very stable conditions as depicted by figure 2.4.
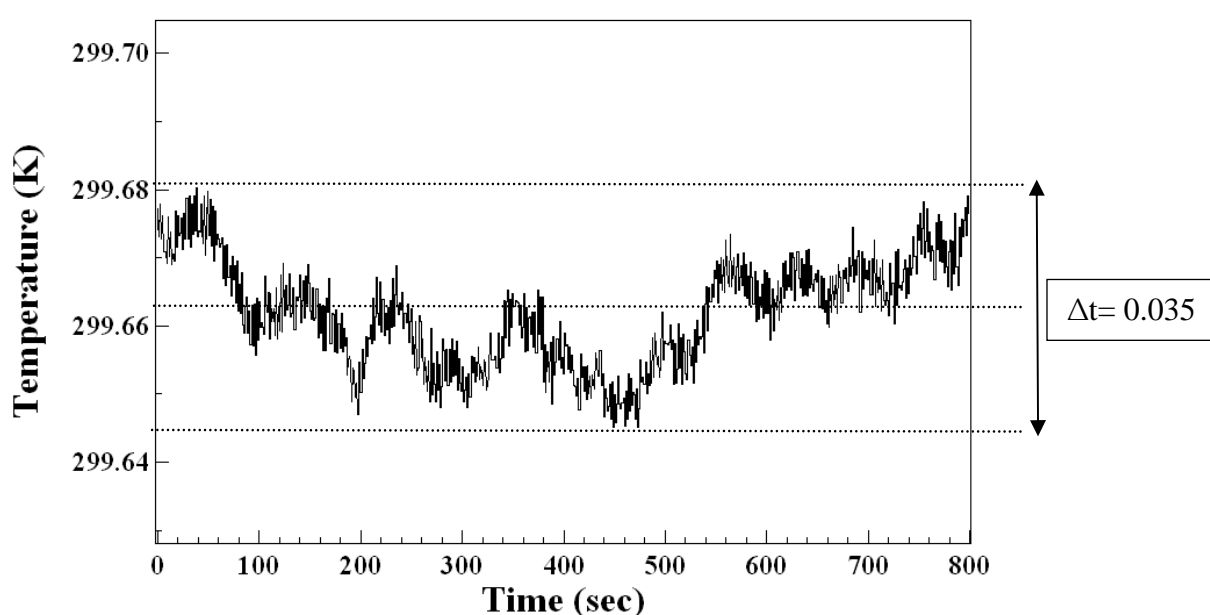
Figure 2.4: *Evolution of system temperature during a generic measurement.*

2.1.2.5 System void volumes: calibration, sample weight-to-volume optimization and error propagation

The evaluation of void volumes is one of the main problems in volumetric apparatus for gas storage measurements.[4,6,9,16,17,18] However the volume calibration procedure was not critically dealt in the past leaving several opened question about its determination and errors.

The inner volumes of the gas piping must be accurately measured. The standard procedure reported in the literature is the expansion of the gas between the

reservoir and the empty or filled sample holder.[9,15] We actually used as a first trial, a procedure in which an object with calibrated volume (an accurately weighted copper cylinder) is introduced in the sample holder volume allowing the determination of its volume by comparison of the gas expansion data. The uncertainty on the copper density and the corrugation of its surface can determine volume errors greater than 1% which propagate to adsorbed moles error bigger than 100% at 8 MPa! As an example, in the literature, this procedure has been carried out filling the sample holder void volume with sea sand[19] or stainless steel rood[20] and expanding hydrogen gas. The two materials do not uptake significant hydrogen moles but in any case it is difficult to know the samples density and roughness. In addition, the procedure establishes that the calibrated volume should be the same size of the void volume[15] but the fittings pipeline connecting the SH and the reservoir volume gives a large contribution to the SH volume and this introduces a significant source of error.

Thus, we developed an alternative procedure for the void volume calibration involving two steps: in the first, we utilize MFC to measure the total void volume (avoiding in this way the use of the calibrated sample). The second step involve the expansion of the gas from the reservoir to the SH volume.

The MFC utilization allows the knowledge of gas moles introduced into the different system void volumes by flux measurements. In fact the volume of the gas admitted by MFC (V_{gas}) and the flux measured (Φ) are connected by the relation

$$\int \Phi(\mathbf{P},\mathbf{T},\mathbf{t})\mathbf{dt} = \mathbf{V_{gas}}(\mathbf{P},\mathbf{T})$$

(2.2)

But the V_{gas} is related to the gas pressure and system void volume by

$$\mathbf{V_{gas}}(\mathbf{P},\mathbf{T}) = \mathbf{K}\cdot\mathbf{V}\cdot\mathbf{P}$$

(2.3)

with

$$K = \frac{T_n}{P_n \cdot T}$$

(2.4)

where T_n and P_n are temperature and pressure at normal condition and T is the system void volume temperature. If the system void volumes are labelled as reported in figure 2.5, the MFC utilization permits to know the total volume $V_{tot}=V_0+V_1+V_2$. The calculation of the three void volumes needs two more relations which can be obtained from the gas expansion from the V_1 volume to either the V_0 or the V_2 void volumes. From this calibration procedure we calculate volume values within the error of 0.5%.
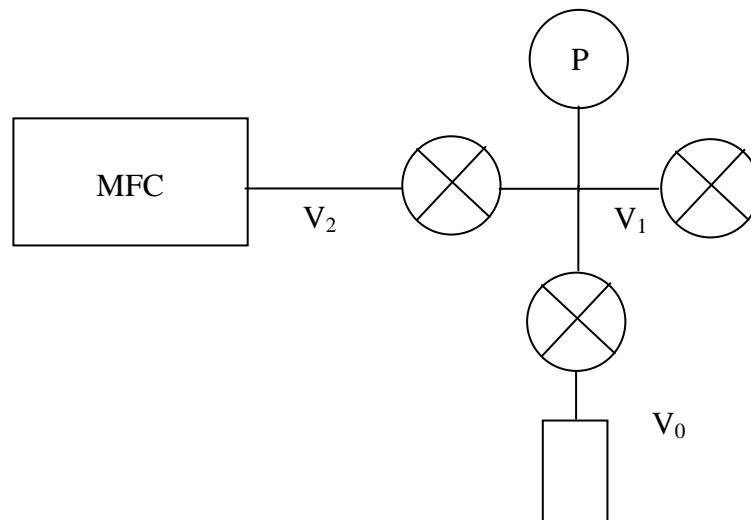
Figure 2.5: *Schematic representation of the system void volumes involved during the calibration procedures.*

However to calculate the error made in the evaluation of the gas adsorbed moles, error propagation has to be performed.

If the sorbed gas moles are calculated by real gas law taking into account the compressibility factor,[7,8] from the expansion between a calibrated reservoir (V_1) and sample holder (V_0) volumes the following relation is obtained

$n_{ads}=P_1[V_1(P_0/P_1-1)-V_0] +P_1'V_0$

(2.5)

where P_i are the normalized pressures, $P_i = P_i/(Z(T_i,P_i)\ RT_i)$ with $Z(T_i,P_i)$ the compressibility factor of the measured gas at the temperature T_i and the pressure P_i. P_0 is the normalized pressure in the calibrated reservoir before the gas expansion in the sample holder volume (SHV), P_1 is the normalized pressure after the expansion in SH volume and the consequent adsorption in the sample, P_1' is obtained as P_1 but it is relative to the previous step. Naturally, in this evaluation the sample volume is removed from the sample holder volume V_0.

If we calculate the maximum error by formula

$$\Delta z = |df/dx|\Delta x + |df/dy|\Delta y + \ldots \qquad (2.6)$$

in case of relation (2.5) the maximum error formula is

$$\Delta\ n_{ads} = (V_1 + V_0)\ \Delta P_1 + V_1\ \Delta P_0 + (P_0 - P_1)\ \Delta V_1 + P_1\ \Delta V_0 + V_0\Delta P_1' + P_1'\Delta V_0 \qquad (2.7)$$

where $\Delta V_1 = \Delta V_0$, $\Delta P_1 = \Delta P_0 = \Delta P_1' = 0.01/RT\ cc^{-1}$. In figure 2.6, the behaviour of the relative error $\Delta n_{ads}/n_{ads}$ versus pressure at different relative error $\Delta V_i/V_i$ is shown. The error values made in the adsorbed moles evaluation enhance dramatically at high pressure. However if better resolved pressure manometers are used with sensitivity of 0.0001 MPa, the error in figure 2.6 decreases more than 50%!
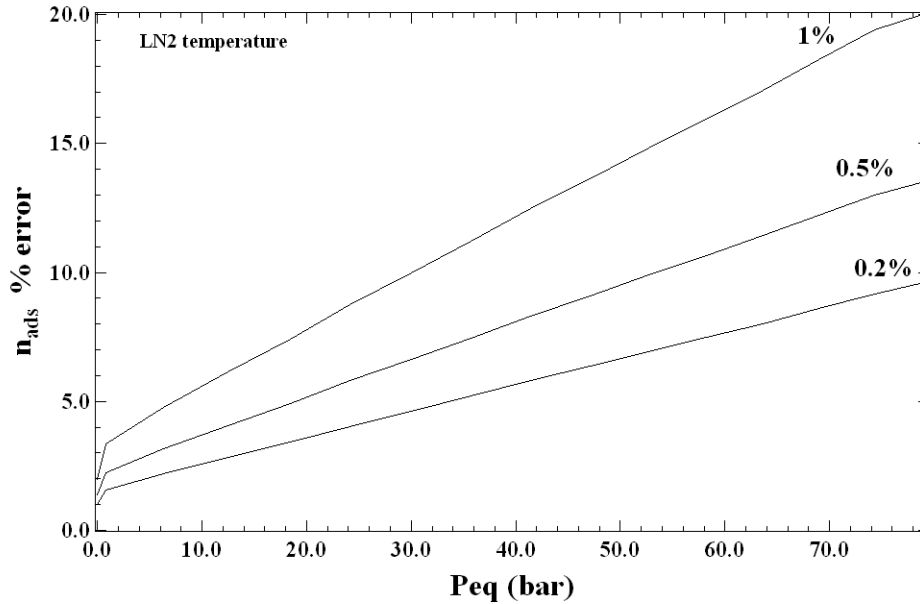
Figure 2.6: *% error of n_{ads} evaluated at different error of the void system volumes at LN_2 temperature. The sample is ZSM-like zeolite.*

As it can be seen in figure 2.6, 0.2% relative error in the system void volumes evaluation minimizes the error in the calculation of n_{ads}. Because of typical system void volumes are ranging between 10 and 800 cc, as reported in the literature,[6,9,12,21] the uncertainty due to the piping and valves cannot be higher than 0.02 and 1.6 cc, respectively.

However the possible error source in the system void volumes determination can be due to additional problems.

The system volumes are connected with two different valves: Manual Valves (MV) and electric valves (EV). The employ of those valves is due to the involved volumes during the experiments. The MV are utilized only in the gases-in line and on the ZT, the EV are used to divide the SH and the reservoir volumes from the rest of the system. The use of EVs is made to fix the system void volume independently if the valves are open or closed, which is, from our point of view, extremely important for the success of the experiments. In literature the most utilized valves are the pneumatic (PV)[2,11] , bellows[10] and needle valves.[13] If PV are concerned, as it is shown in figure 2.7, its volume changes between its opening and closure, instead the volume of our EV remains constant between the on- and off-status. The choice of PV valves can give rise to volumes uncertainty of 1% which results in error of >20% in

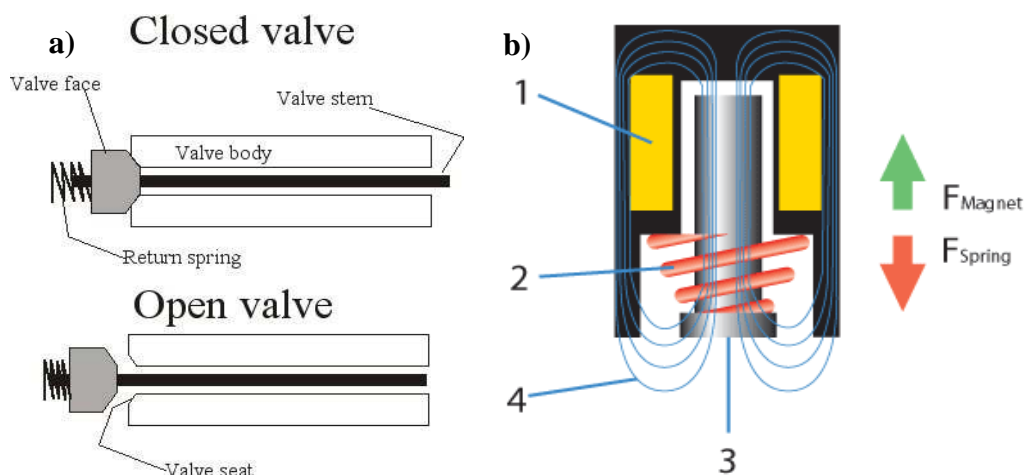the calculation of the wt% gas adsorbed from the sample under investigation (see volumes calibration section).

Figure 2.7: *Schematic view of on and off status in (a) PV and (b) EV.*

Rouquerol et al.[15] advise the use of gases during the calibration with the same virial coefficient B_m as the adsorptive specie in the volume calibration procedure, since the correction due to this coefficient can be significantly different from one gas to the other. Nevertheless, for the preparation of the hydrogen sorption measurements, we do not use helium gas as reported in the literature[4] but the same gas utilized in the sorption measurements. Here the conditions are favourable (very low gas condensation at RT) and cross testing the volume evaluation results by using He_2 or H_2 we found identical values.

To be more accurate in the volume calibration procedure, sample holder with smooth surface should be utilized otherwise it will behave as porous material and it could changes the equilibrium and dynamical sorption properties of the investigated sample. In addition the expanded gas could condensates easily on the sample holder with rough surface during the sorption measurements at low temperature.

The choice of the system void volumes values fulfil two requirements: 1) the gas adsorbed moles are less than the moles expanded into the void volume (Wang and Suda relation[2]), 2) the reservoir and sample holder void volumes do not differ too much.

The first condition requires $n_{exp} \geq n_{ads}$, where the n_{exp} are the gas moles expanded to the sample holder void volume. If $PV = Zn_{exp}RT$ we obtain the relation

$$V \geq wt\% \cdot R \cdot T \cdot m / (MP) \qquad\qquad (2.8)$$

where M is the gas molecular weight.

In silicalite-1 the wt% of hydrogen adsorbed at 0.1 MPa and 77 K is 0.7%, if 0.2 mg are measured, the sample holder void volume has to fulfil the relation V≥ 4.5 cc. In our case the sample holder void volume is 5.8 cc.

The second condition has to be fulfilled because considering formula (2.8), the error made on the evaluation of the wt% depends on the pressures difference between the reservoir volume before the valve opening and the sample holder volume after the valve opening. In particular, if the reservoir and sample holder void volumes are too different, the pressures difference enhances and thus, the error made on the adsorbed moles evaluation increases.

2.1.2.6 Sample properties

In order to perform accurate experiments and calculate exactly the gas adsorbed moles, different sample properties have to be evaluated: sample volume, adsorbed gas density, gas compressibility, gas diffusion time and SSA.

The insertion of the sample in the apparatus causes a reduction of the relative sample holder volume which is utilized into the relation (2.6).[5] According to this reduction, a non trivial question raises in the volumetric evaluation of the sorbed gas concerning the sample volume. In principle, this volume has to be considered as volume inaccessible to the sorbed gas specie. In addition, the same sample has different apparent volumes if gases with different "molecular radius" are considered. Furthermore, when meso- and micro-porous materials are concerned, several other points have to be considered such as regarding the empty internal volumes originated from the material porous structure. In particular for material with high specific surface area (SSA), it is usual to refer the sample volume to the material skeleton density. To overcome these problems, we implemented an "in-situ" gas pycnometry technique by using He_2 gas.[16] As a first step, after the sample insertion and eventual under vacuum heating procedure, we perform a series of gas expansion at low pressure (below 1 atm) and RT. Using low pressures, we avoid the

effects described by Malbrunot et al.,[21] i.e. the He_2 gas partial adsorption from the sample at higher pressures. Error less than 1% in the skeleton sample volume evaluation has been obtained.

An additional topic to be considered when high SSA samples are investigated is the increment of the sample volume during the adsorption of gas molecules (moles in excess, n_{exc}).[15,16] Naturally, this extra-volume is negligible for low SSA samples due to the very small thickness of the adsorbed layer. In general the volume occupied from the physisorbed molecules is

$$V_{ads}= v_o*n_{ads} \tag{2.9}$$

where v_o is the volume occupied from 1 mole of condensed gas (molar volume). As an example, in literature there are many works about the density of physisorbed hydrogen on carbon materials[22] or MOF[23] which show values close to the liquid hydrogen value (v_0 = 28.25 cc/mol; density = 70.8 kg/m^3)[22] or even lower (v_0 = 37.73 cc/mol; density = 53 kg/m^3).[23] In order to choose the best value, we tried to find out the lowest density (highest molar volume) for its liquid phase on the basis of the following consideration: the physisorption temperatures (77 K or even more) is usually largely higher than the H_2 critical temperature (T_c = 33.145 K) while the measured H_2 pressures go beyond the critical pressure (P_c = 1.2964 MPa). For those reasons the film molar volume takes at least the liquid hydrogen value at the melting point (T_m = 14.1 K), i.e. 28.25 cc/mol. Having this as a boundary, the molar volume could increase by changing the H_2/surface interaction: well packed liquid-like hydrogen films are expected to be characterized from low physical interaction energies. In fact, the low interaction energies (few meV/molecule) will be effective in physisorption leaving a high lateral mobility of the adsorbed molecules whose density could be at maximum that of the liquid phase of the molecular specie.[24]

This parameter could be determined also by molecular dynamics calculations. In any case the method is not totally reliable because the modelled internal surface of the porous sample does not represent strictly the real structure.

Considering a typical mesoporous sample with 0.7 g/cc apparent density (i.e. the quantity of powder with which we can fill a volume unit) adsorbing up to 3 wt% of

H_2, we obtain a maximum value of $V_{ads} = (0.085 - 0.11)$ cc of condensed H_2 per each cc of the sample holder V_0 which is ~2% of its value. The fact that these volumes are comparable makes strictly necessary to take V_{ads} into account for the evaluation of the volume for the free diffusion of the gas in the evaluation of the n_{ads} by formula (2.5). So, we end with two strictly related quantities, V_{ads} and n_{ads}, whose evaluation is not independent. We adopted a recursive routine that allowed the calculation of these quantities in self-consistent way. This routine converges rapidly (7-9 loops) making it a reliable tool to avoid the effects of the sample volume expansion due to the adsorbed gas layer. Keeping in mind all this discussion, the PcT isotherms of silicalite-1 present different behaviour taking into account the n_{exc} contribution (see figure 2.8), as expected.
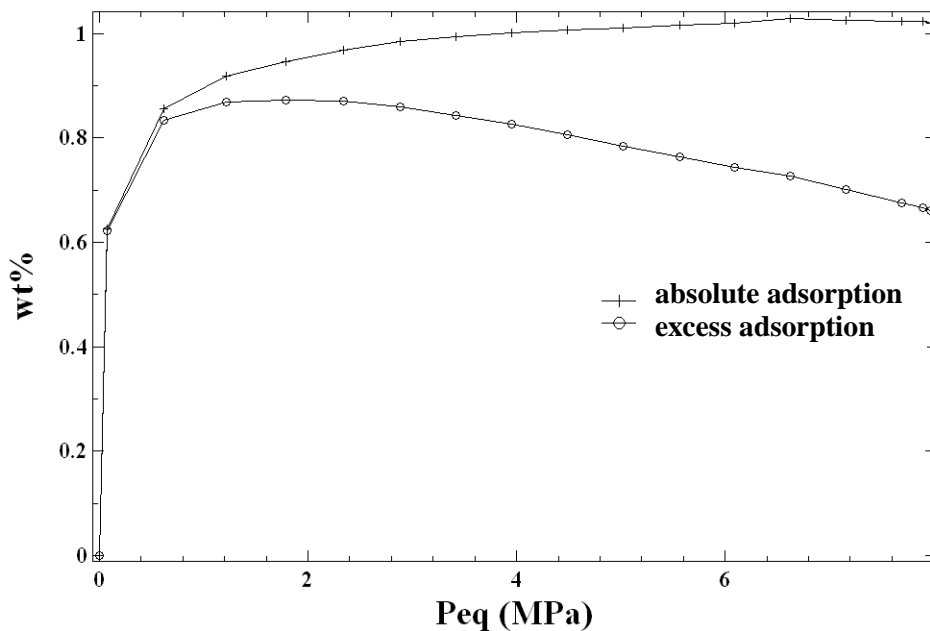
Figure 2.8: *PcT isotherms of silicalie-1 considering the n_{exc} contribution to the sample apparent volume.*

2.2   Thermal Desorption Spectroscopy

Thermal desorption spectroscopy (TDS) is a technique which is widely applied in surface science[25] and in catalysis[26] to characterize the energetics of adsorbates on surfaces. For the desorption of hydrogen it is commonly applied to investigate metal hydrides and complex hydrides.[27,28]   Recently, has been used to study hydrogen

desorption at low temperatures which involves a small isosteric heat of adsorption (~5 kJ/mol)[29] .

The experimental setup used for obtaining desorption spectra of physisorbed hydrogen is demonstrated on fig. 1. The sample cell, (1), made of copper and the thermocouple, (2), are introduced into a copper block, (3), in order to warrant good thermal contact between sample and thermocouple. The copper block is surrounded by a resistive heater, (5), and can be connected to the cold finger of a flowing helium cryostat, (4), which allows cooling down to 20 K. With a heat controller the temperature can be regulated with different heating rates. The desorbed gases are analyzed by a quadrupole mass spectrometer, (7), which detects masses in the range from 1 to 100 amu and possesses a sensitivity of $2 \cdot 10^{-11}$ mbar.
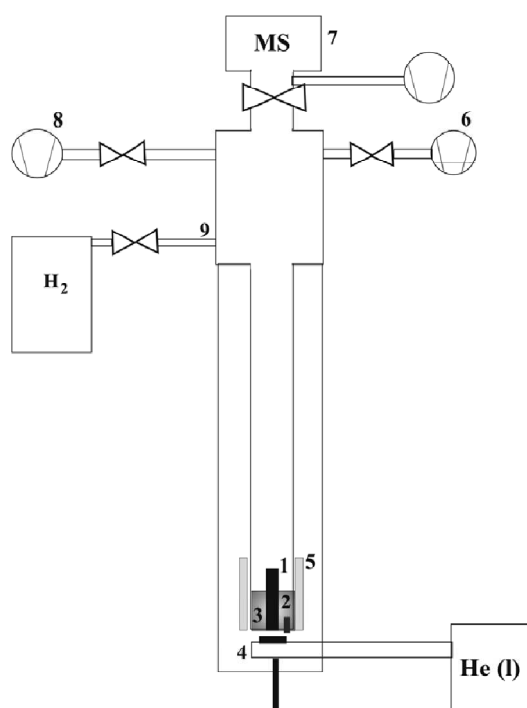
Figure 2.9: *Setup for thermal desorption spectroscopy. The indexed parts are: sample holder (1), thermocouple (2), copper block (3), He cryostat (4), heater (5), pressure gauge (6), mass spectrometer with turbo molecular pump (7), turbo molecular pump (8), hydrogen inlet (9).*

Before the TDS measurements, the samples have been annealed at 378 K in high vacuum (higher than 10^{-5} mbar) for at least 8h to remove moisture and contaminations. Afterwards, at room temperature hydrogen pressure of 25 mbar

was inserted into the chamber and the sample was slowly cooled down to approximately 20 K. In these conditions, in a number of samples, surface coverage with hydrogen is similar to the coverage at 77 K and high pressures.[29] The sample was held at 20 K for approximately 30min. Following this the chamber was evacuated for 20 min (final pressure ~10^{-7}mbar) to remove the non-adsorbed hydrogen molecules and to minimize the background noise of the mass spectrometer. This diminishing is assigned to hydrogen attached to chamber walls and is gradually removed so to have as less contribution in the spectrum as possible. Finally, the temperature program was started with a constant heating rate of 0.01 K s^{-1} and the signal of the desorbed hydrogen was recorded from the mass spectrometer. The procedure was repeated with heating rates of 0.03 K s^{-1} and 0.1 K s^{-1}. Desorption spectra were recorded in the region of (20 – 140) K. In addition the masses 1 and 18 of atomic hydrogen and water, respectively, were measured.

TDS is often used to calculate the activation energy of desorption from the temperature of the desorption maximum. Here, two methods are proposed, which base on the measurement of the peak-maximum position: For coverage independent desorption parameters and first-order kinetics the activation energy for desorption correlates to the temperature of the peak maximum or the centroid temperature in a multipeak spectrum T_m and to the heating rate β, according to the Redhead's peak maximum method:[30]

$$E = RT_m \left[ln \left(\frac{\nu T_m}{\beta} \right) - 3.64 \right] \tag{2.10}$$

Here ν is the pre-exponential factor for desorption, which describes the frequency of vibration of the hydrogen molecule in the adsorbed phase. This equation is usually applied to determine E from a single spectrum, however a value for ν has to be chosen. The usual choice is 10^{13} s^{-1}. The second method is based on the heating rate variation.[30] The method requires a number of spectra corresponding to the same initial coverage, but measured with different heating rates.

$$ln \frac{T_m^2}{\beta} = \frac{E}{RT_m} + ln \frac{E}{\nu R} \tag{2.11}$$

Plotting $\ln(T^2_m/\beta)$ versus $1/T_m$ for different heating rates provides the activation energy of desorption, E, from the slope. This method requires at least a change of one order of magnitude in β to give accurate values of the activation energy of desorption.

2.3 Scanning Electron Microscopy (SEM)[31]

Scanning electron microscope is one of the most versatile instruments for examining the microstructural characteristics of porous solids. High resolution that can go beyond 2,5 nm and three-dimensional view are characteristic principles of this instrument. The variety of the attained signals (x-rays, Auger electrons etc) provides rich information regarding surface's composition and additionally can be studied crystallographic, magnetic and electronic characteristics of the materials. A scanning electron microscope is composed of:

- The luminescence source: Electron gun
- The vacuum system
- The electromagnetic lenses
- The deflection coil
- The object's lens
- The signal detector
- The signal transformation system to images
- The sample holder area
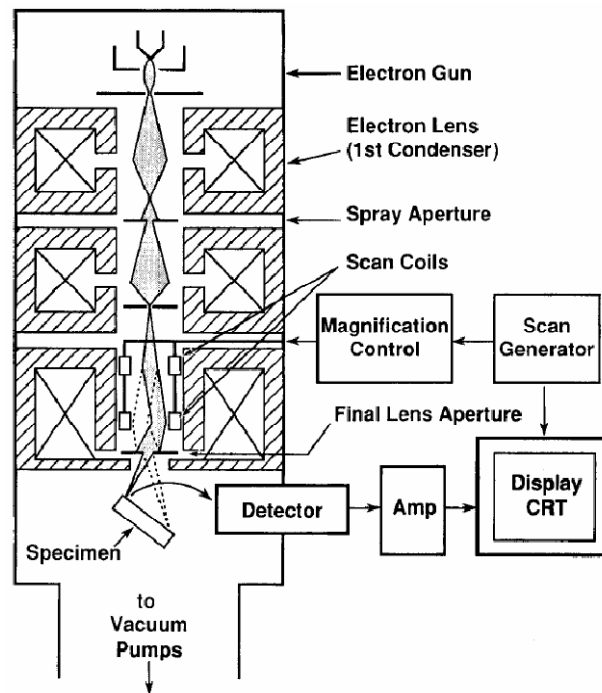
Figure 2.10: *Schematic presentation of a SEM apparatus*

The scanning procedure takes place through interactions between sample's surface and the electronic beam. Between the produced signals there are secondary electrons, electrons diffusing inside the surface, a continuum characteristic of the x-rays, auger electron emissions and photons of various energies. The resolution of a particular SEM signal is determined primarily by the excitation volume and not by the magnitude of the secondary probe. The energy of the beam electrons lies in between (1 – 30) keV. When the beam arrives in the surface there can be either elastic or inelastic diffusion. The first results from the interactions between the beam electrons and the atoms of the material provoked by significant deviations on the occurring directions. The second is produced from the inelastic interaction between the beam's electrons and the material's bonds.

The inelastic diffusion is directly responsible for the production of the signals used for the surface's examination. In fact, the interaction with the Coulomb field of the atoms verifies energy loss and emission of characteristic x-rays.

Below 10 nm the electrons diffusing from the primary beam get strongly absorbed through recombination with the gap that is created during the diffusion process and

in some insulator materials there are produced photons with wave lengths in the visible or the near infrared giving therefore a visible luminescence.

The intensity of backscattered electrons can be correlated to the atomic number of the element within the sampling volume. Hence, some qualitative elemental information can be obtained. The analysis of characteristic X-rays emitted from the sample gives more quantitative elemental information. Such X-ray analysis can be confined to analytical volumes as small as 1 cubic micron.

The Scanning Electron Microscope we used (Quanta FEG 400 (FEI)) operates in the e-SEM mode, which is *environmental*-SEM and allows operation in very low vacuum conditions (≤ 20 Torr) with the possibility to collect secondary electron with an appropriate detector (GSED). The gas ionization process on the sample allows the compensation of the charge product by the electron beam on the surface. In this way it is possible to analyze also non conductive sample without a pre-metallization. Moreover, operating in a relative *high* pressure permits to study sample with a high content of volatile substances, like water, polymer and etc. Cooling the sample close to or below 0 °C is possible to work in a condition of 100% relative humidity.

2.3.1   Morphological and Structural Correlation

Morphological investigation is linked to the long range order probed by XRD.[32] In particular, the crystal habit of the sample is strictly determined by the existence of an ordering of the building blocks in the long range and to the stability of the external surfaces of the crystal. This correlation is depicted on figures 2.11 & 2.12 where the existence of a hexagonal long range order in the BB_C16_25_Si, shown by the XRD patterns, is promptly recognized in the SEM image.

XRD
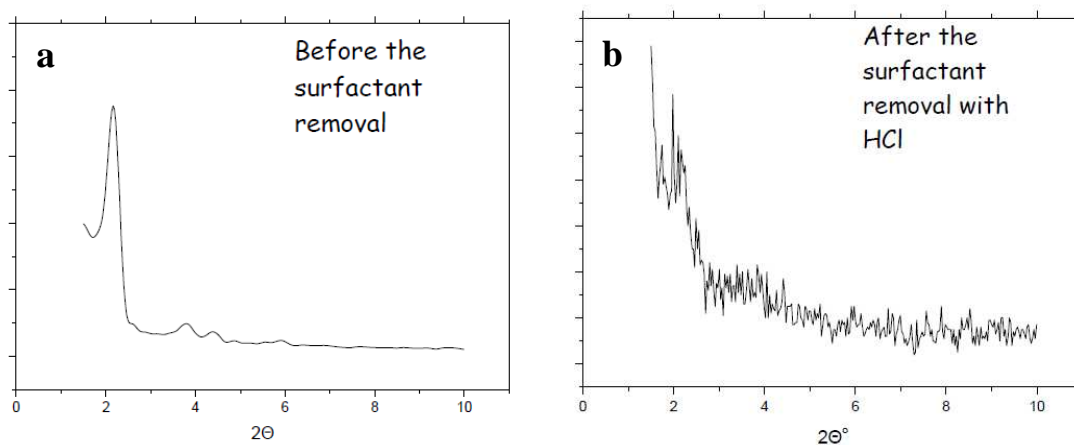
SEM

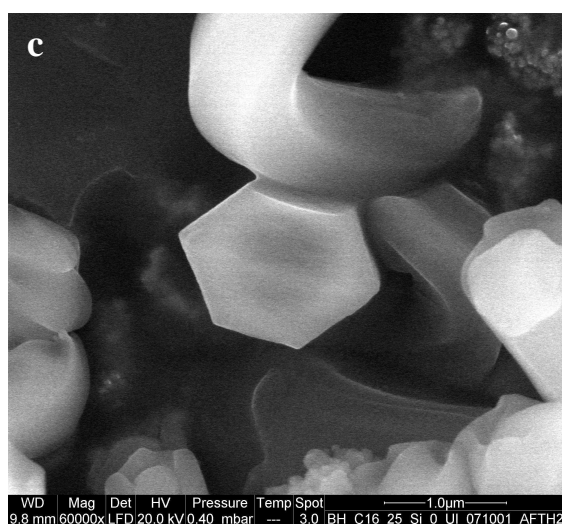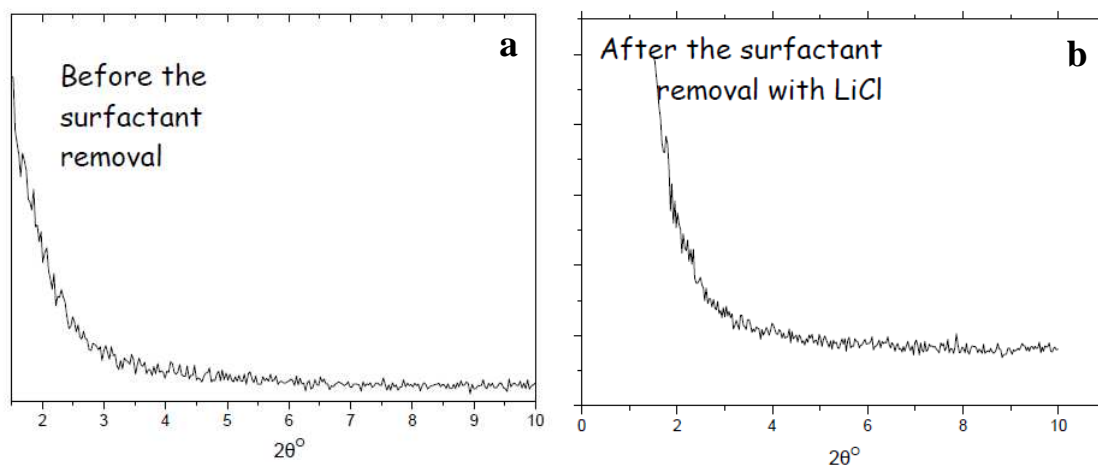**Figure 2.11:** *XRD patterns before (a) and after surfactant removal (b) of a quasi-hexagonal PNO. SEM image demonstrates the morphology of this material (c).*
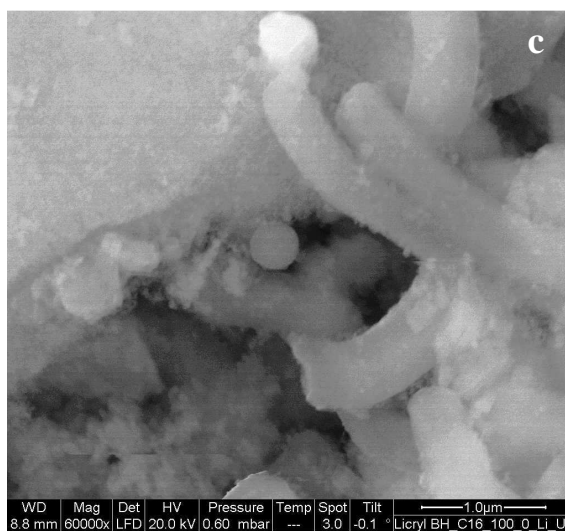
XRD

SEM

Figure 2.12: *XRD patterns before (a) and after surfactant removal (b) of an amorphous PNO. SEM image demonstrates the morphology of this material (c).*

49

Bibliography Chapter 2

(1)   Panella, B.; Hirscher, M.; Roth, S. *Carbon*, **2005**, *43*, 2209-2214.
(2)   Wang, X. L.; Suda, S. *Journal of Alloys and Compounds*, **1995**, *231*, 660-665.
(3)   Maccallini, E., Policicchio, A., Kalantzopoulos, G. *et al. in preparation*, **2009**.
(4)   Broom, D. P. *International Journal of Hydrogen Energy*, **2007**, *32*, 4871-4888.
(5)   Blach, T. P.; Gray, E. M. *Journal of Alloys and Compounds*, **2007**, *446*, 692-697.
(6)   Zielinski, J. M., Coe, C. G., Nickel, R. J. *et al. Adsorption-Journal of the International Adsorption Society*, **2007**, *13*, 1-7.
(7)   http://webbook.nist.gov. The compressibility was calculated taking into account the inverse of H_2 molar density in the NIST data, multiplied for pressure and divided for the ideal gas constant and temperature.
(8)   Perry, R.H.; Green, D.W.; Maloney, J.O. *Perry's chemical engineers' handbook*, 7th edition ed., McGraw-Hill, New York, **1997**.
(9)   Belmabkhout, Y.; Frere, M.; De Weireld, G. *Measurement Science & Technology*, **2004**, *15*, 848-858.
(10) Blackman, J. M.; Patrick, J. W.; Snape, C. E. *Carbon*, **2006**, *44*, 918-927.
(11) Checchetto, R.; Trettel, G.; Miotello, A. *Measurement Science & Technology*, **2004**, *15*, 127-130.
(12) Ramaprabhu, S.; Rajalakshmi, N.; Weiss, A. *International Journal of Hydrogen Energy*, **1998**, *23*, 797-801.
(13) Sun, J., Jarvi, T. D., Conopask, L. F. *et al. Energy & Fuels*, **2001**, *15*, 1241-1246.
(14) Hirschfelder, J.O.; Curtiss, C.F.; Bird, R.B. *Molecular Theory of Gases and Liquids*, ed., Wiley, New York, **1954**.
(15) Rouquerol, F.; Rouquerol, J.; Sing, K. *Adsorption by powders & porous solids*, ed., Academic Press, London, **1999**.
(16) Sircar, S. *Aiche Journal*, **2001**, *47*, 1169-1176.
(17) Broom, D. P.; Moretto, P. *Journal of Alloys and Compounds*, **2007**, *446*, 687-691.
(18) Beeri, O., Cohen, D., Gavra, Z. *et al. Journal of Alloys and Compounds*, **1998**, *267*, 113-120.
(19) Panella, B., Kossykh, L., Dettlaff-Weglikowska, U. *et al. Synthetic Metals*, **2005**, *151*, 208-210.
(20) Lee, Y. W.; Clemens, B. M.; Gross, K. J. *Journal of Alloys and Compounds*, **2008**, *452*, 410-413.
(21) Malbrunot, P., Vidal, D., Vermesse, J. *et al. Langmuir*, **1997**, *13*, 539-544.
(22) Zuttel, A., Wenger, P., Sudan, P. *et al. Materials Science and Engineering B-Solid State Materials for Advanced Technology*, **2004**, *108*, 9-18.
(23) Lee, J. Y., Pan, L., Kelly, S. R. *et al. Advanced Materials*, **2005**, *17*, 2703-+.
(24) Karger, J; Ruthven, D.M. *Diffusion in zeolites and other microporous solids*, ed., John Wiley & Sons, **1992**.
(25) King, D. *Surface Science*, **1975**, *47*, 384-402.
(26) Weiss, W.; Ranke, W. *Progress in Surface Science*, **2002**, *70*, 1-151.
(27) Mueller, U., Schubert, M., Teich, F. *et al. J. Mater. Chem.*, **2006**, *16*, 626-636.
(28) F. Schüth, K.S.W. Sing, J. Weitkamp *Handbook of Porous Solids*, October 2002 ed., Wiley-VCH, Weinheim, 2, **2002**.
(29) Panella, B., Hones, K., Muller, U. *et al. Angewandte Chemie-International Edition*, **2008**, *47*, 2138-2142.

(30)   Dejong, A. M.; Niemantsverdriet, J. W. *Surface Science*, **1990**, *233*, 355-365.
(31)   J.I.Goldstein, H.Yakovitz *Practical Scanning Electron Microscopy*, 1rst ed., Plenum Press, New York, **1975**.
(32)   Klein, Cornelis and Cornelius Hurlbut Jr. *Manual of Mineralogy*, 20th ed., Wiley, **1985**.

3. Periodic Nanoporous Organosilicas

3.0.1   Samples' description

In the following chapter I will present the adsorption properties and the morphological and structural characterization of ordered and disordered PNOs obtained by changing the synthesis parameters in order to tune their chemical and physical properties.

The varied synthesis parameters are:

1) surfactant used (e.g., with or without pyridine group) and its chain length, in order to change the pores size distribution and the specific pore volumes;

2) the sample aromaticity, in order to change the physical interaction between the adsorbent and the adsorbate;

3) different substitutional atoms in the pore walls, in order to enhance the hydrogen storage capacity. Isomorphous substitution of Si^{4+} by Al^{3+} can create anionic charges in the organosilica network;

4) insertion of polar atoms (e.g. Li^+) in order to attract more hydrogen molecules;

5) substitution of the starting material with phenyl triethoxy silane. Phenyl rings can create point charge in the surface.

This strategy will be applied either on the samples synthesized making use of 1,4-Bis(triethoxysilyl)-benzene (BTB) as the starting material[1] or on the samples obtained making use of 4,4-Bis-triethoxy-biphenyl (DBTB) as the starting material.[2] Also samples will be categorized on whether basic or acid conditions were used during the synthesis and their effect on sorption properties will be examined.

The samples will be named according to different labels which correspond to the previous synthesis parameter (see detailed description below). In particular the samples need 5 labels in the form *A_B_C_D_E*. On this sample code name the letters represent:

A) On this label I assign the starting material (BTB≡B and DBTB≡D) and if the sample is synthesized in basic (B) or acid (A) conditions (Figure 3.1).

1,4 bis(triethoxysilyl) benzene

1,1'-Biphenyl, 4,4'-bis(trimethoxysilyl)
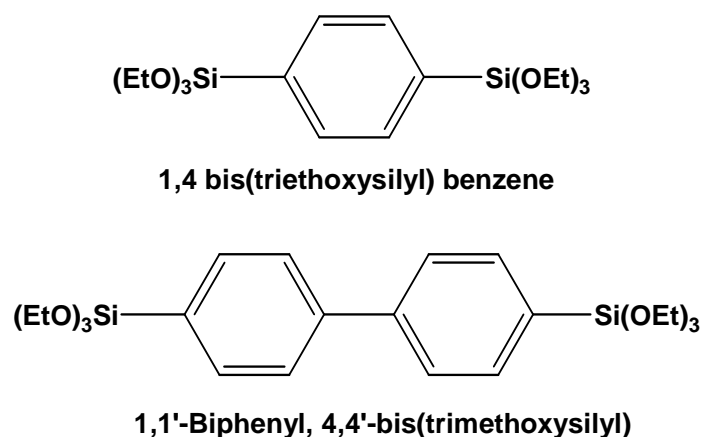
Figure 3.1: *Organosilane groups 1,4 bis(triethoxysilyl)benzene (BTB) & 4,4 bis(triethoxysilyl)-biphenyl (DBTB) used as precursors for PNO synthesis.*

B) This label corresponds to the surfactant utilized. The possible surfactants are either alkyl-trimethylammonium halides of the type $R(CH_3)_3N^+Br^-$ or alkyl-pyridinium halides of the type $RPyBr^-$ (Figure 3.2). In particular the $RPyBr^-$ surfactant has been utilized in the acid conditions while the $R(CH_3)_3N^+Br^-$ in the basic conditions.

Alkyl-pyridinium Halides

Alkyl-trimethylammonium Halides
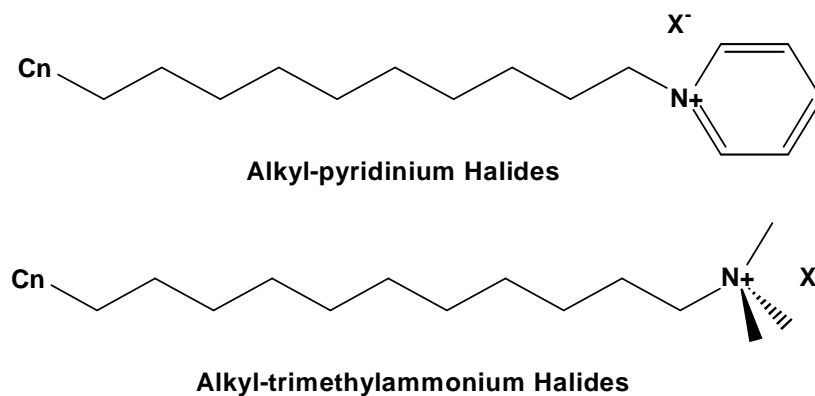
Figure 3.2: *$R(CH_3)_3N^+X^-$ and $RPyX^-$ surfactants used (X=Br, R's length varies between 10-18 carbon atoms).*

On this label the numerical value represents the carbon atoms present in the main chain of the surfactant. This value changes in the range (10 − 18) carbon atoms.

C) This label indicates the percentage of the BTB or DBTB in the starting material. When no supplementary starting material is used the percentage is 100%.

D) This label represents the supplementary material utilized to substitute the starting one. The compound used here is tetraethoxysilane (TEOS) (Figure 3.3). When the supplementary material is not utilized, the label is 0.
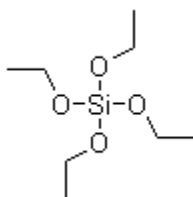
Figure 3.3: *Tetraethoxysilane (TEOS).*

E) The last label indicates eventually, added doping atoms. Here doping took place with Li^+ cations.

For instance BA_C16Py_40_Si means sample was synthesized under acid conditions (A), having BTB as precursor (B), hexadecyl-trimethyl-pyridinium-ammonium-bromide (CTPyABr) was the surfactant used having 16 carbon atoms length (C16Py), the percentage of BTB was 40 (40) so the ratio between was 40 : 60 over the supplementary material (Si) and no doping took place within the synthesized matrix. Instead DB_C10_100_Li means sample was synthesized under basic conditions (B), having DBTB as precursor (D), decyl-trimethyl-ammonium-bromide (DTABr) was the surfactant used possessing 10 carbon atoms length (C10), the percentage of DBTB was 100 so there was no supplementary precursor (100) and lastly, sample was doped with Li^+ cations (Li).

For each sample we obtained the PcT isotherms at liquid nitrogen temperature and the experimental data fitted by Tóth equation (see section 1.2.2, formula 1.12). From the fitting parameters results we can have estimation about the trend of the samples adsorption properties. Furthermore, SSA and porosity were measured with the common Brunauer-Emmet-Teller (BET) technique with N_2 as the probing molecule. Density was measured with pycnometry measurements with He_2 as a probe molecule (see experimental part). Images with Scanning Electron Microscopy (SEM)

– when provided – and x-ray diffraction patterns in the angle range of 1.5˚ − 10˚ degrees were received to extract more information on the morphology and crystallinity of the samples structure.

For each series of sample introduced above, I will present the combined morphological and structural characterization by SEM, BET and XRD techniques. Afterwards the adsorption isotherms, obtained by PcT apparatus, will be analysed by Tóth equation and number of molecules per nm^2 (see section 1.3 for more details). The combination of all the experimental results will be discussed in order to extract the relation between adsorption and structural/morphological properties. Finally, preliminary results on the diffusion coefficient analysis will be shown on a single sample series.

The structural characterization data will be summarized on the tables without to show the BET plots and the XRD patterns and referencing only to the ordering/disordering of the pores arrangement from the observation of the peaks at lower 2 theta (see figures 2.11 and 2.11 in the experimental section).

3.0.2   Synthesis

Crystalline and amorphous organosilane nanoporous materials through sol – gel method[3] using organosilane or non compounds as precursors were synthesized. Surfactants were chosen to possess different chain length. Cation exchange of Li^+ or H^+ was used for the removal of the surfactants.

Samples synthesized under basic conditions were made by the group of Associated Professor Dimitrios Gournis in the Department of Materials Science & Engineering of the University of Ioannina (Greece)[1], whereas samples under acid conditions were prepared by the group of Associated Professor Pantelis Trikalitis in Department of Chemistry of the University of Crete (Greece)[2].

---

[1] Email address: dgourni@cc.uoi.gr
[2] Email address: ptrikal@chemistry.uoc.gr

3.0.2.1 Synthesis procedure under basic conditions

The typical synthesis procedure requires the following mol ratio of the utilized materials: 1.00 Si : 557 H_2O : 4 NaOH (6M solution) : 0.96 surfactant.[1] 57.46 g H_2O, then 4.1 ml NaOH (6M) and lastly 2.18 g of surfactant slowly are inserted into a polypropylene bottle. 30 minutes of stirring follow in temperature of 50 – 60˚C till a transparent solution is produced. Following this, 2.4 ml of precursor (BTB or DBTB) is added drop by drop while vigorous stirring takes place in ambient temperature. Afterwards, solution is stirred into sonication bath for 20 minutes and mechanical stirring for 20 hours is following after all amount of precursor is added. Then, solution is sealed with parafilm and kept at 95˚C under static conditions for 20 hours. Following this, solution cools down in ambient temperature and is placed for centrifugation in order to obtain the final produced powder (cetrifugation parameters: t=10 minutes, speed: 3.5 krpm). After it, powder is washed with distilled water. Cetrifugation and washing with distilled water was repeated 2 more times. Finally, powder is left to dry in ambient temperature.

Removal of surfactants takes place with H^+ cations. 0.5 g of synthesized material are placed into a bottle with 125 ml of ethanol and 4.5 g of HCl 36% into reflux at 70˚C for 8 hours.

3.0.2.2 Organisilica synthesis using BTB and TEOS as precursors under basic conditions[1,4]

The typical synthesis procedure is the same as the one described above. In a second polypropylane bottle, mixtures of BTB over tetraethoxysilane (TEOS) are inserted in ratios of 0%, 25%, 75% and 100% BTB:TEOS and stirred for 30 minutes. Precursors are added into initial solution drop by drop while solution being stirred. Following this procedure continues as above. Removal of surfactants takes place as descibed above.

3.0.2.3 Organosilica synthesis using BTB and Aluminum isopropoxide as precursors under basic conditions[5]

The typical synthetic procedure is the following one. 20.5 g of H_2O, 11.2 g Na_4OH and 0.44 g of the surfactant are inserted in a polypropylene bottle of 150 ml. Mixture is stirred for 40 minutes and then 1.81 g of BTB and 0.22 g of Aluminum isopropoxide (precursors) are added in the solution under vigorous stirring in ambient temperature. Solution is stirred for 24 hours and after it is airproofly sealed with parafilm is kept in 100˚C for 24 hours under static conditions. Following this, bottle is left to cool down in ambient temperature. Cetrifugation of the solution takes place and is repeated 2 times with washing with distilled water in the intervals. (Centrifugation parameters: t=10 minutes, speed: 3.5 krpm). Finally, synthesized powder is spead on a glass to dry in ambient temperature. Surfactant removal is carried out in the same way as described above.

3.0.2.4 Organosilica synthesis with 4,4 Bis-Triethoxysilyl-Biphenyl (DBTB) as precursor[2]

The synthetic procedure is carried out like this: in a polypropylene bottle of 150 ml there are added 59.4 g H_2O (3.3 mol), 5.06 ml NaOH (6M) (30.4 mmol) and lastly 1.16 g (3.2 mmol) of the surfactant. Then, 1.16 ml (3.2mmol) of the precursor is added dorp by drop under vigorous stirring in ambient temperature. Solution is stirred for 20 hours and after it is sealed airproofly is placed in 95˚C for 22 hours under static conditions. Following this, solution is left to cool down in ambient temperature and is centrifugated. Cetrifugation is repeated 2 times with distilled water washing to take place between each cetrifugation. (Cetrifugation parameters: t=10 minutes, speed: 3.5 krpm). Surfactant removal was carried out with H^+ cation exchange as described above.

3.0.2.5 Doping with Li⁺ cations[6,7]

0.5g of sample synthesized under the procedure described in section 3.0.2.1 or 3.0.2.3 was introduced into a bottle and have been through reflux at 70˚C for 8 hours, with 125 ml of LiCl solution in ethanol 1N.

3.0.2.6 Synthesis procedure under acid conditions[8]

In a typical synthetic procedure 53.2 g of H_2O, 0.4 g of the surfactant and 23.1 ml of HCl (36% w/w) are mixed together. 1 g of the precursor is added and the mixture is stirred at 273 K for 1 hour and a second stirring at 318 K for 24 hours is following. The white solution obtained is filtered and washed repeatedly with distilled water in order to receive the white powder. Synthesized powder is placed into HCl solution in ethanol (3 ml HCl 36% w/w in 50 EtOH) to remove the surfactant. Finally, the material is heated in 573 K for 120 minutes in the presence of air.

3.0.2.7 Organosilica synthesis under acid conditions with BTB and TEOS as precursors

The typical synthetic procedure is the same as the one described above. In a separate bottle mixtures of BTB over TEOS are inserted in ratios of 0 : 100, 40 : 60, 67 : 33 and 100 : 0. Mixtures are stirred for 30 minutes in ambient temperature. Then precursors are added into the initial solution, stirred for 60 minutes in ambient temperature and a second stirring in 318 K for 24 hours is coming after. Synthetic procedure as well as surfactant removal continues as described above.

3.0.2.8 Organosilica synthesis with 4,4 Bis-Triethoxysilyl-Biphenyl (DBTB) as precursor under acid conditions

As synthesis procedure is followed the same like the one described in section 3.0.2.6 by making use of DBTB instead of BTB.

3.0.2.9 Doping with Li$^+$

0.5g of sample synthesized under the procedure described in section 3.0.2.6 or 3.0.2.8 was introduced into a bottle and have been through reflux at 70˚C for 8 hours, with 125 ml of LiCl solution in ethanol 1N.

3.0.2.10 Sustitution of BTB with phenyl groups[9]

The typical synthesis procedure, is composed of the procedure described at section 3.0.2.7 with BTB and phenyl triethoxy silane as precursors.

3.1 PNOs synthesized under basic conditions

3.1.1 Surfactant's main chain length variation

3.1.1.1 Structure and morphology

The synthesis of this series samples gives rise to fully disordered assembling of the pores by XRD data. Their structural characteristics are summarized at table 3.1 as received from pycnometry, BET with N_2 at 77 K and XRD diffraction. SSA enhances with the increase of surfactant chain length. In the same time, the disordering introduces a wide pore size distribution by BET measurement (not shown here).

| Sample | Density (cm^3g^{-1}) | BET | | XRD | |
		Specific Surface Area (m^2g^{-1})	Pore diameter (nm)	Crystallinity	Lattice parameter a_0 (nm)
BB_C10_100	1.51 ± 0.03	654	1.92	Fully Disordered	-
BB_C12_100	1.49 ± 0.02	688	1.37	Fully Disordered	-
BB_C16_100	1.50 ± 0.05	864	1.86	Fully Disordered	-
BB_C18_100	1.47 ± 0.04	855	1.37	Fully Disordered	-

Table 3.1: *Concentrative table containing all samples' data presented above.*

If the samples present XRD pattern, this will be related to particular morphology which reflects the microscopic ordering (see section 2.4.1 at experimental chapter). On the other hand, not well defined morphological shape of the sample would be connected to microscopic disordering (no XRD pattern). In the present series, SEM images (figures 3.4a – 3.4d) verify the disordered arranging of the pores arrangement.
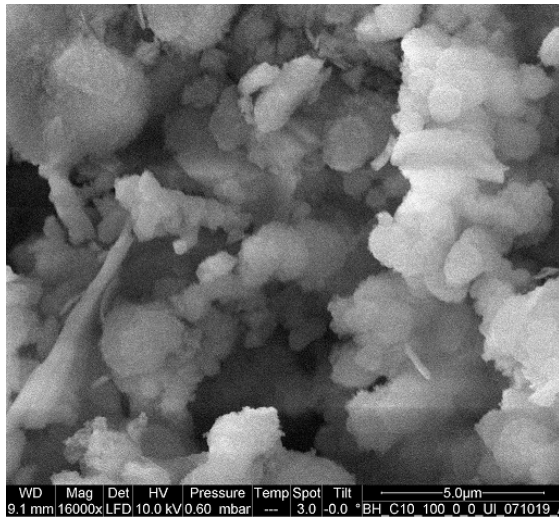
Figure 3.4a: *SEM images for the BB_C10_100 sample.*
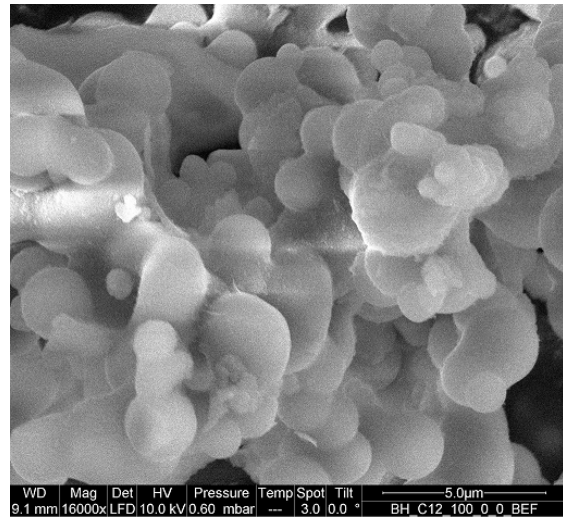
Figure 3.4b: *SEM images for the BB_C12_100 sample.*
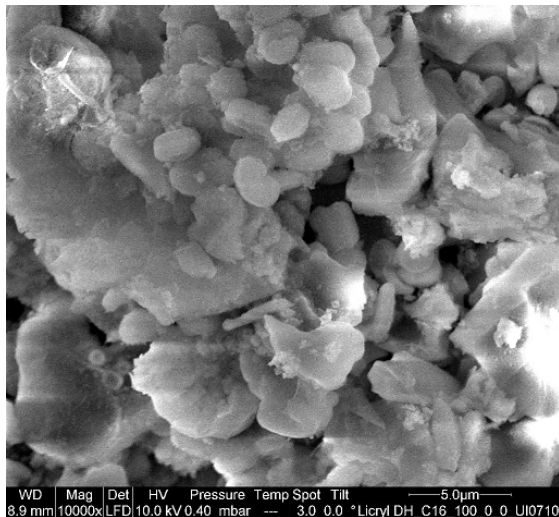
Figure 3.4c: *SEM images for the BB_C16_100 sample.*
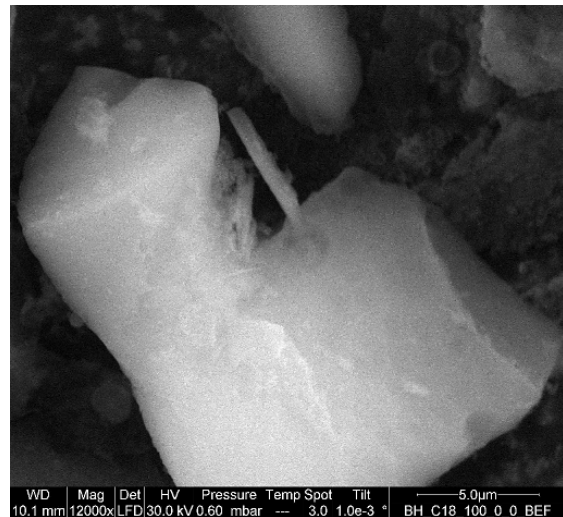
Figure 3.4d: *SEM images for the BB_C18_100 sample.*

3.1.1.2 Volumetric measurements, Tóth model application & sorption properties analysis

In figure 3.5 it is depicted, as an example, the adsorption isotherm obtained at 77 K for the sample BB_C10_100. All 4 samples gave Type I isotherms of the same shape, like figure 3.5. In table 3.2 the values of Tóth equation parameters are summarized (see section 1.2.2).
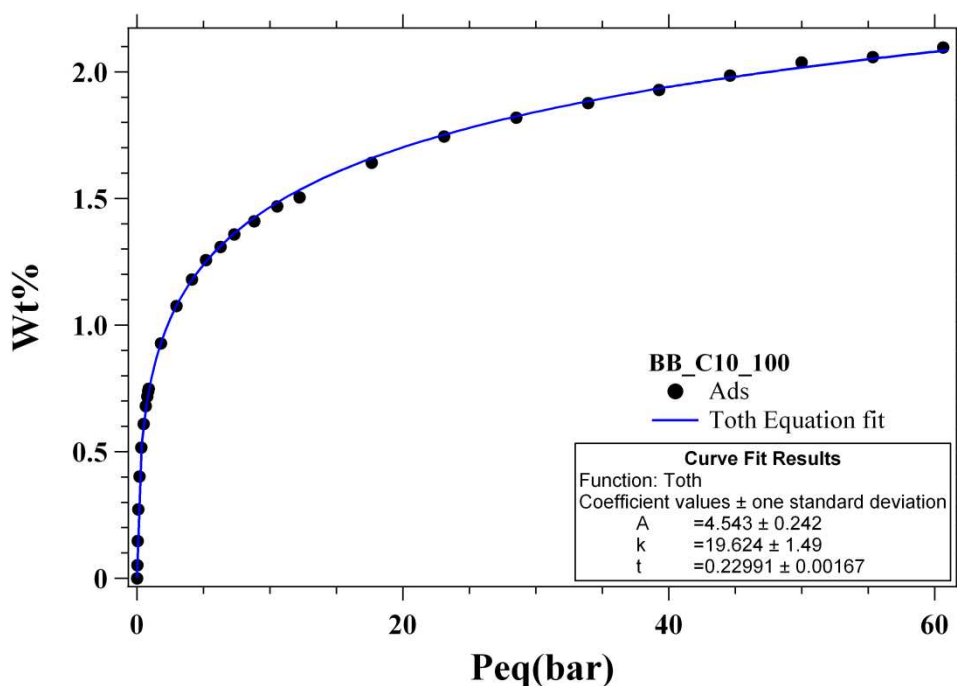
Figure 3.5: *Adsorption isotherm obtained at 77 K for the BB_C10_100 sample, fitted with the Tóth model.*

	BB_C10_100	BB_C12_100	BB_C16_100	BB_C18_100
A	4.5 ± 0.2	4.00 ± 0.01	3.2 ± 0.1	3.0 ± 0.2
K	20 ± 1	0.85 ± 0.01	0.74 ± 0.03	0.6 ± 0.1
t	0.230 ± 0.002	0.297 ± 0.001	0.353 ± 0.002	0.582 ± 0.007

Table 3.2: *Tóth equation fitting parameters for the samples BB_C10_100, BB_C12_100, BB_C16_100 & BB_C18_100.*

The sample BB_C10_100, which was synthesized using the shorter surfactant, exhibits a particularly high K-value. According to the meaning of the Tóth equation, this result is related to an enhancement of binding energy between the H_2 molecules and the adsorbent pore walls. On the other hand, this sample exhibits a large pore distribution from 1,2 to 4 nm radius that combined with its fully disordered structure and the shortest surfactant chain length could activate additional adsorption process

as capillarities providing an environment of high affinity to hydrogen molecules. Additionally, shorter surfactant's main chain means higher pores curvature and therefore due to this, the interaction between the adsorbent and the adsorbate could be further enhanced[10] . Moreover this complex structure seems to get saturated with hydrogen faster than other samples. The K-value, which is connected to the adsorption energy, decreases as the length of surfactant's main chain increases. As expected, smaller pores favor hydrogen's hosting on the surface.[10,11,12] As far as t-value is concerned, the increase of surfactant's main chain creates structures with more homogeneous adsorption sites.

Figure 3.6 shows the number of H_2 molecules per nm^2 that each surface can host at theoretical maximum storage capacity that can exhibit as it derives from the Tóth fitting model (A-value). The use of surfactant with shorter main chain strongly increases the hosting capacity of the material resulting into the creation of a surface with higher affinity to H_2.

Molecules per square nm

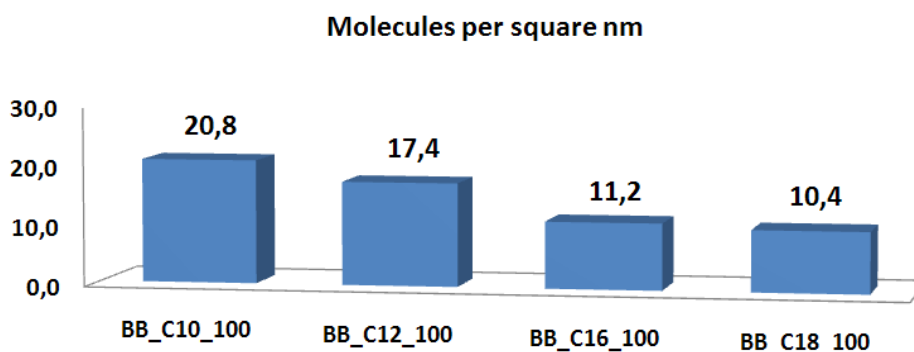**Figure 3.6:** *Number of molecules per surface's nm^2 at theoretical maximum storage capacity for the BB_C1x_100 samples*

Therefore, according to the discussion of section 1.3, the sample BB_C10_100 adsorbs more than one monolayer of H_2 molecules and therefore its porosity (curvature plus pore size distribution) enhances the hydrogen storage capacity compared to the samples of the same series.

3.1.2 Effect of aromaticity in the walls of PNOs

3.1.2.1 Structure and morphology

The addition of BTB in the position of TEOS (see section 3.0.2.2) causes disordering in the structure going from hexagonal to partly disordered – hexagonal structures and finally to a complete disordered array of porous tubes in the solid material (see table 3.3).

Sample	Density (cm^3g^{-1})	BET		XRD	
		Specific Surface Area (m^2g^{-1})	Pore diameter (nm)	Crystallinity	Lattice parameter a_0 (nm)
BB_C16_0_Si	2.8 ± 0.3	953	1.43	Mes. Hexagonal P6mm	4.59
BB_C16_25_Si	1.9 ± 0.1	636	1.88	Mes Disordered Hexagonal	4.23
BB_C16_75_Si	1.72 ± 0.06	1052	1.86	Mes. Disordered	5.05 & 4.15
BB_C16_100	1.50 ± 0.05	864	1.86	Fully Disordered	-

Table 3.3: Concentrative table containing all samples' data presented above.

Substitution of TEOS with BTB creates a less dense structure. SEM images (figure 3.7a – 3.7d) demonstrate the macro-structure of the 4 samples at magnification of 5μm. The increase of concentration of BTB in the walls gradually disorders the structure. At small concentrations of BTB (figure 3.7a & 3.7b) can be seen the hexagonal tubes which reflect the long range structural ordering obtained by XRD. Moreover, the addition of higher amount of BTB increases the average pore size of the samples.
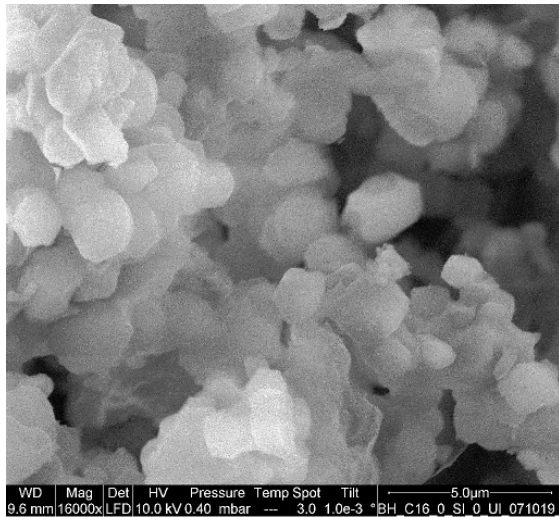
Figure 3.7a: *SEM images for the BB_C16_0_Si sample.*
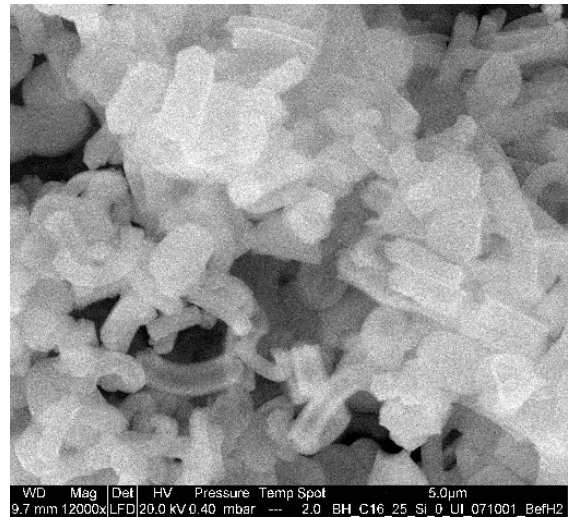
Figure 3.7b: *SEM images for the BB_C16_25_Si sample.*
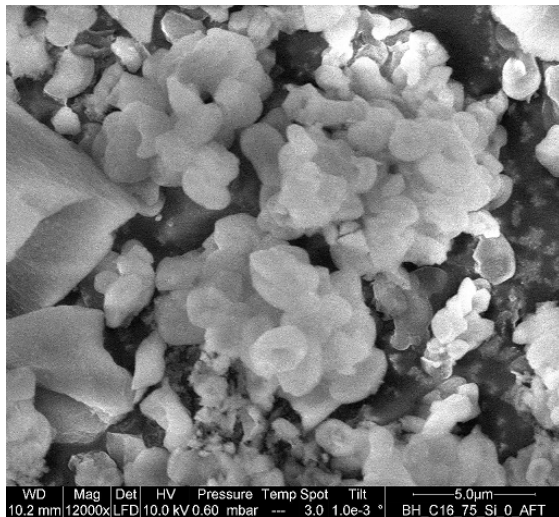
Figure 3.7c: *SEM images for the BB_C16_75_Si sample.*
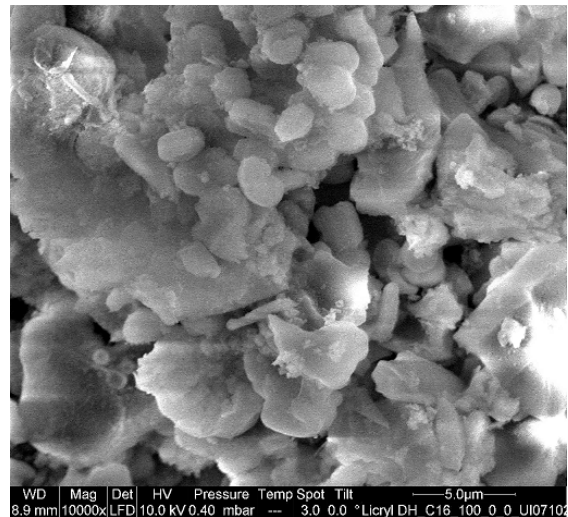
Figure 3.7d: *SEM images for the BB_C16_100 sample.*

3.1.2.2 Volumetric measurements, Tóth model application & sorption properties analysis

In figure 3.8 it is depicted the adsorption isotherm obtained at 77 K for the sample BB_C16_25_Si. All the series samples gave Type I isotherms of the same shape like figure 3.8. In table 3.4 the values of Tóth equation parameters are summarized.
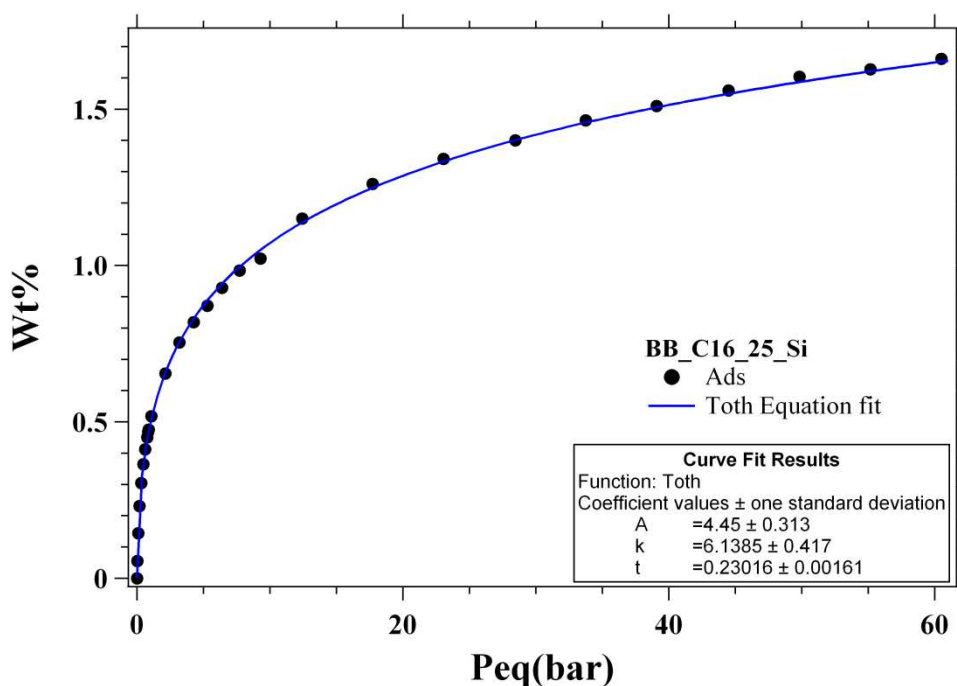
Figure 3.8: *Adsorption isotherm obtained at 77 K for the BB_C16_25_Si sample, fitted with the Tóth model.*

	BB_C16_0_Si	**BB_C16_25_Si**	**BB_C16_75_Si**	**BB_C16_100**
A	3.2 ± 0.1	4.4 ± 0.3	4.80 ± 0.03	3.2 ± 0.1
K	1.11 ± 0.05	6.1 ± 0.4	3.7 ± 0.4	0.74 ± 0.03
t	0.359 ± 0.003	0.231 ± 0.002	0.261 ± 0.003	0.353 ± 0.002

Table 3.4: *Tóth equation fitting parameters for the samples BB_C16_0_Si, BB_C16_25_Si, BB_C16_50_Si, BB_C16_75_Si & BB_C16_100.*

Hydrogen's maximum storage capacity is favored when there is a combination of 25% of BTB and 75% of TEOS as starting materials. This is related to an enhancement of the SSA (see table 3.3). From the other side, the calculation of the number of H_2 molecules per nm^2 demonstrates that the surface which host more hydrogen molecules is the BB_C16_25_Si sample (see figure 3.9). Still, this sample exhibits a double layer hydrogen storage capacity while the other samples can host more than

a monolayer. Regarding the energy of adsorption, comparing that series sample with the previous one, the K-value is higher in these hybrid materials. On the other hand, t-value is particularly low in the hybrid samples where the use of 2 precursors could favor the presence of adsorption sites with different hydrogen binding energy giving rise in this case to heterogeneous adsorption properties.

Molecules per square nm
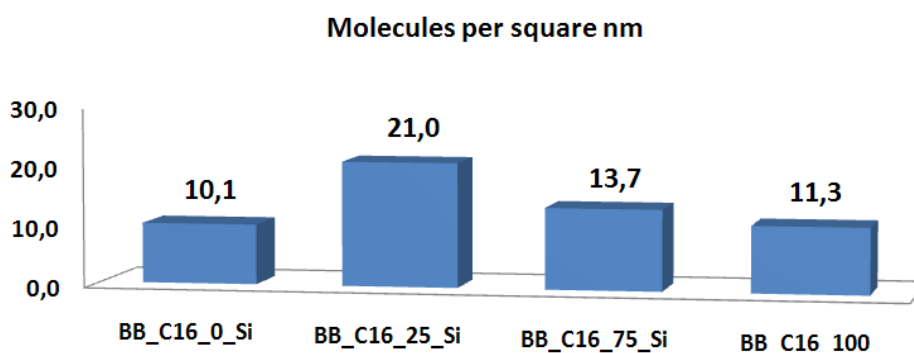
Figure 3.9: *Number of molecules per surface's nm² at theoretical maximum storage capacity for the BB_C1x_100 samples*

Hybrid synthesized materials exhibit highest number of molecules that their surface can host at maximum storage capacity as it is yield from the A-value. Small percentage of BTB in the silica network enhances interaction. Use of a single precursor exceeds the monolayer creation but is not as efficient as in the case where both of the precursors are utilized.

3.1.3 Substitution of BTB with Al^{3+} cations and insertion of Li^+

3.1.3.1 Structure and morphology

Table 3.5 summarizes the samples' structural characteristics as received from He_2 pycnometry at room temperature, nitrogen's BET at 77 K and x-ray diffraction. Introducing Al^{3+} cations in the structure does not induce any change in the

crystallinity. Pore diameter remains the same even after the introduction of Li$^+$ cations in the pores. Nevertheless, the BB_C16_90_Al_Li gave a decreased density and a much smaller SSA. Combining these two results together could be said that the introduction of Li$^+$ blocked the pores resulting in bigger not accessible sample volume and therefore smaller sample skeletal volume producing higher skeletal density. As a result neither nitrogen nor helium could enter in the blocked pores giving rise maybe to underestimated density and SSA values.

Sample	Density (cm^3g^{-1})	BET		XRD	
		Specific Surface Area (m^2g^{-1})	Pore diameter (nm)	Crystallinity	Lattice parameter a_0 (nm)
BB_C16_100	1.50 ± 0.05	864	1.86	Fully Disordered	-
BB_C16_90_Al	1.77 ± 0.08	750	1.88	Fully Disordered	-
BB_C16_90_Al_Li	1.31 ± 0.03	238	1.88	Fully Disordered	-

Table 3.5: *Concentrative table containing all samples' data presented above.*

3.1.3.2 Volumetric measurements, Tóth model application & sorption properties analysis

In figure 3.10 there are seen the adsorption isotherms acquired at 77 K for the samples BB_C16_90_Al, BB_C16_90_Al_Li & BB_C16_100 as the reference material. All samples' experimental data were fitted with Tóth equation. In table 3.6 the values of Tóth equation parameters are summarized.
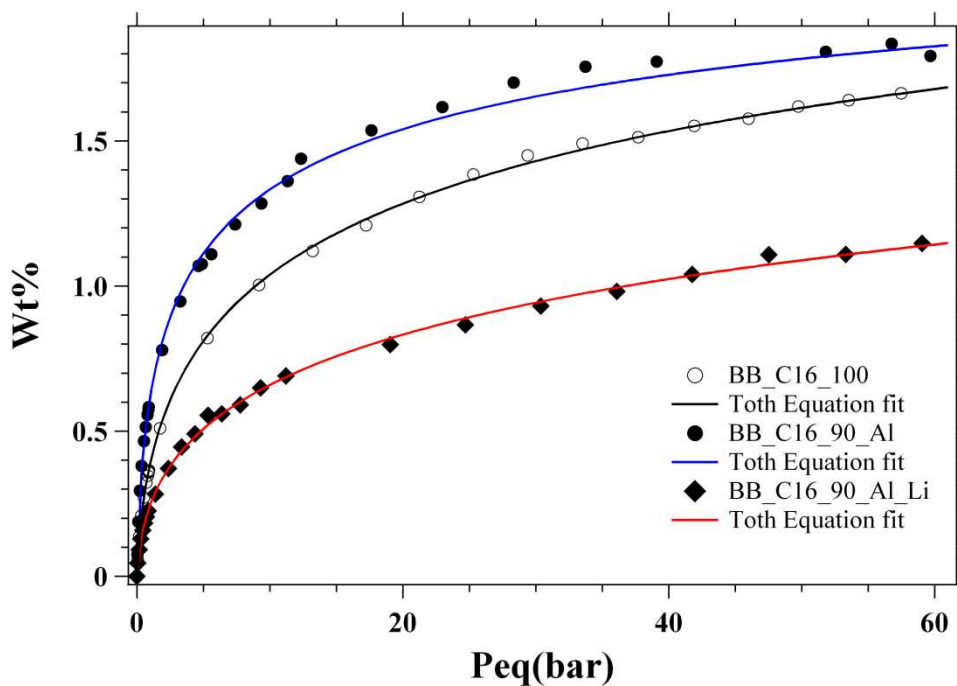
Figure 3.10: *Adsorption isotherms obtained at 77 K for the BB_C16_90_Al, BB_C16_90_Al_Li & BB_C16_100 samples, fitted with the Tóth model.*

	BB_C16_100	**BB_C16_90_Al**	**BB_C16_90_Al_Li**
A	3.2 ± 0.1	2.5 ± 0.1	3.74 ± 0.08
K	0.74 ± 0.03	1.8 ± 0.2	1.0 ± 0.1
t	0.353 ± 0.002	0.413 ± 0.008	0.254 ± 0.003

Table 3.6: *Tóth equation fitting parameters for the samples BB_C16_100, BB_C16_90_Al & BB_C16_90_Al_Li.*

Partial substitution of BTB with Al^{3+} cations increases the hydrogen storage capacity in relatively small pressures. On the other hand, the SSA values of BB_C16_100 is higher than in BB_C16_90_Al, therefore the hydrogen storage capacity enhancement has to be attributed to the increasing of the adsorption energy between the pore walls and the adsorbate. In fact the K-value of the sample where partial substitution with Al^{3+} cations has been obtained (table 3.6) is higher. From the other point of view, initial BB_C16_100 material yields a higher theoretical maximum storage

capacity for its higher SSA value. Doping of the sample with Li$^+$ creates a sample that does not possess promising storage properties in applicative pressures but exhibits an interesting theoretical maximum capacity showing a continuous ascent in the adsorption curve. By taking into consideration the number of H$_2$ molecules the surface can host as it derives from the theoretical maximum storage capacity, is depicted in figure 3.11.
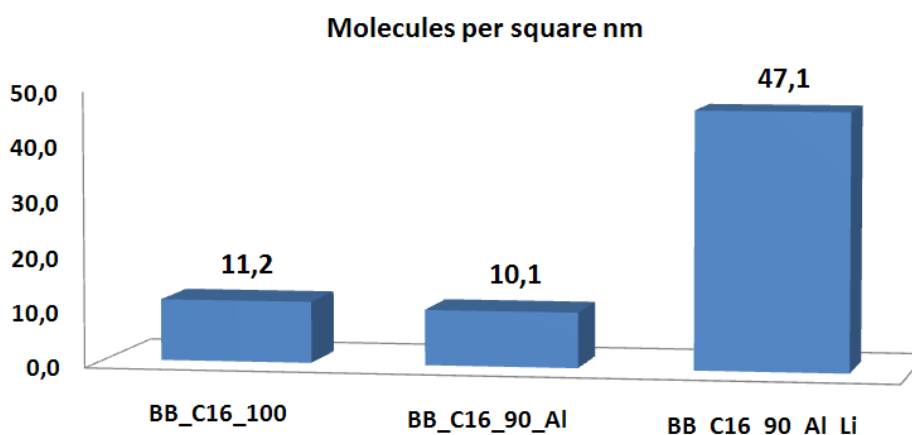
Figure 3.11: *Number of molecules per surface's nm^2 at theoretical maximum storage capacity for the BB_C16_90_Al_x samples.*

According to the considerations of the Tóth fitting model, it was calculated that the BB_C16_90_Al_Li can host up to the unusual number of 47 molecules of H$_2$ per nm^2, that is 5 times the monolayer capacity. However, the diversity of this value can be attributed to the inaccuracy of BET method when nitrogen is used which underestimates the SSA.

3.1.4   Doping PNOs with Li$^+$ cations

3.1.4.1 Structure and morphology

Table 3.7 resumes the samples' structural characteristics as obtained from He$_2$ pycnometry at room temperature, nitrogen's BET at 77 K and x-ray diffraction.

Sample	Density $(cm^3 g^{-1})$	BET		XRD	
		Specific Surface Area $(m^2 g^{-1})$	Pore diameter (nm)	Crystallinity	Lattice parameter a_0 (nm)
BB_C16_100	1.50 ± 0.05	864	1.86	Fully Disordered	-
BB_C16_100_Li	1.9 ± 0.2	484	1.84	Fully Disordered	-

Table 3.7: *Concentrative table containing all samples' data presented above.*

Doping the initial material with Li^+ cations leaves the pore size unaltered whereas density increases indicating that introduction of Li^+ into pores was successful because the accessible pore volumes of the samples should be unaltered while the weight increases because of the Li^+ presence. However the Li^+ insertion results in a severely reduced SSA value maybe due to the covering of the internal pores walls by Li atoms.
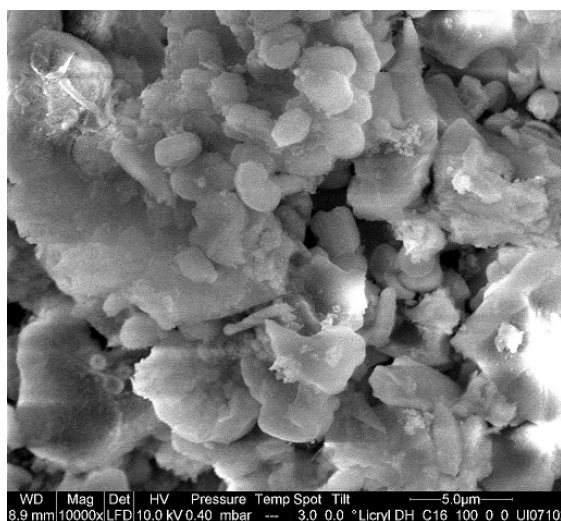

Figure 3.12a: *SEM images for the BB_C16_100 sample.*
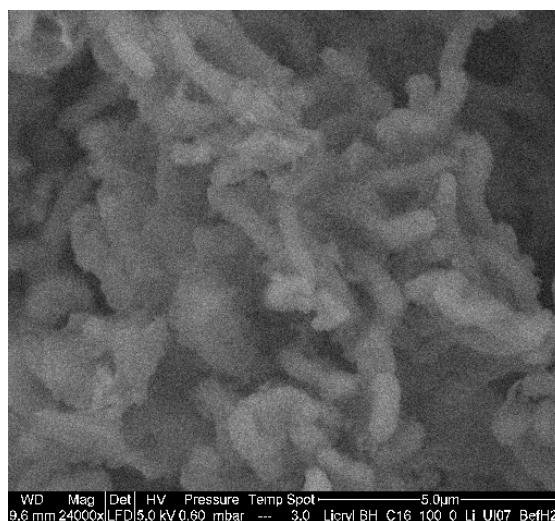
Figure 3.12b: *SEM images for the BB_C16_100_Li sample.*

SEM images obtained for initial and doped material demonstrate lacking of long range structure that XRD showed. Tubes are visible but no order exists between them (figures 3.12a & 3.12b).

3.1.4.2 Volumetric measurements, Tóth model application & sorption properties analysis

In figure 3.13 there are seen in comparison the adsorption isotherms received at 77 K for the samples BB_C16_100 & BB_C16_100_Li. Both isotherms' experimental data were fitted with Tóth fitting equation. In table 3.8 the values of Tóth equation parameters are resumed.

Figure 3.13: *Adsorption isotherms acquired at 77 K for the BB_C16_100 & BB_C16_100_Li samples, fitted with the Tóth model.*

	BB_C16_100	BB_C16_100_Li
A	3.2 ± 0.1	1.43 ± 0.02
K	0.74 ± 0.03	0.61 ± 0.07
t	0.353 ± 0.002	0.637 ± 0.022

Table 3.8: *Tóth equation fitting parameters for the samples BB_C16_100 & BB_C16_100_Li.*

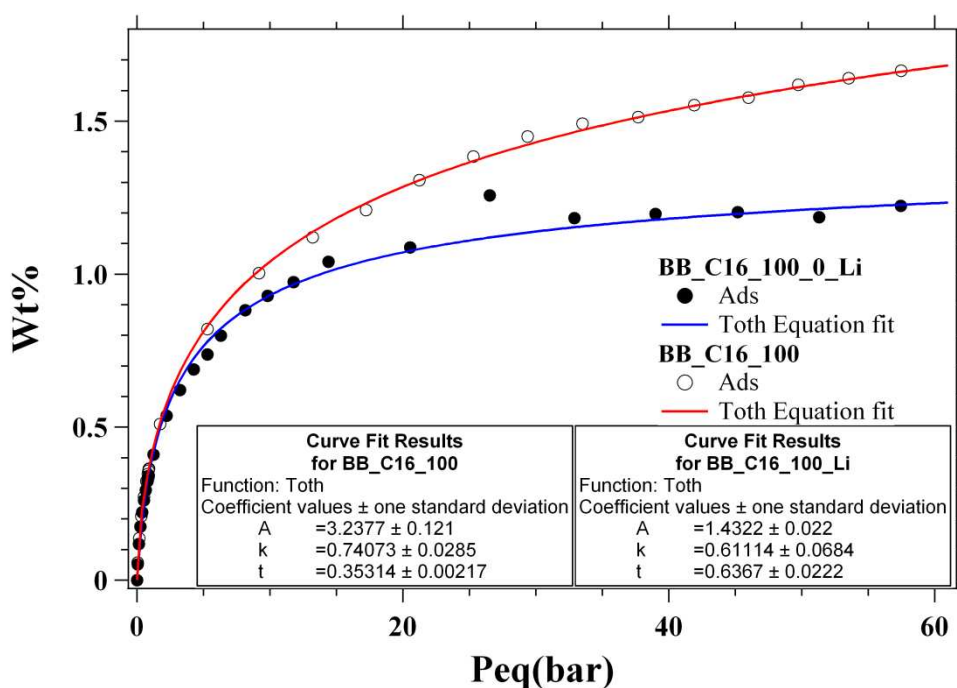Summarizing the data of table 3.8, smaller SSA value is related to minor amount of hosted hydrogen on the sample surface. However we could expect an enhancement of the hydrogen storage capacity on the Li^+ doped sample due to the interaction induced from the Li atoms. However the decrease of the hydrogen storage capacity indicates that Li atom should be oxidized losing its point charge and therefore its peculiarity to attract hydrogen molecules. According to this last discussion, we can explain the decrease of the K-value by Li^+ doping too.

Molecules per square nm
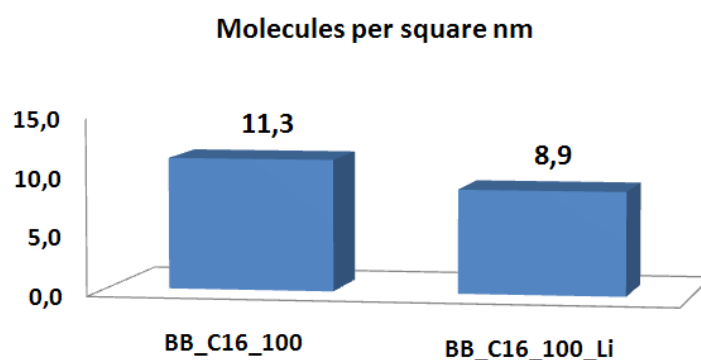
Figure 3.14: *Number of molecules per surface's nm^2 at theoretical maximum storage capacity for the BB_C16_100_x samples*

As expected from the previous analysis, despite of its small SSA, the doped sample does not show higher number of molecules per nm^2 compared to the starting sample (see figure 3.14).

3.1.5   Conclusions

The samples created under condensation in basic conditions exhibit sorption capacity that is reversely proportional to the length of the surfactant used. Shorter surfactant enhances energy of formation and diminishes long range order. If TEOS is exchanged with BTB we can find the right composition between starting material and BTB in order to enhance the hydrogen storage capacity. Hybrid materials having 2 precursors demonstrate enhanced sorption properties. Incorporation of Al^{3+} into the organosilane framework succeeds to increase the interaction of H_2 molecules

with the surface in relatively small pressures. The samples doped with Li^+ do not present any hydrogen storage capacity improvement for two reasons: 1) the Li^+ is not successful inserted into the samples pores and 2) the Li atoms are oxidized.

3.2 PNOs synthesized under basic conditions with the organo-bis-silicalite (4,4 Bis-Triethoxysilyl-Biphenyl (DBTB)) as precursor

3.2.1 Surfactant's main chain length variation PNOs with DBTB as precursor

3.2.1.1 Synthesis, structure and morphology

The increase of surfactant's length results in an increase of the principle pore size as pore distribution demonstrates. Table 3.9 collects the data as received from pycnometry (see corresponding PcT section), BET with N_2 at 77 K and XRD diffraction. Within the experimental error, samples skeletal densities are similar. Longer surfactant seems to induce order in the synthesized material as XRD patterns indicate. Principle pore size increases with the increase of surfactant's length whereas SSA exhibits small variations.

Sample	Density (cm^3g^{-1})	BET		XRD	
		Specific Surface Area (m^2g^{-1})	Pore diameter (nm)	Crystallinity	Lattice parameter a_0 (nm)
DB_C10_100	1.41 ± 0.02	795	1.86	Fully Disordered	-
DB_C16_100	1.25 ± 0.06	827	1.95	Disordered	-
DB_C18_100	1.35 ± 0.07	723	2.10	Mes. Hexagonal	-

Table 3.9: *Concentrative table containing all samples' data presented above.*

3.2.1.2 Volumetric measurements, Tóth model application & sorption properties analysis

In figure 3.15 it is depicted the adsorption isotherm acquired at 77 K for the sample BB_C10_100. All other samples gave Type I isotherms of the same shape like figure 3.15. In table 3.10 the values of Tóth equation parameters are summarized.
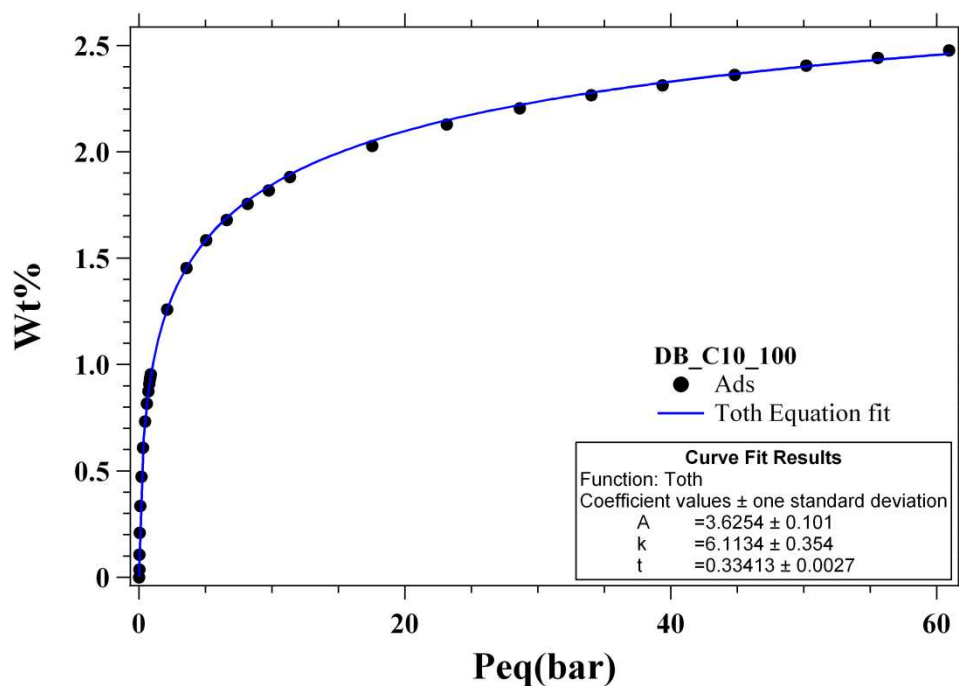
Figure 3.15: *Adsorption isotherm obtained at 77 K for the DB_C10_100 sample, fitted with the Tóth model.*

	DB_C10_100	DB_C16_100	DB_C18_100
A	3.6 ± 0.1	3.20 ± 0.02	2.8 ± 0.1
K	6.1 ± 0.4	0.46 ± 0.06	0.33 ± 0.05
t	0.334 ± 0.003	0.388 ± 0.009	0.44 ± 0.02

Table 3.10: *Tóth equation fitting parameters for the samples DB_C10_100, DB_C12_100, DB_C16_100 & DB_C18_100.*

Increasing the surfactant's length gradually decreases the theoretical maximum storage capacity, as observed in the same BB samples series. Narrower pores are favored since energy potential increases with the decrease of pore size [10,13]. Same picture is reflected on the K-value: the narrower pore size is related to higher surface's attraction to hydrogen.
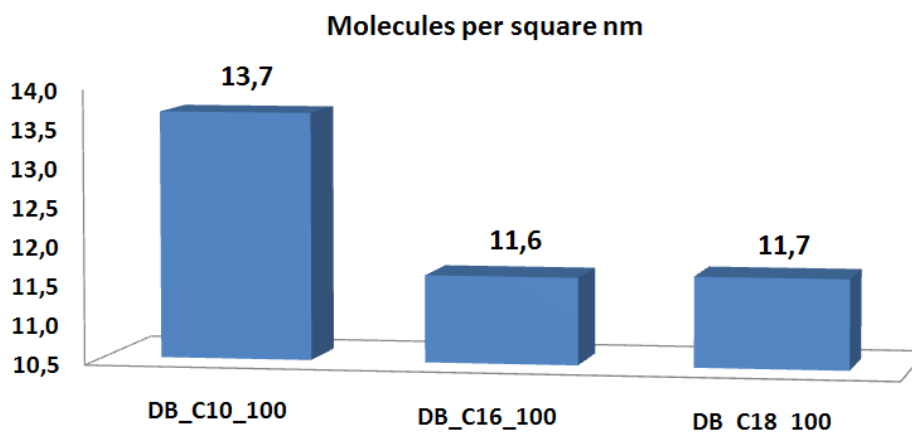
Figure 3.16: *Number of molecules per surface's nm^2 at theoretical maximum storage capacity for the DB_C1x_100_x samples*

Shorter surfactant gives a surface that can host the highest number of H$_2$ molecules per surface unit (figure 3.16). Longer surfactant's effect is considered efficient since more than one monolayer's creation is reached.

3.2.2 Doping PNOs synthesized with DBTB as precursor, with Li$^+$ cations

3.2.2.1 Structure and morphology

Table 3.11 contains the samples' structural characteristics as received from He$_2$ pycnometry at room temperature, nitrogen's BET at 77 K and x-ray diffraction.

Sample	Density (cm^3g^{-1})	BET		XRD	
		Specific Surface Area (m^2g^{-1})	Pore diameter (nm)	Crystallinity	Lattice parameter a_0 (nm)
DB_C10_100	1.41 ± 0.02	795	1.86	Fully Disordered	-
DB_C10_100_Li	1.54 ± 0.03	223	1.81	Fully Disordered	-

Table 3.11: *Concentrative table containing all samples' data presented above.*

The addition of Li^+ cations into the pristine material reduces severely the SSA probably. Morever, the decrease of the hydrogen storage capacity indicates that Li atom should be oxidized losing its point charge and therefore its peculiarity to attract hydrogen molecules (see section 3.1.4.2). Again, the Li^+ insertion results in a severely reduced SSA value maybe due to the covering of the internal pores walls by Li atoms.

3.2.2.2 Volumetric measurements, Tóth model application & sorption properties analysis

In figure 3.17 there are demonstrated in comparison the adsorption isotherms received at 77 K for the samples DB_C10_100 & DB_C10_100_Li. Both isotherms' experimental data were fitted with Tóth fitting equation. In table 3.12 the values of Tóth equation parameters are resumed.
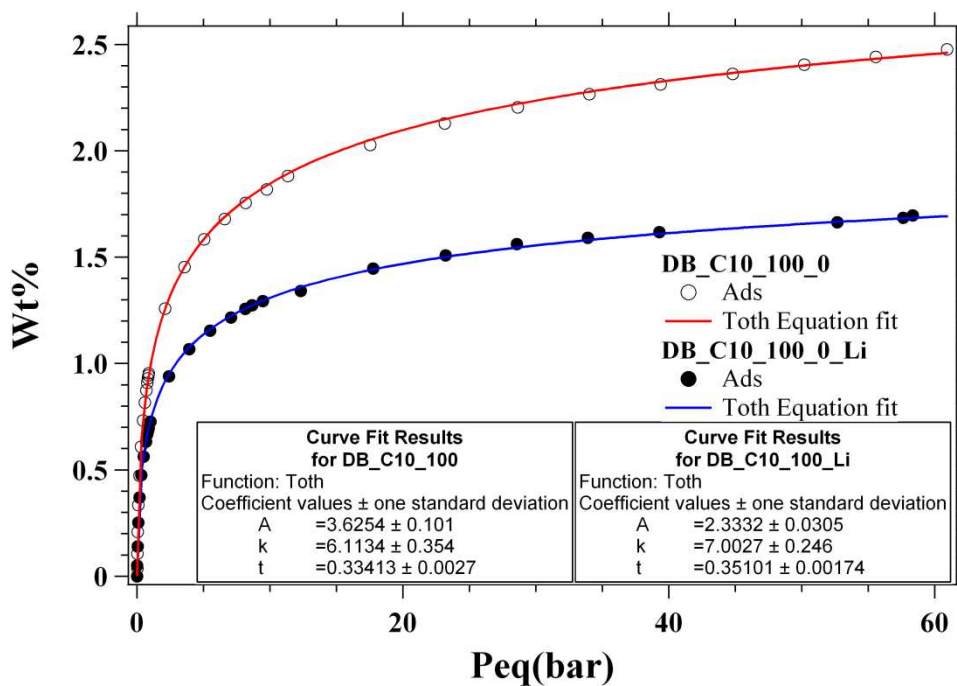
Figure 3.17: *Adsorption isotherms acquired at 77 K for the BB_C16_100 & BB_C16_100_Li samples, fitted with the Tóth model.*

	DB_C10_100	DB_C10_100_Li
A	3.6 ± 0.1	2.33 ± 0.03
K	6.1 ± 0.4	7.0 ± 0.3
t	0.334 ± 0.003	0.64 ± 0.02

Table 3.12: *Toth equation fitting parameters for the samples DB_C10_100 & DB_C10_100_Li.*

Comparing the adsorption properties of the two samples, K-value remained in the same magnitude. The narrower pore distribution we are having in DB_C10_100_Li, is depicted on the t-value whereas the theoretical maximum storage capacity has decreased after the Li^+ cations insertion.

Figure 3.18: *Number of molecules per surface's nm^2 at theoretical maximum storage capacity for the DB_C10_100_x samples*
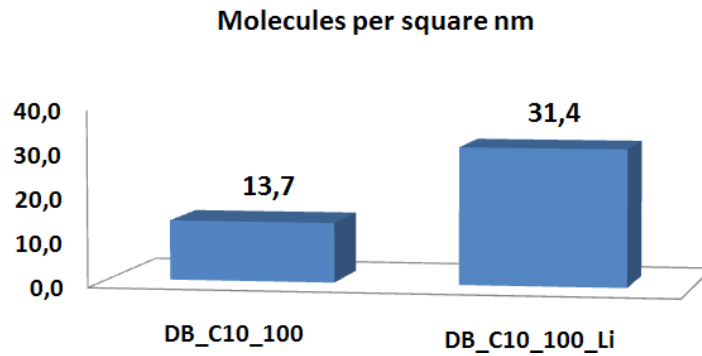
In figure 3.18 is depicted the amount of molecules per nm^2 that each surface can host at theoretical maximum coverage. By making the considerations that Tóth model is making and BET's accuracy, it was calculated that doping PNOs that have DBTB as the starting material with Li$^+$ cations results in a surface that can host more than 2,5 times the H$_2$ molecules the initial surface can host.

As a conclusion, introduction of Li$^+$ into pores was successful because the accessible pore volumes of the samples should be unaltered while the weight increases because of the Li$^+$ presence but the reduced SSA that Li$^+$ cations insertion creates, is responsible for the lower hydrogen storage capacity depicted both in the adsorption isotherms and Tóth model's extracted values.

3.2.3 Conclusions

In PNOs synthesized in basic conditions with DBTB as precursor, surfactant's chain length can affect the pore size created. Smaller pores increase the interaction between hydrogen and surface whereas maximum storage capacity is enhanced as well. Li$^+$ insertion alters the sample's porosity and reduces the measured SSA therefore a clear estimation of doping's effect in sorption properties could not be obtained.

3.3 PNOs synthesized under acid conditions

3.3.1 Surfactant's main chain length variation

3.3.1.1 Structure and morphology

Table 3.13 summarizes the samples' structural characteristics as received from He_2 pycnometry at room temperature, nitrogen's BET at 77 K and x-ray diffraction.

Sample	Density (cm^3g^{-1})	BET		XRD	
		Specific Surface Area (m^2g^{-1})	Pore diameter (nm)	Crystallinity	Lattice parameter a_0 (nm)
BA_C12Py_100	1.57 ± 0.02	963	< 1.6	Cubic Pm3n	-
BA_C14Py_100	1.8 ± 0.1	983	1.6	Disordered Cubic	-
BA_C16Py_100	1.5 ± 0.04	1024	< 1.6	Disordered Cubic	-
BA_C18Py_100	2.2 ± 0.2	1073	2.5	Hexagonal P6m	4.8

Table 3.13: *Concentrative table containing all samples' data presented above.*

Increasing the length of surfactant in basic conditions induces slightly increase in the SSA of the synthesized material. Crystallinity exists only in case of C_{12} and C_{18} surfactants length whereas C_{12} and C_{16} gave the smaller pore size. Density is related to the pore size trend: samples with smaller pore size have minor density.

3.3.1.2 Volumetric measurements, Tóth model application & sorption properties analysis

In figure 3.19 is demonstrated as an example the adsorption isotherm obtained at 77 K for the sample BA_C16Py_100. All 4 samples gave Type I isotherms of the same

shape like figure 3.19. In table 3.14 the values of Tóth equation parameters are summarized.
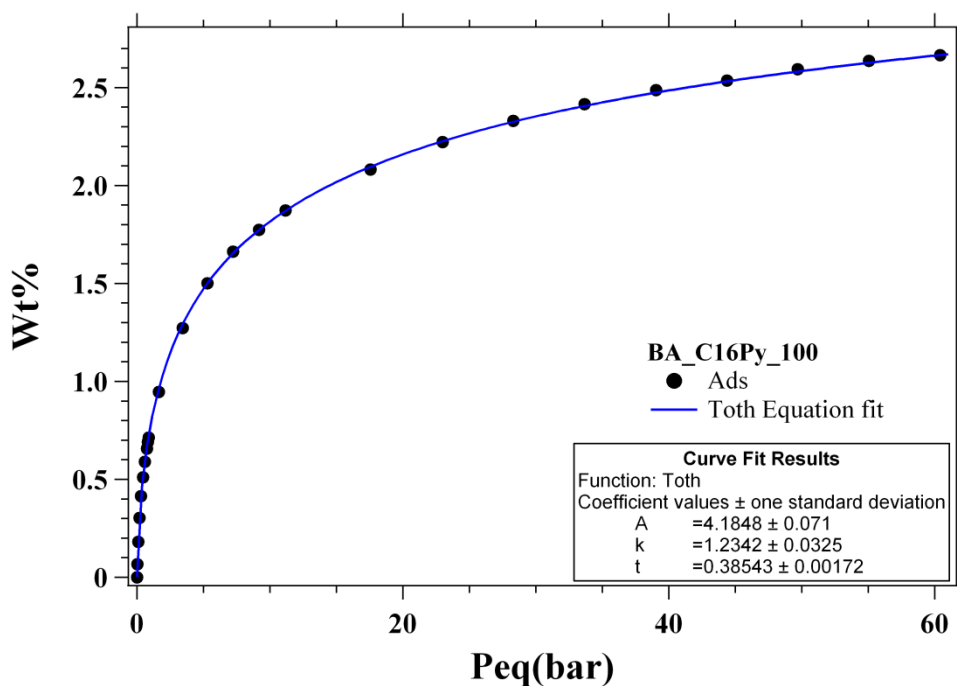

Figure 3.19: *Adsorption isotherm obtained at 77 K for the BA_C16Py_100 sample, fitted with the Tóth model.*

	BA_C12Py_100	BA_C14Py_100	BA_C16Py_100	BA_C18Py_100
A	2.52 ± 0.08	2.5 ± 0.1	4.18 ± 0.07	2.32 ± 0.03
K	1.7 ± 0.2	1.6 ± 0.3	1.23 ± 0.03	0.91 ± 0.06
t	0.47 ± 0.01	0.445 ± 0.002	0.385 ± 0.002	0.63 ± 0.01

Table 3.14: *Tóth equation fitting parameters for the samples BA_C12Py_100, BA_C14Py_100, BA_C16Py_100 & BA_C18Py_100.*

The increase of pore size results in gradual decrease of K-value which means weaker interaction of hydrogen with the samples surface. This could be due to the reduced pore size and therefore the enhanced pore curvature which increases the interaction between the hydrogen molecules and the PNOS walls[14,15,16] . Additionally, the

smaller the pore size, the higher the A-value (table 3.13 & 3.14). On the other hand, also heterogeneity affects the maximum hydrogen storage capacity. A combination of all these parameters permits to get the best maximum storage capacity on the BA_C16Py_100 sample. In figure 3.20 is depicted the amount of molecules per nm^2 that each surface can host at theoretical maximum coverage.
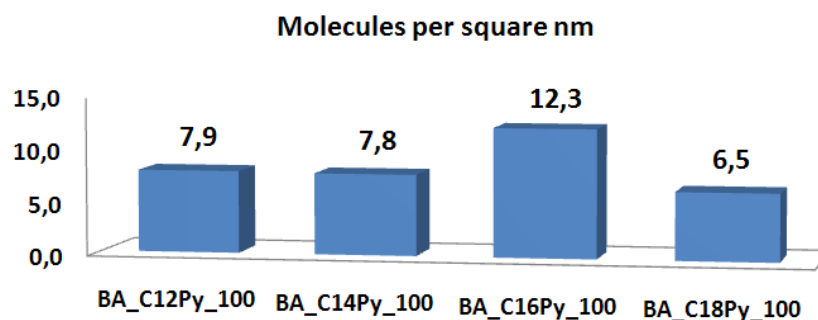

Figure 3.20: *Number of molecules per nm^2 at theoretical maximum storage capacity for the BA_C1xPy_100 samples.*

Heterogeneity appears to be critical for hydrogen's accumulation in the pores. Crystalline samples fulfilled a monolayer of surface coverage, whereas the sample with the C_{14} surfactant despite its almost disordered structure results into same surface coverage.

3.3.2   Effect of aromaticity in the walls of PNOs

3.2.2.1 Structure and morphology

Table 3.15 summarizes the samples' structural characteristics as obtained from He_2 pycnometry at room temperature, nitrogen's BET at 77 K and x-ray diffraction.

| Sample | Density (cm^3g^{-1}) | BET | | XRD | |
		Specific Surface Area (m^2g^{-1})	Pore diameter (nm)	Crystallinity	Lattice parameter a_0 (nm)
BA_C16Py_0_Si	2.8 ± 0.1	1399	2.1	Hexagonal P6m	-
BA_C16Py_40_Si	1.9 ± 0.1	1155	2.5	-	-
BA_C16Py_100	1.52 ± 0.04	1024	< 1.6	Disordered Cubic	-

Table 3.15: *Concentrative table containing all samples' data presented above.*

Substitution of Si with BTB creates lighter and therefore less dense materials; in the same time, more free space exists between each Si-O-Si bridge since the bulk BTB increases the distance between Si atoms which should result in less denser samples. The combination of the two phenomena gives the density trend showed in table 3.15. Additionally SSA decreases but in all cases remains above 1000 m^2g^{-1} that is amongst the highest for this class of materials.[17] Insertion of BTB in the matrix creates disordering whereas pore size is larger when both precursors are used.

3.3.2.2 Volumetric measurements, Tóth model application & sorption properties analysis

In figure 3.21 the adsorption isotherm obtained at 77 K is depicted as an example for the sample BH_C16_40_Si. All samples series gave Type I isotherms of the same shape like figure 3.21. In table 3.16 the values of Tóth equation parameters are resumed.
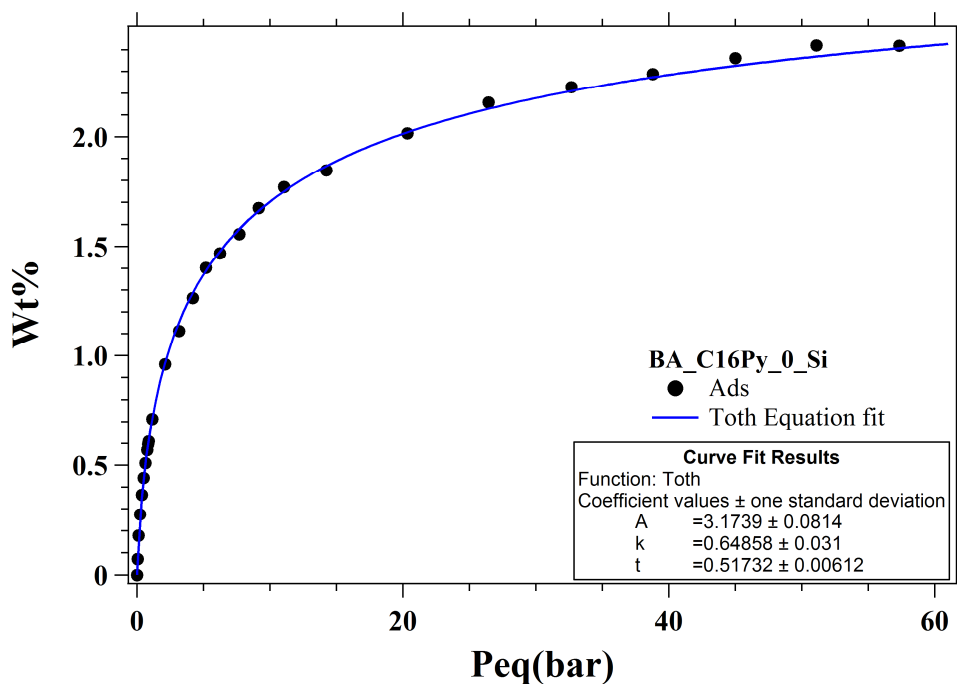
Figure 3.21: *Adsorption isotherm obtained at 77 K for the BA_C16Py_0_Si sample, fitted with the Tóth model.*

	BA_C16Py_0_Si	BA_C16Py_40_Si	BA_C16Py_100
A	3.17 ± 0.08	2.51 ± 0.02	4.18 ± 0.07
K	0.65 ± 0.03	0.92 ± 0.01	1.23 ± 0.03
t	0.517 ± 0.006	0.603 ± 0.009	0.385 ± 0.002

Table 3.16: *Tóth equation fitting parameters for the samples BA_C16Py_0_Si, BA_C16Py_40_Si & BA_C16Py_100.*

The introduction of BTB disorders the pores arrangement as t-value is demonstrating. K-values as well as theoretical maximum storage capacity are strongly enhanced in the case of the BA_C16Py_100 that exhibits the highest disordering. Insertion of BTB augments the interaction of hydrogen with the surface (K-value). In figure 3.22 is depicted the amount of molecules per nm^2 that each surface can host at theoretical maximum coverage.
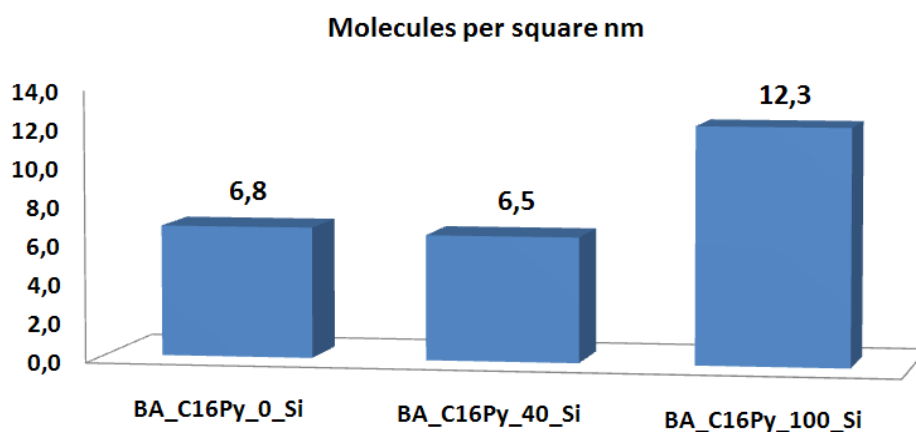
Figure 3.22: *Number of molecules per nm² at theoretical maximum storage capacity for the BA_C16Py_x_Si samples.*

Hybrid materials of TEOS and BTB do not seem to favor hydrogen's attraction to surface. BB_C16Py_100 still possess the surface that attracts higher number of hydrogen molecules; benzene ring appears to attract hydrogen's polarized molecule more than the electronegative Si.

3.3.3   Doping PNOs synthesized under acid conditions with Li$^+$ cations

3.3.3.1 Structure and morphology

Table 3.17 summarizes the samples' structural characteristics as acquired from He$_2$ pycnometry at room temperature, nitrogen's BET at 77 K and x-ray diffraction.

Sample	Density (cm³g⁻¹)	BET		XRD	
		Specific Surface Area (m²g⁻¹)	Pore diameter (nm)	Crystallinity	Lattice parameter a₀ (nm)
BA_C16Py_100	1.52 ± 0.04	1024	< 1.6	Disordered Cubic	-
BA_C16Py_100_Li	1.28 ± 0.04	932	2.2	Fully Disordered	-

Table 3.17: *Concentrative table containing all samples' data presented above.*

The disordering of the BA_C16Py_100 sample does not change after doping with Li⁺. The similar SSA indicates that the Li doping has been successful. In addition the Li⁺ insertion into the samples creates a pore enlargement which results in a smaller skeletal sample density.

3.3.3.2 Volumetric measurements, Tóth model application & sorption properties analysis

In figure 3.23 there are seen in comparison the adsorption isotherms obtained at 77 K. Both isotherms' experimental data were fitted with Tóth fitting equation. In table 3.11 the values of Tóth equation parameters are summarized.
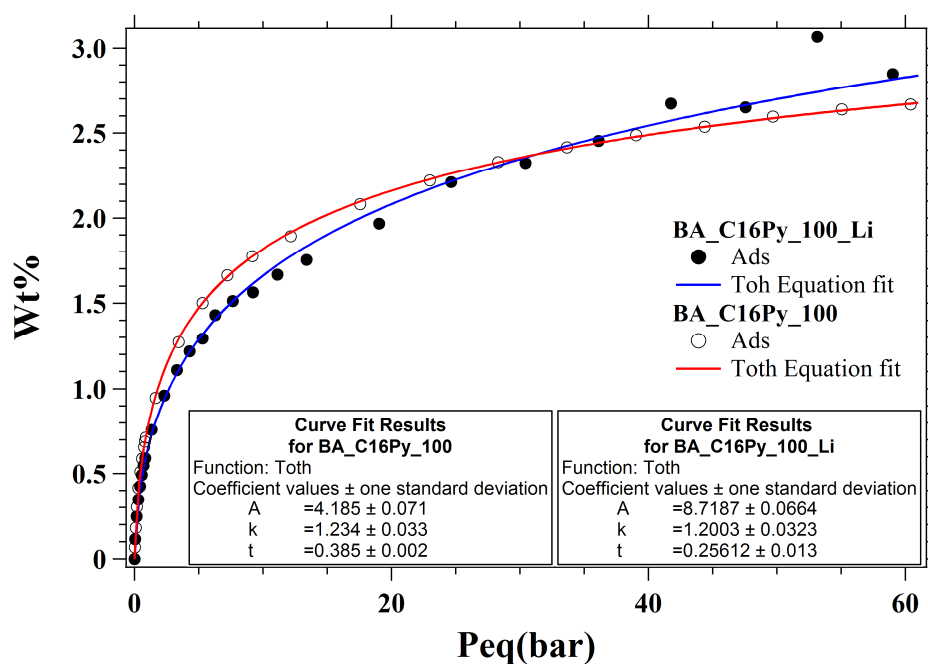

Figure 3.23: *Adsorption isotherms acquired at 77K for the BA_C16Py_100 & BA_C16Py_100_Li samples, fitted with the Tóth model.*

	BA_C16Py_100	BA_C16Py_100_Li
A	4.19 ± 0.07	8.72 ± 0.07
K	1.23 ± 0.03	1.20 ± 0.03
t	0.385 ± 0.002	0.26 ± 0.01

Table 3.18: *Tóth equation fitting parameters for the samples BA_C16Py_100, BA_C16Py_100_Li.*

The sample with Li^+ presents higher hydrogen storage capacity while the K-value are within the error equal. However at moderately small pressures (figure 3.23), the BA_C16Py_100 sample appears to have slightly higher adsorption capacity than BA_C16Py_100_Li. On the other hand at pressure values over 40 bar the wt% of the two samples cross-meet (see figure 3.23) resulting in higher hydrogen storage capacity in the BA_C16Py_100_Li sample. The results could be related to the formation of multi layered structure of adsorbed hydrogen molecules due to the induced dipole on the adsorbed hydrogen molecules due to the presence of the Li^+ ions[18,19,20,21,22] thus increasing the surface's affinity to hydrogen as also figure 3.24 demonstrates. On the other hand the t-value is smaller in the doped samples which, according to the Tóth equation discussion (see figure 1.6, at Fundamentals section), could indicate the activation of additional adsorption process at higher pressure values.
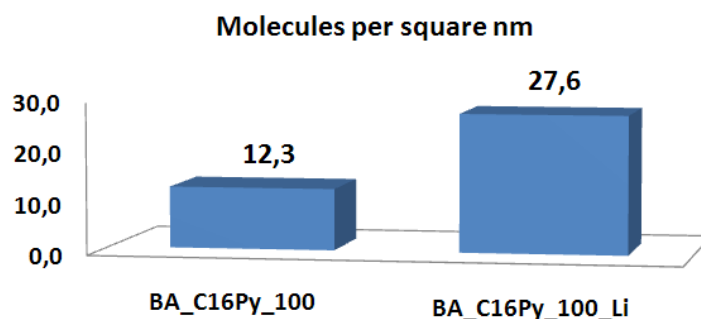

Figure 3.24: *Number of molecules per nm^2 at theoretical maximum storage capacity for the BA_C16Py_100_x samples*

In spite of the similar adsorption capacity, Li$^+$ doped surface attracts more hydrogen molecules per surface unit. An increase of the SSA to this kind of surface could create a promising hydrogen storage material.

3.3.4   Substitution of BTB with phenyl groups

3.3.4.1 Structure and morphology

Table 3.19 summarizes the samples' structural characteristics as received from He$_2$ pycnometry at room temperature, nitrogen's BET at 77 K and x-ray diffraction.

Sample	Density (cm^{3}g^{-1})	BET		XRD	
		Specific Surface Area (m^{2}g^{-1})	Pore diameter (nm)	Crystallinity	Lattice parameter a$_0$ (nm)
BA_C16Py_100	1.52 ± 0.04	1024	< 1.6	Disordered Cubic	-
BA_C16Py_95_ph	2.0 ± 0.1	1066	2.4	Disordered	-
BA_C16Py_89_ph	1.5 ± 0.1	1107	1.8	Cubic Pm3n	-

Table 3.19: *Concentrative table containing all samples' data presented above.*

Substitution of BTB with phenyl triethoxy silane in the matrix increases the SSA. In the same time, the sample with the 95% of BTB shows an enhancement of the skeletal density which is related to pores enlargement. This could be due to the allocation of phenyl groups into the samples structures (either on the surface either on the bulk skeletal sample). This particular modification by phenyl groups gives rise to perfect Pm3n (cubic) symmetry into the sample with 89% of BTB. In any case, this discussion will require more investigation in the future.

3.3.4.2 Volumetric measurements, Tóth model application & sorption properties analysis

In figure 3.25 there are seen the adsorption isotherms of the samples acquired at 77 K. The BA_C16Py_100 is presented as the reference material. In table 3.20 the values of Tóth equation parameters are summarized.
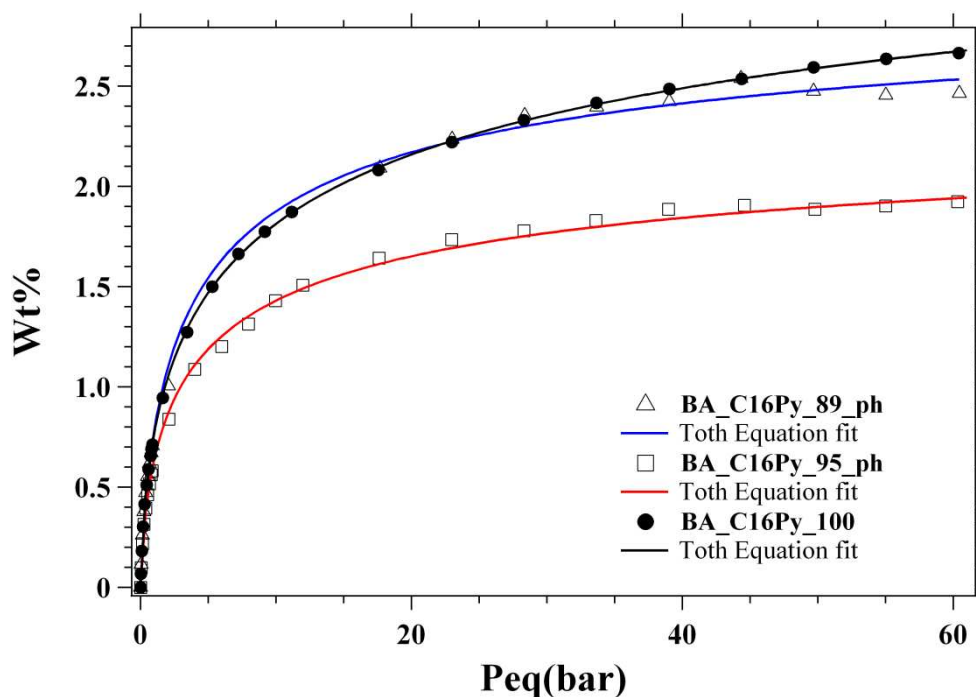

Figure 3.25: *Adsorption isotherms received at 77K for the BA_C16Py_89_ph, BA_C16Py_95_ph & BA_C16Py_100 samples, fitted with the Tóth model.*

	BA_C16Py_100	BA_C16Py_95_ph	BA_C16Py_89_ph
A	4.19 ± 0.07	2.5 ± 0.1	3.10 ± 0.02
K	1.23 ± 0.03	1.2 ± 0.1	0.77 ± 0.07
t	0.385 ± 0.002	0.479 ± 0.008	0.55 ± 0.01

Table 3.20: *Tóth equation fitting parameters for the samples BA_C16Py_100, BA_C16Py_95_ph & BA_C16Py_89_ph.*

During the substitution of BTB with phenyl groups porous lattice is expected to become more flexible. Due to the flexibility that single covalent bond provides, phenyl groups are able to turn around single bond's axis increasing therefore the accessibility of hydrogen to the surface. In any case, the insertion of phenyl groups decrease the maximum hydrogen storage capacity which is mainly due to the decrease of the adsorption energy between the pore walls and the hydrogen molecules (see K-value in table 3.20). However the sample with higher number of phenyl group presents higher hydrogen storage capacity which is mainly due to the higher SSA (see table 3.19). This type of functionalization gives one monolayer of hydrogen molecules considering the number of H_2 molecules per nm^2 depicted in figure 3.26.
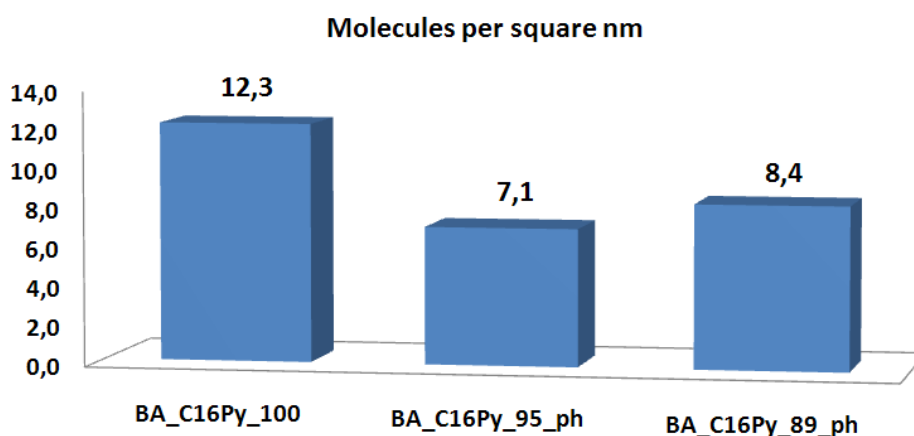

Molecules per square nm

Figure 3.26: *Number of molecules per nm^2 at theoretical maximum storage capacity for the BA_C16Py_x_ph samples*

3.3.5 Conclusions

Periodic nanoporous organosilicas synthesized under acid conditions gave type I isotherms that are typical for microporous materials.[23] SSA was in the interval of 950 – 1200 m^2g^{-1} a value high enough for this class of materials and a connection with the skeleton density was observed. At least, 2% of hydrogen storage capacity at 60 bar and 77 K was achieved from all the samples. Disordering appears as a critical

factor in sorption properties. Doping the surface with Li^+ cations strongly enhances the hydrogen storage capacity of the structure. Heterogeneity plays important role in the maximum storage capacity and in the mechanism hydrogen accommodates on the adsorbent.

3.4 PNOs synthesized under acid conditions with the organo-bis-silicalite (4,4 Bis-Triethoxysilyl-Biphenyl (DBTB)) as precursor

3.4.1 Functionalization with phenyl-triethoxy-silane

3.4.1.1 Structure and morphology

Table 3.21 presents the data as obtained from pycnometry, BET with N_2 at 77 K and XRD diffraction. The partial substitution of DBTB with phenyl-triethoxy-silane increases the SSA whereas an accurate pore size could not be obtained because experimental sensitivity of BET technique by N_2 molecules could not explore such as pore size. Density increases with the crystallinity of the prepared sample; disordered structures appear less dense.

Sample	Density (cm^3g^{-1})	BET		XRD	
		Specific Surface Area (m^2g^{-1})	Pore diameter (nm)	Crystallinity	Lattice parameter a_0 (nm)
DA_C16Py_100	1.33 ± 0.02	720	<1.6	Mes. Hexagonal	-
DA_C16Py_90_ph	1.18 ± 0.02	994	<1.6	Disordered	-
DA_C16Py_80_ph	1.88 ± 0.08	1081	<1.6	Mes. Hexagonal	-

Table 3.21: *Concentrative table containing all samples' data presented above.*

3.4.1.2 Volumetric measurements, Tóth model application & sorption properties analysis

In figure 3.27 are depicted the adsorption isotherms of the samples acquired at 77 K. All samples gave Type I isotherms and the experimental data were fitted with Tóth

model's equation. In table 3.22 there are summarized the values of the parameters of the Tóth equation applied for all the 3 samples.
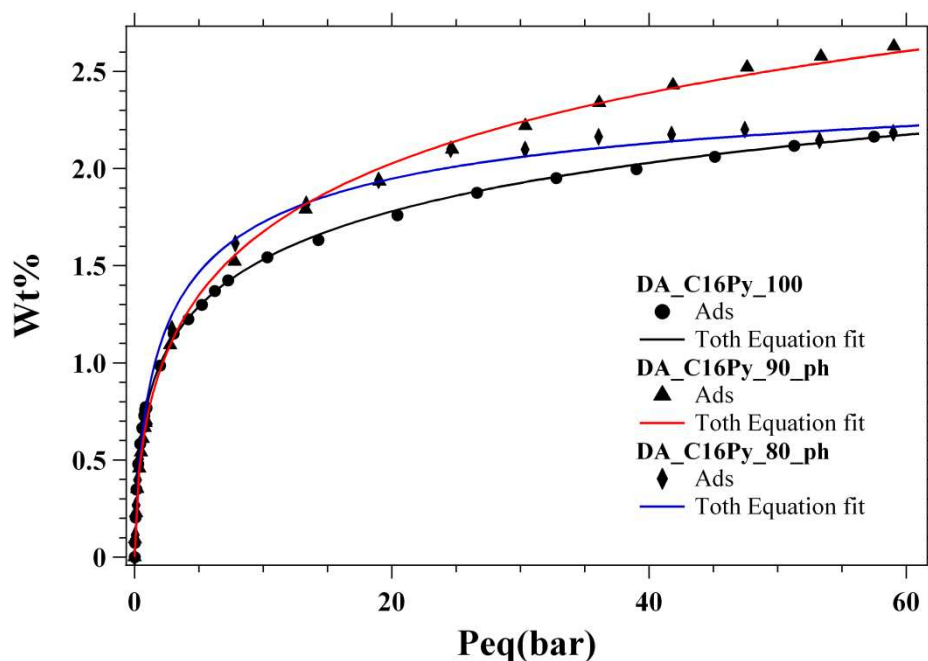

Figure 3.27: *Adsorption isotherms obtained at 77 K for the DA_C16Py_100, DA_C16Py_90_ph & DA_C16Py_80_ph samples, fitted with the Tóth model.*

	DA_C16Py_100	DA_C16Py_90_ph	DA_C16Py_80_ph
A	4.5 ± 0.2	6.54 ± 0.03	2.7 ± 0.1
K	14 ± 1	3.09 ± 0.3	1.4 ± 0.1
t	0.242 ± 0.002	0.255 ± 0.002	0.52 ± 0.01

Table 3.22: *Tóth equation fitting parameters for the samples DA_C16Py_100, DA_C16Py_90_ph & DA_C16Py_80_ph.*

Insertion of phenyl groups into the pore structure decreases the interaction of the surface with hydrogen according to the smaller K-value (see table 3.22). However the sample with 10% of phenyl groups has higher hydrogen storage capacity because of its higher SSA.
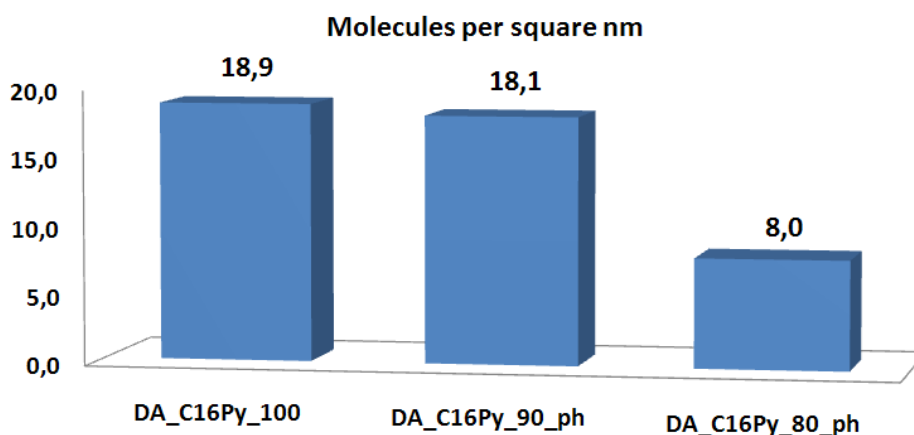
Figure 3.28: *Number of molecules per nm² at theoretical maximum storage capacity for the DA_C16Py_x_ph samples*

In any case the number of hydrogen molecules adsorbed per nm² in the unmodified and modified sample with 10% of phenyl groups is similar, confirming, in this way, that the smaller hydrogen storage capacity is just due to the smaller SSA value.

3.4.2   Conclusions

Synthesizing Periodic Nanoporous Organosilicas with DBTB as precursor creates materials with enhanced interaction with hydrogen. Pore size lies in low values for this class of materials[2,24] and ordered structure does not enhance the sorption capacity. The substitution with phenyl groups does not reinforce the interaction between surface pore samples and hydrogen molecules; however hydrogen storage capacity increases because of the SSA enhancement.

3.5 Comparisons

3.5.1 Effect of acid and basic conditions in PNOs with BTB as precursor

3.5.1.1 Structure and morphology

Table 3.23 contains the samples' structural characteristics as obtained by He_2 pycnometry at room temperature, nitrogen's BET at 77 K and x-ray diffraction.

Sample	Density (cm^3g^{-1})	BET		XRD	
		Specific Surface Area (m^2g^{-1})	Pore diameter (nm)	Crystallinity	Lattice parameter a_0 (nm)
BB_C16_100	1.50 ± 0.05	864	1.86	Fully Disordered	-
BA_C16Py_100	1.52 ± 0.04	1024	< 1.6	Disordered Cubic	-

Table 3.23: *Concentrative table containing all samples' data presented above.*

Within the error, samples density is the same since chemical constituents are common. Acid conditions seem to favor the creation of nanopores and high SSA whereas basic conditions give fully disordered structure that as discussed above enhances the adsorption properties.

3.5.1.2 Volumetric measurements, Tóth model application & sorption properties analysis

In figure 3.29 there are seen in comparison the adsorption isotherms obtained at 77 K for the 2 samples. Both isotherms experimental data were fitted with Tóth fitting equation. In table 3.24 the values of Tóth equation parameters are summarized.
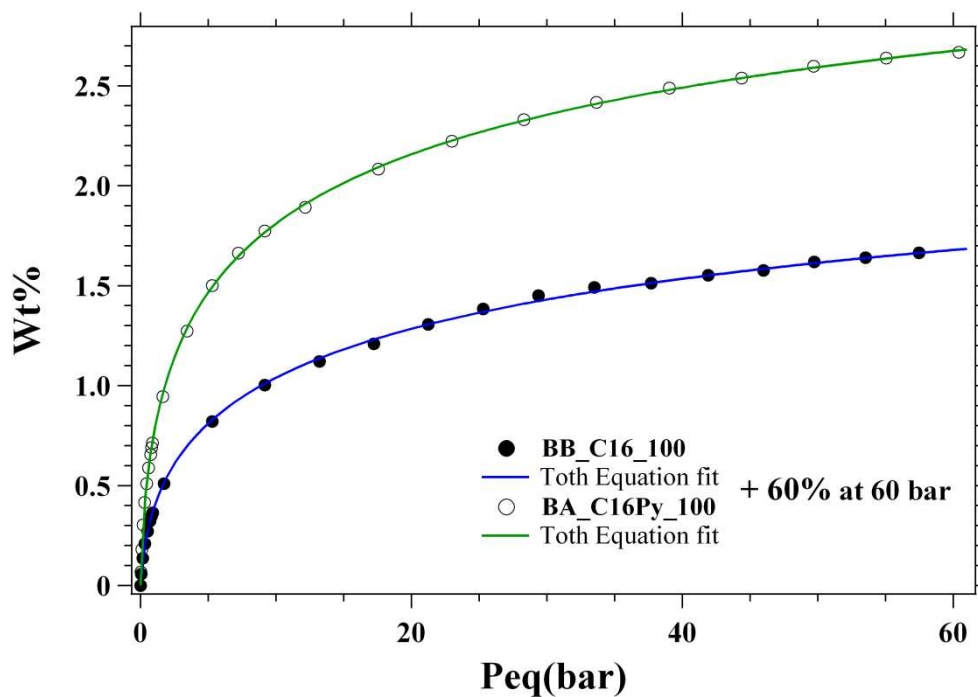
Figure 3.29: *Effect of acid/basic synthesis conditions in sorption properties.*

	BB_C16_100	**BA_C16Py_100**
A	3.3 ± 0.1	4.19 ± 0.07
K	0.74 ± 0.03	1.23 ± 0.03
t	0.353 ± 0.002	0.385 ± 0.002

Table 3.24: *Tóth equation fitting parameters for the BB_C16_100, BA_C16Py_100 samples.*

The idea that adsorption isotherm is giving, is verified by the Tóth equation fit. Under acid conditions, interaction is stronger giving almost double capacity in low pressures (0 – 5 bar) and arriving at +60% more at 60 bar.
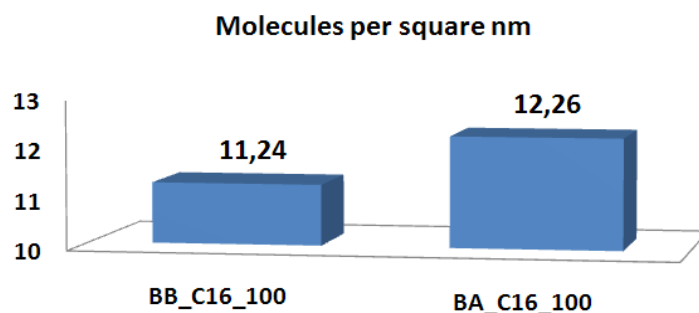
Figure 3.30: *Number of molecules per nm² at theoretical maximum storage capacity for the BB_C16_100 & BA_C16Py_100 samples*

As far as surface's hosting capacity is concerned acid conditions are favorable in respect to basic conditions of synthesis although in both conditions more than monolayer coverage is created (figure 3.30).

3.5.2 Effect of mono- and bi-phenyl ring in PNOs synthesized under basic conditions

3.5.2.1 Structure and morphology

Table 3.25 contains the samples' structural characteristics as acquired by He_2 pycnometry at room temperature, nitrogen's BET at 77 K and x-ray diffraction.

| Sample | Density (cm^3g^{-1}) | BET | | XRD | |
		Specific Surface Area (m^2g^{-1})	Pore diameter (nm)	Crystallinity	Lattice parameter a_0 (nm)
BB_C10_100	1.51 ± 0.03	654	1.92	Fully Disordered	-
DB_C10_100	1.41 ± 0.02	795	1.86	Fully Disordered	-

Table 3.25: *Concentrative table containing all samples' data presented above.*

The use of biphenyl in the starting material decreases the pore size and enhances SSA when synthesis takes place under basic conditions. A small decrease in density favors the hydrogen storage capacity in terms of materials weight. In both cases crystal order is not found under these synthesis conditions.

3.5.2.2 Volumetric measurements, Tóth model application & sorption properties analysis

In figure 3.31 there are seen in comparison the adsorption isotherms obtained at 77 K for the 2 samples. Both isotherms experimental data were fitted with Tóth fitting equation. In table 3.26 the values of the Tóth equation parameters are summarized.
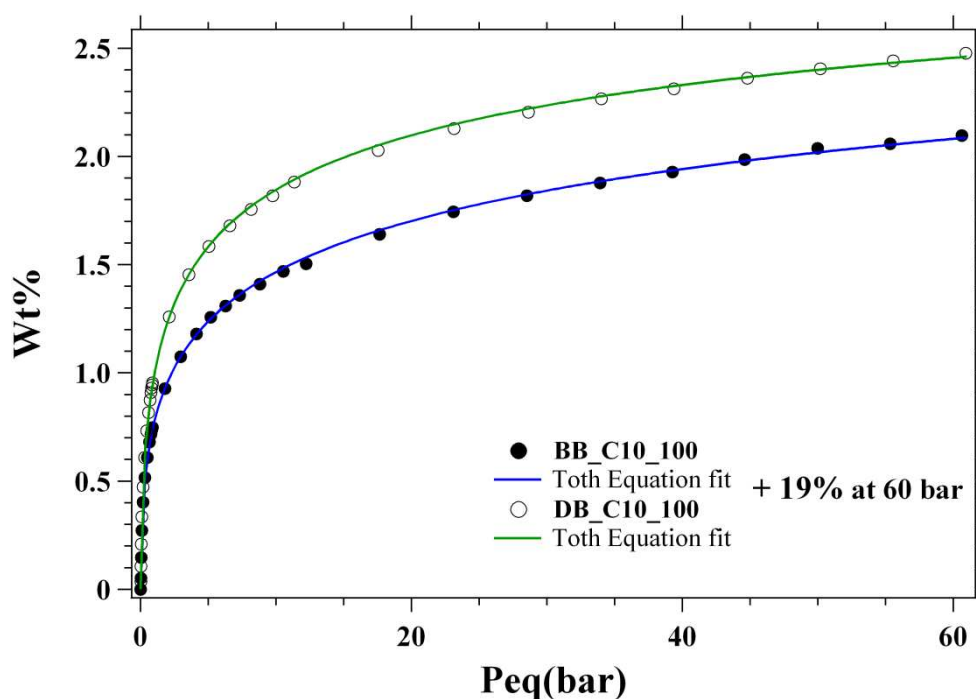

Figure 3.31: *Effect of mono- and bi-phenyl ring in the precursor in the sorption properties. Synthesis was carried out in basic conditions.*

	BB_C10_100	DB_C10_100
A	4.5 ± 0.2	3.6 ± 0.1
K	19 ± 1	6.1 ± 0.4
t	0.230 ± 0.002	0.334 ± 0.003

Table 3.26: *Tóth equation fitting parameters for the BB_C10_100, DB_C10_100 samples.*

In relatively low pressures use of biphenyl enhances adsorption properties due to the presence of the biphenyl rings as predicted. On the other hand, the large heterogeneity that BB_C10_100 is exhibiting makes it efficient, in comparison to mono-phenyl, only in relatively high pressures. Comparing with the biphenyl material, this does not consist it a viable solution from application's point of view.
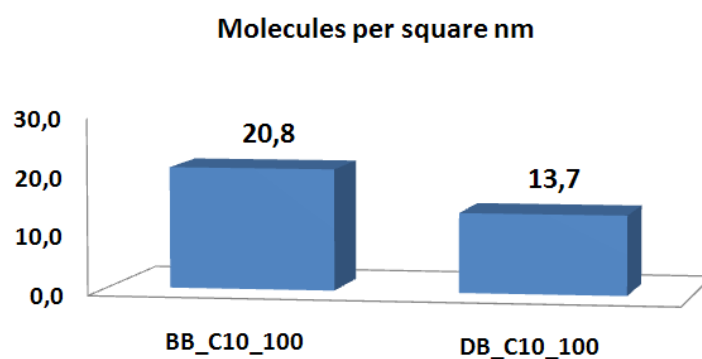

Figure 3.32: *Number of molecules per nm^2 at theoretical maximum storage capacity for the BB_C10_100 & DB_C10_100 samples.*

From surface's hosting capacity and regardless to gravimetric hydrogen storage capacity, the shorter BTB creates a surface that hosts 50% more hydrogen molecules in respect to DBTB in basic conditions (figure 3.32).

3.5.3 Effect of mono- and bi-phenyl ring in PNOs synthesized under acid conditions

3.5.3.1 Structure and morphology

Table 3.27 contains the samples' structural characteristics as obtained from He_2 pycnometry at room temperature, nitrogen's BET at 77 K and x-ray diffraction.

Sample	Density (cm^3g^{-1})	BET		XRD	
		Specific Surface Area (m^2g^{-1})	Pore diameter (nm)	Crystallinity	Lattice parameter a_0 (nm)
BA_C16Py_100	1.52 ± 0.04	1024	< 1.6	Disordered Cubic	-
DA_C16Py_100	1.33 ± 0.02	720	<1.6	Mes. Hexagonal	-

Table 3.27: *Concentrative table containing all samples' data presented above.*

The use of biphenyl ring in the precursor under acid conditions produces a lighter material. Principle pore size in both cases remains below 1.6 nm, a pore size that favors hydrogen adsorption.[11] On the hand, SSA is decreased and crystallinity from almost disordered shifts to quasi-hexagonal.

3.5.3.2 Volumetric measurements, Tóth model application & sorption properties analysis

In figure 3.33 there are seen in comparison the adsorption isotherms obtained at 77 K for the 2 samples. Both isotherms experimental data were fitted with Tóth fitting equation. In table 3.28 the values of the Tóth equation parameters are shown.
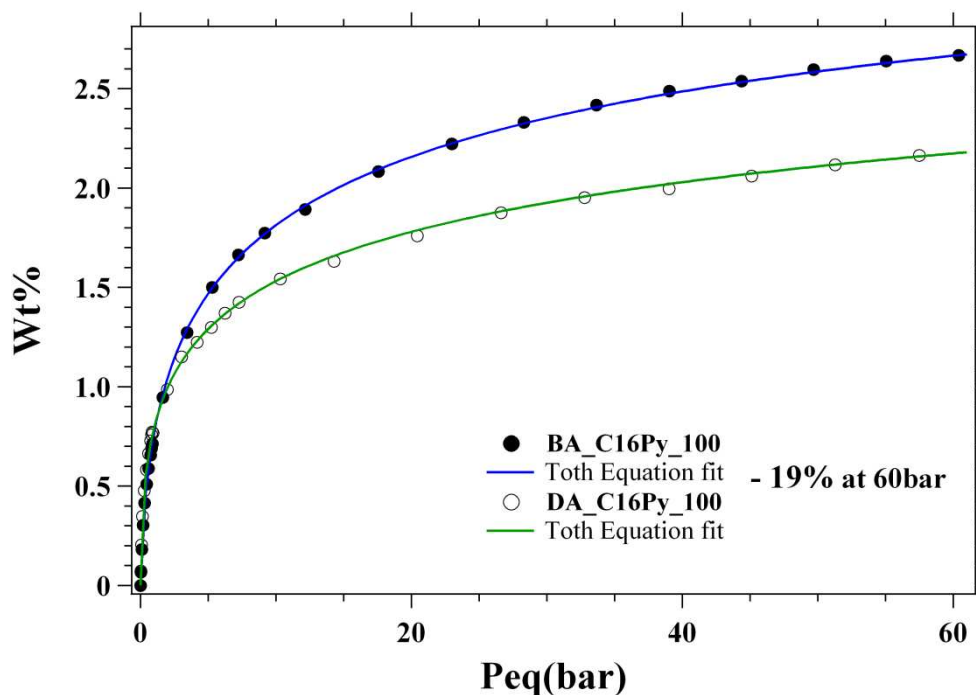
Figure 3.33: *Effect of mono- and bi-phenyl ring in the precursor in the sorption properties. Synthesis was carried out in acid conditions.*

	BA_C16Py_100	DA_C16PY_100
A	4.19 ± 0.07	4.5 ± 0.2
K	1.23 ± 0.03	14 ± 1
t	0.385 ± 0.002	0.242 ± 0.002

Table 3.28: *Tóth equation fitting parameters for the BB_C10_100, DB_C10_100 samples.*

A closer look in the (0 – 2) bar region will reveal higher uptake for the biphenyl sample. Nevertheless, after 3 bar mono-phenyl sample outclasses having at 60 bar 19% higher hydrogen storage capacity. The difference can be attributed to the difference in SSA. On the other hand, according to the Tóth model biphenyl sample can accommodate more hydrogen at its maximum theoretical storage capacity. In figure 3.34 the maximum number of molecules per nm^2 the surface can host is depicted.
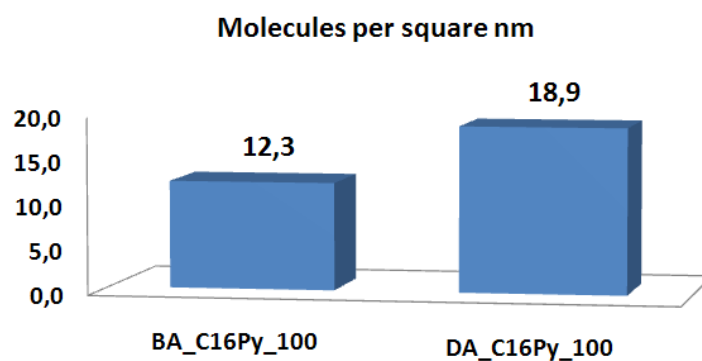
Figure 3.34: *Number of molecules per nm^2 at theoretical maximum storage capacity for the BA_C16Py_100 & DA_C16Py_100 samples.*

The biphenyl sample attracts more hydrogen molecules on its surface. The existence of the second phenyl group enhances the interaction strength by 60% (figure 3.34).

3.5.4 Effect of bi-phenyl ring as precursor in PNOs synthesized under basic or acid conditions

3.5.4.1 Structure and morphology

Table 3.29 contains the samples' structural characteristics as acquired from He$_2$ pycnometry at room temperature, nitrogen's BET at 77 K and x-ray diffraction.

Sample	Density (cm^{3}g^{-1})	BET		XRD	
		Specific Surface Area (m^{2}g^{-1})	Pore diameter (nm)	Crystallinity	Lattice parameter a$_0$ (nm)
DB_C16_100	1.25 ± 0.06	827	1.95	Disordered	-
DA_C16Py_100	1.33 ± 0.02	720	<1.6	Mes. Hexagonal	-

Table 3.29: *Concentrative table containing all samples' data presented above.*

Basic synthesis conditions create a more disordered structure with higher SSA whereas acid conditions give smaller pore size and partial crystallinity. Density in the error remains the same since same chemical constituents were used.

3.5.4.2 Volumetric measurements, Tóth model application & sorption properties analysis

In figure 3.35 there are seen in comparison the adsorption isotherms obtained at 77 K for the 2 samples. Both isotherms experimental data were fitted with Tóth fitting equation. In table 3.30 the values of the Tóth equation parameters are demonstrated.
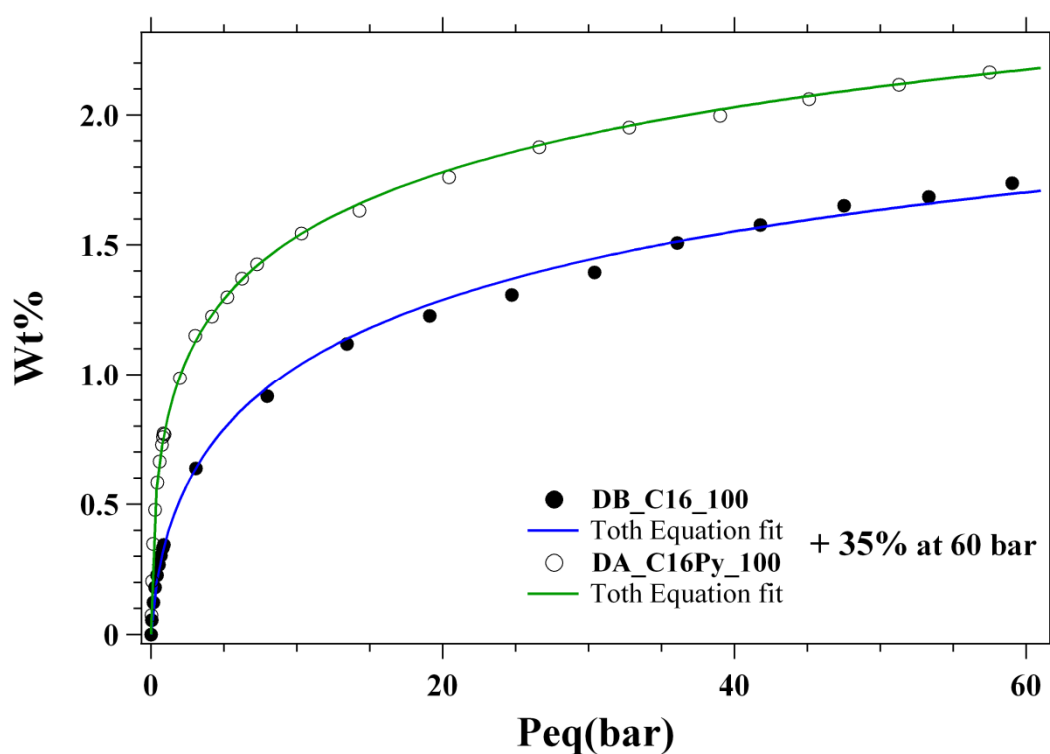
Figure 3.35: *Effect of the synthesis conditions (acid/basic) in sorption properties when DBTB is used as precursor.*

	DB_C16_100	DA_C16Py_100
A	3.20 ± 0.02	4.5 ± 0.2
K	0.46 ± 0.06	14 ± 1
t	0.388 ± 0.009	0.242 ± 0.002

Table 3.31: *Tóth equation fitting parameters for the DB_C16_100, DA_C16Py_100 samples.*

Acid conditions strongly favor the adsorption properties when DBTB as precursor is used. In the range (0 – 1) bar hydrogen storage capacity is double for the DA_C16Py_100 and in the end of scale predominates by 35%. Applying the Tóth equation A-value is 50% higher and K-value reflects the strong interaction that the sample exhibits. Given that the acid-synthesized sample possesses a short-range order in contrast to the disordered of the basic-synthesized one, turns out that in this case pore size determines the hydrogen storage capacity.
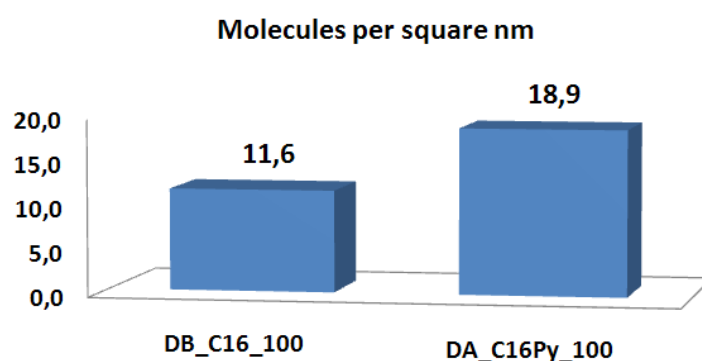

Figure 3.36: *Number of molecules per nm^2 at theoretical maximum storage capacity for the DB_C16_100 & DA_C16Py_100 samples.*

Biphenyl sample synthesized under acid conditions can host 50% more hydrogen molecules at maximum storage capacity (figure 3.36). The figure above verifies that principle role in the storage properties plays the smaller pore size.

3.5.5 Effect of Li⁺ cations doping under basic and acid conditions

3.5.5.1 Structure and morphology

Table 3.32 contains the samples' structural characteristics as received from He_2 pycnometry at room temperature, nitrogen's BET at 77 K and x-ray diffraction.

Sample	Density $(cm^3 g^{-1})$	BET		XRD	
		Specific Surface Area $(m^2 g^{-1})$	Pore diameter (nm)	Crystallinity	Lattice parameter a_0 (nm)
BB_C16_100_Li	1.9 ± 0.2	484	1.84	Fully Disordered	-
BA_C16Py_100_Li	1.28 ± 0.04	932	2.2	Fully Disordered	-

Table 3.32: *Concentrative table containing all samples' data presented above.*

Synthesis under acid conditions creates sample with higher SSA. Doping with Li⁺ cations seems to have been successful due to the similar value SSA that has been obtained in respect to the initial material (see section 3.3.3.1). In addition the Li⁺ insertion into the samples creates a pore enlargement which results in a smaller skeletal sample density. On the other hand, basic conditions gave a heavier, bulkier material of heavily reduced SSA. Disordering of the initial material after the doping was preserved under both conditions.

3.5.5.2 Volumetric measurements, Tóth model application & sorption properties analysis

In figure 3.37 there are seen in comparison the adsorption isotherms obtained at 77 K for the 2 samples. Both isotherms experimental data were fitted with Tóth fitting equation. The values of the Tóth equation parameters are shown in table 3.33.
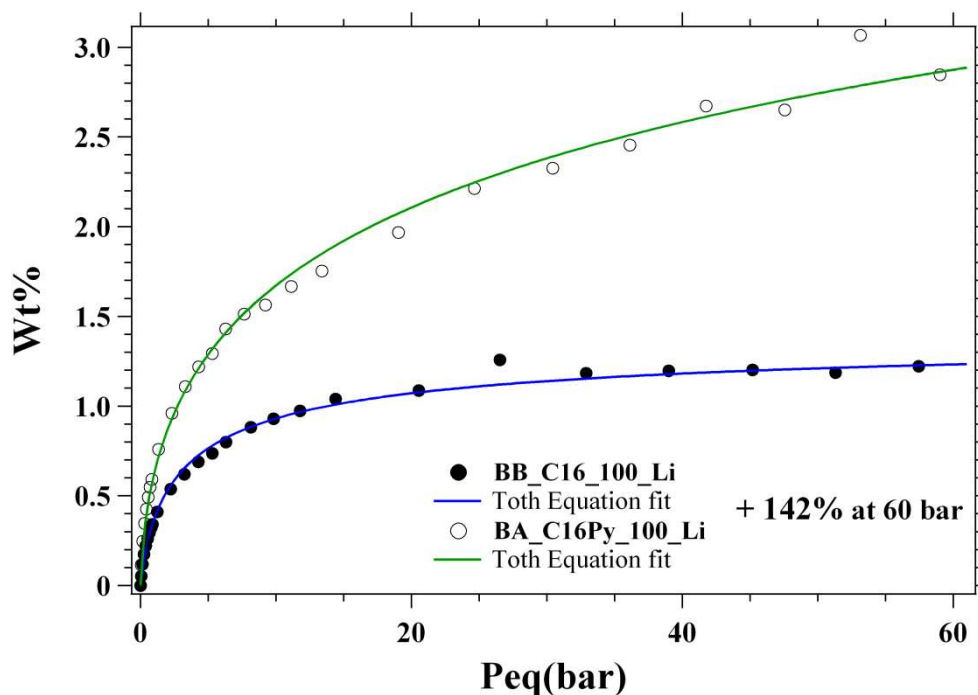
Figure 3.37: *Effect of Li$^+$ cations doping in sorption properties in acid/basic conditions of synthesis.*

	BB_C16_100_Li	BA_C16Py_100_Li
A	1.43 ± 0.02	8.57 ± 0.08
K	0.61 ± 0.07	0.9 ± 0.2
t	0.64 ± 0.02	0.268 ± 0.007

Table 3.33: *Tóth equation fitting parameters for the BB_C16_100_Li, BA_C16Py_100_Li samples.*

Tóth fitting enhances the idea that adsorption isotherms are depicting. Synthesis under acid conditions favors the interaction of hydrogen with surface. Lighter skeleton and double SSA are the critical factors that produce such promising adsorption behavior. Hydrogen is attracted stronger both in low and high pressures whereas the disorder and the wide pore distribution that t-value is indicating, enhance the hydrogen storage capacity in relatively high pressures. The higher enthalpy that K-value is suggesting is seen on the graph by the higher hydrogen storage capacity that BA_C16_100_Li is exhibiting in low pressures.
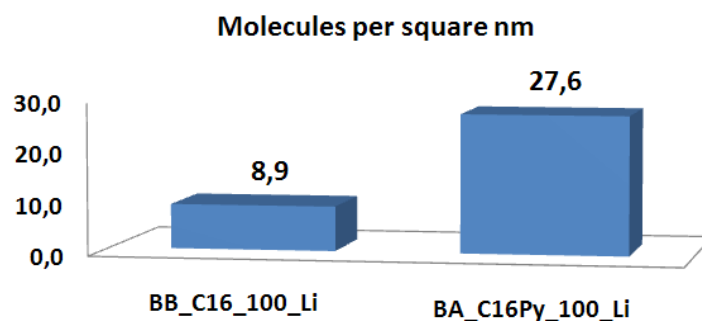
Figure 3.38: *Number of molecules per nm^2 at theoretical maximum storage capacity for the BB_C16_100_Li & BA_C16Py_100_Li samples.*

The surface of the BA_C16Py_100_Li given its SSA as measured by BET and the considerations made by Tóth model, favors hydrogen adsorption capacity. According to it, hosted molecules outnumber the one monolayer that BB_C16_100_Li can host by 3 times (figure 3.38).

3.5.6   Conclusions

Acid appear as favorable conditions in terms of crystallinity, SSA and uptake of hydrogen. Doping of materials in the edge of nanoporous/microporous scale with Li$^+$ needs further investigation and improvement in the doping procedure. Nevertheless, Li$^+$ cations do enhance surface's interaction with hydrogen. From adsorption point of view theoretical calculations are verified from experiment.[19] The existence of biphenyl in the precursor enhances the interaction and gives higher hydrogen storage capacity in relatively low pressures. Disorder and wide pore distribution are favoring sorption properties but on the other hand also nanopores (<1.6 nm) provide better environment for hydrogen adsorption enhancing the hydrogen interaction with the adsorbent.

In the case of Li$^+$ insertion, either under basic conditions or under acid conditions insertion was successful but in basic conditions Li was oxidized therefore losing its

ability to attract the polarized hydrogen molecules. Apart from this, in basic conditions less hydrogen uptake was observed. On the other hand, high pressure in the sample under acid conditions seems to activate a different adsorption mechanism that needs further investigation.

Regarding the contribution of the surfactant chain length, both in basic and acid conditions shorter surfactant chain enhances the hydrogen storage capacity. Longer surfactant chain increases the sample's homogeneity.

Lastly, Si substitution with BTB enhances clearly the adsorption properties under acid conditions. BTB increases the heterogeneity arriving close to saturation in lower pressures than the others. Basic conditions give high heterogeneity in mixtures of Si and BTB whereas materials with single precursor exhibit higher homogeneity and lower interaction with hydrogen.

3.6   Preliminary diffusion analysis

According to the analysis of the dynamical properties on the hydrogen adsorption measurements by PcT apparatus presented in the section 1.4 of chapter 1, the diffusion coefficient can be extracted from the pressure versus time graphs. In this section the dynamical adsorption data analysis of the basic sample series with different surfactant chain length is presented.

In order to reproduce the experimental data, the formula (see section 1.4, formula 1.16) has been utilized. However the data of BB_C10_100_0 cannot be well fitted with this model. On the other hand if we observe the fitting result (see figure 3.39) it seems that the diffusion is described by double diffusion. In fact if the BET measurement of that sample is analyzed double peak in the pore size distribution is observed due to two different pores size (see figure 3.40). Therefore we expect in this case double diffusion coefficient. Instead, the BET measurements of the other samples of the series present only one peak in the pore size distribution (not shown here), therefore the choice of single diffusion is correct.

According to this discussion, the diffusion coefficients D_0 for the four samples considered are reported in table 3.34. The diffusion coefficient calculated by fitting procedure considers also the square grain size (l^2) which in average is equal to the four sample, i.e. (1-2) µm (see figure 3.4a-d).

	BB_C10_100		BB_C12_100	BB_C16_100	BB_C18_100
D/l^2 (sec^{-1})	0.0036	0.016	0.027	0.016	0.015

Table 3.34: *Diffusion coefficient normalizes to the square grain size (D/l^2) calculated on the considered samples series. The relative error is 10%.*

The data of table 3.34 underline that all the samples, except for the sample with the C_{12} surfactant length, present, in the error, the same diffusion coefficient (~0.016 sec^{-1}). However the sample with the C_{10} surfactant length presents an additional

diffusion mechanism due to the second peak in figure 3.40. The higher diffusion coefficient of the C_{12} sample can be related to the smaller uptake observed in the C_{12} sample up to 60 bar (not shown here). On the other hand, the smaller diffusion coefficient of C_{10} sample is related to higher H_2 uptake. Therefore we can claim that higher uptake is connected to slower kinetics. This is a parameter which has to be considered as an application point of view, because it is important to know the adsorption and releasing time of the hydrogen molecules.
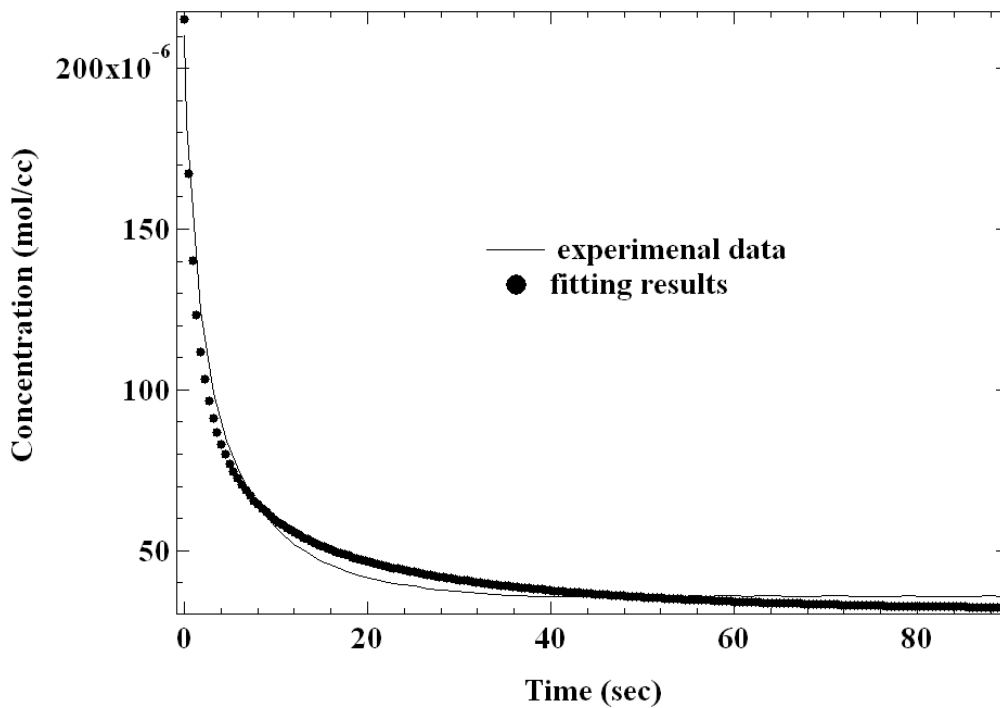
Figure 3.39: *Diffusion analysis according to the formula 1.16 in the BB_C10_100 sample.*
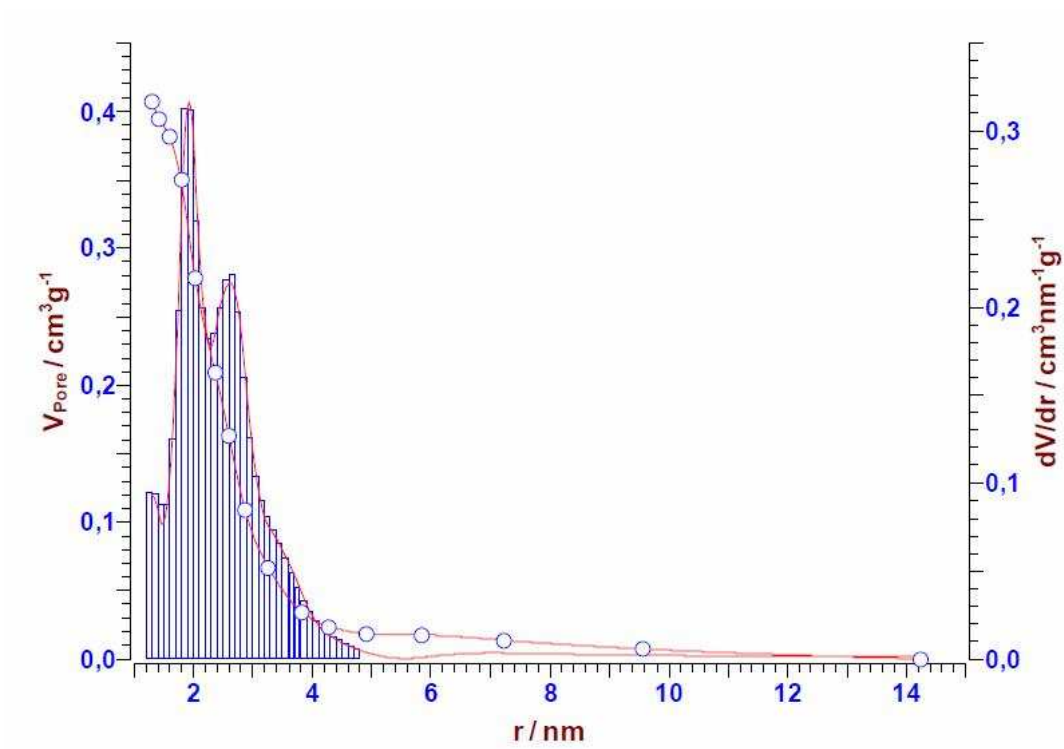
Figure 3.40: *Pore size distribution of the sample BB_C10_100 obtained by BET technique.*

Bibliography Chapter 3

(1) Asefa, T., MacLachlan, M. J., Coombs, N. *et al. Nature*, **1999**, *402*, 867-871.
(2) Kapoor, M. P.; Yang, Q. H.; Inagaki, S. *Journal of the American Chemical Society*, **2002**, *124*, 15176-15177.
(3) C.J. Brinker, G.W. Scherer *The Physics and Chemistry of Sol-Gel Processing*, ed., Academic Press, **1990**.
(4) Inagaki, S., Guan, S., Ohsuna, T. *et al. Nature*, **2002**, *416*, 304-307.
(5) Xia, Y. D.; Wang, W. X.; Mokaya, R. *Journal of the American Chemical Society*, **2005**, *127*, 790-798.
(6) Klontzas, E.; Tylianakis, E.; Froudakis, G. E. *J. Phys. Chem. C*, **2008**, *112*, 9095-9098.
(7) Froudakis, G. E. *Nano Lett.*, **2001**, *1*, 531-533.
(8) Binas, V.; Trikalitis, P. *in preparation*, **2009**.
(9) Binas, V.; Trikalitis, P. *in preparation*, **2009**.
(10) Yushin, G., Dash, R., Jagiello, J. *et al. Advanced Functional Materials*, **2006**, *16*, 2288-2293.
(11) Latroche, M., Surble, S., Serre, C. *et al. Angewandte Chemie-International Edition*, **2006**, *45*, 8227-8231.
(12) Lin, X., Telepeni, I., Blake, A. J. *et al. Journal of the American Chemical Society*, **2009**, *131*, 2159-2171.
(13) Gogotsi, Y., Portet, C., Osswald, S. *et al. Int. J. Hydrog. Energy*, **2009**, *34*, 6314-6319.
(14) Panella, B.; Hirscher, M.; Roth, S. *Carbon*, **2005**, *43*, 2209-2214.
(15) Rzepka, M.; Lamp, P.; de la Casa-Lillo, M. A. *J. Phys. Chem. B*, **1998**, *102*, 10894-10898.
(16) Nijkamp, M. G., Raaymakers, Jemj, van Dillen, A. J. *et al. Applied Physics a-Materials Science & Processing*, **2001**, *72*, 619-623.
(17) Hoffmann, F., Cornelius, M., Morell, J. *et al. J. Nanosci. Nanotechnol.*, **2006**, *6*, 265-288.
(18) Mavrandonakis, A., Klontzas, E., Tylianakis, E. *et al. Journal of the American Chemical Society*, **2009**, *131*, 13410-13414.
(19) Mavrandonakis, A., Tylianakis, E., Stubos, A. K. *et al. J. Phys. Chem. C*, **2008**, *112*, 7290-7294.
(20) Mpourmpakis, G., Tylianakis, E., Papanikolaou, D. *et al. J. Nanosci. Nanotechnol.*, **2006**, *6*, 3731-3735.
(21) Blomqvist, A., Araujo, C. M., Srepusharawoot, P. *et al. Proceedings of the National Academy of Sciences of the United States of America*, **2007**, *104*, 20173-20176.
(22) Han, S. S.; Goddard, W. A. *Journal of the American Chemical Society*, **2007**, *129*, 8422-+.
(23) IUPAC *Pure & Applied Chemistry*, **1985**, *57*, 603.
(24) Hoffmann, F., Cornelius, M., Morell, J. *et al. Angewandte Chemie-International Edition*, **2006**, *45*, 3216-3251.

4. Zeolites: Gas solubility and mobility in modified and unmodified zeolites

4.1 Introduction

The synthesis of new materials for gas separation is a big issue in the energy market for purification of gas mixtures, and in particular great attention is paid to the purification of hydrogen.[1] In this context organic[2] and inorganic[3] membranes play an important role and compete in this research field. However the optimal material to separate the gas has to offer high gas flux and selectivity[2] at a reasonable cost.

To obtain all these goals, organic-inorganic mixed matrix membranes (MMMs) have been proposed[4] in order to exploit the advantages of both polymers and inorganic compounds. MMMs in fact are potentially able to couple the ease of formation and low cost of polymeric membranes with the superior selectivity, permeability and resistance of inorganic materials.

Among the most used inorganic materials for MMMs are zeolites.[5] Zeolites, characterized by well defined micropores within their structures, are used for gas separation, catalysis[6,7,8] and for water softening in detergents. The selectivity of zeolite membranes to small sized molecules like H_2 and CO_2 is poor because the size of the molecules is similar. In order to improve the H_2/CO_2 separation factor, a modification of the zeolite pores and of the membrane defects by silylation has been proposed.[9] The zeolite surface functionalization and/or the reduction of the pore size should modify the gas transport through the zeolite in order to obtain the best membrane selectivity.

However the H_2 diffusion and adsorption into the modified zeolite is important too, in order to know the dynamical and equilibrium sample properties in applicative conditions.

The modification of zeolite frameworks by covalently bound organic molecules either externally or internally to the micropores could transform those materials in

organic-inorganic hybrid composites able to fulfil the requirement of several applications.[9,10]

Different type of modifications by organic molecules have been developed in the literature.[11,12,13,14] The modification of zeolite with organo-silane molecules is one of the most important reaction studied in the literature[13] which allows to the zeolite to be reactive and connected with different composites like polymers. In this way the so-called "mixed matrix" materials are synthesised which combines the advantages of each phase: high selectivity of the zeolite and advantageous mechanical properties associated to easy processing and economical return of the polymers. The grafting of organo-silane molecules with reactive functional groups allows to the out-modified zeolite its bonding with polymers.[15]

In the present study, the hydrogen adsorption capacity is experimentally measured. The hydrogen choice is dictated from the small size of the molecule (the only gas with a smaller size is helium) in order to have an upper limit to the gas selectivity of the zeolite. Very recently Dong et al.[16] tested the hydrogen adsorption capacity of different zeolite with different pore size and they report the hydrogen adsorption capacity in combination with channel size of zeolites and the best result is related to the closer size of kinetic diameter of a hydrogen molecule and zeolite pores.

In this chapter we tested the hydrogen adsorption of the starting zeolite (silicalite-1, MFI type) and modified with different organo-silane molecules by Pressure-concentration-Temperature (PcT) isotherms obtained in pressure range (0 – 80) bar and at 77 K and 300 K by Sievert's type apparatus. The same samples have been characterized by Thermal Desorption Spectroscopy (TDS) in the temperature region (20 – 120) K. Additionally, XRD and SEM techniques were utilized. A discussion of the sorption properties of the investigated materials at equilibrium and dynamical conditions is also presented.

4.2   Synthesis

The silicalite-1 zeolites have been prepared from a synthesis mixture of the following composition (in oxides):

8.8 $(C_3H_7)_4NBr : 5\ Na_2O : 0,125\ Al_2O_3 : 100\ SiO_2 : 1250\ H_2O$

obtained by dissolving the right amount of tetrapropylammonium bromide (>99%, Fluka, purum) in a freshly prepared 30% sodium hydroxide solution (pellets, 98,6%, Baker analyzed), followed by the addition of the rest of distilled water, and finally by precipitated SiO_2 (BHD). Aluminum was contained as an impurity mainly in the silica, and its content measured by means of atomic absorption spectroscopy (Perkin Elmer AAS 380). The homogenized gel was loaded in a teflon lined stainless steel autoclave and heated at 170 °C for 30 hours. The solid was filtered and washed with plenty of water up to a neutral pH, and dried at 100°C for 12 hours.

The silicalite-1 has been modified with different organosilane molecules: Cl_3SiCH_3, $Cl_2Si(CH_3)_2$, $ClSi(CH_3)_3$ and $Cl_3Si(CH_2)_2(CF_2)_8F$. For the sake of clarity the sample modified with the last molecules will be called fluorinated silicalite-1.

4.3   Results – Discussion

4.3.1   Structural and morphological characterization

The XRD patterns of the starting and modified materials (see figure 4.1) show the typical peaks of silicalite-1, MFI topology.[17]
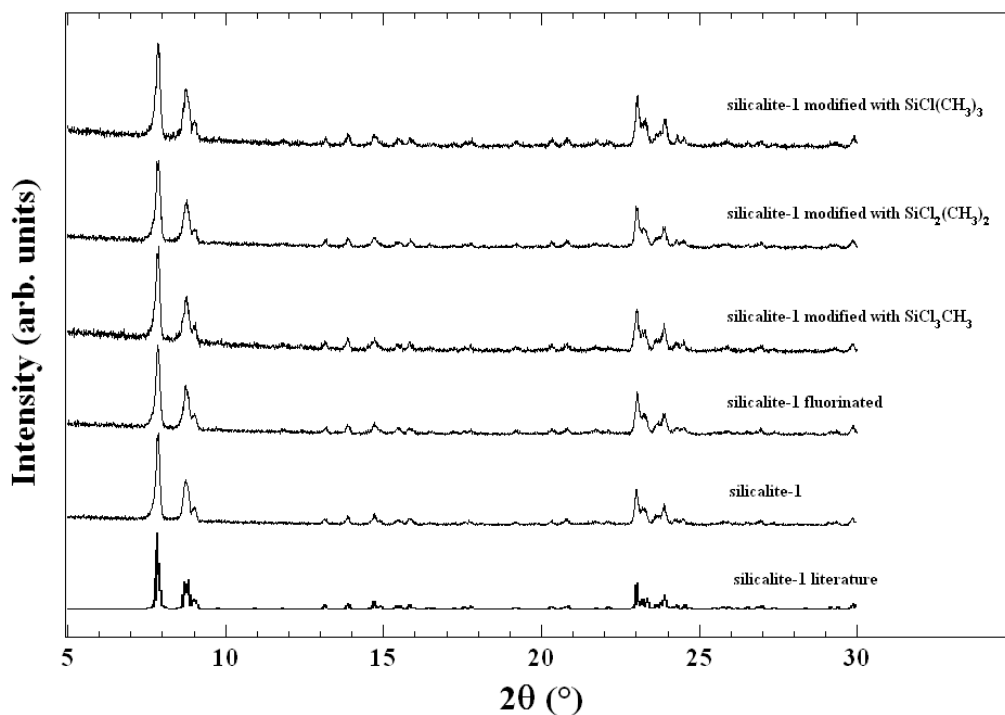
Figure 4.1: *XRD patterns of silicalite-1 before and after the modifications.*

The modification of silicalite-1 by organosilane molecules does not produce any structural change in the zeolite[18] . In any case, if differences are observed in the XRD pattern, they are only present in the peaks intensity and broadening of the lower-order reflections due to the smaller crystallite size, or a higher degree concentration of disordering.[14,19] The XRD patterns do not present any cristobalitic phase which should introduce an intense peak at ~10° 2θ.[20]

The SEM pictures (see figure 4.2 for silicalite-1) show the typical morphology of silicalite-1 with intergrowth structures of zeolites[21] indicating an average grain size of 20 μm which is unchanged after the modification.
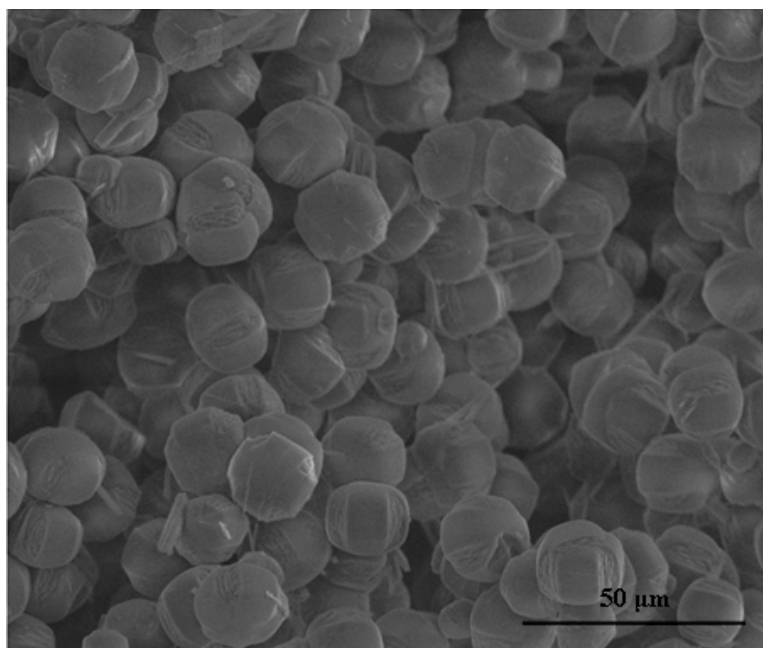
Figure 4.2: *SEM picture of silicalite-1.*

The successful functionalization obtained by organo-silane molecules is confirmed by EDX analysis obtained by SEM. In the EDX spectra of the sample Cl, Na and Al signals ≤1% have been measured (see table 4.1). Those values do not affect the PcT isotherms because can be included in the experimental error done by the adsorption measurements.

	Si %	O %	Al %	Na %	Cl %	F %
Silicalite-1	34.5	63.0	0.5	2.0	-	-
Silicalite-1 fluorinated	38.2	57.7	0.6	2.3	-	1.2
Silicalite-1 modified with SiCl$_3$CH$_3$	37.4	59.4	0.5	1.9	0.8	
Silicalite-1 modified with SiCl$_2$(CH$_3$)$_2$	36.3	60.1	0.6	2.1	0.9	-
Silicalite-1 modified with SiCl(CH$_3$)$_3$	35.2	61.0	0.6	2.2	1.0	-

Table 4.1: *Atomic percentage of the modified and unmodified silicalite-1 obtained by EDX.*

4.3.2 PcT analysis

PcT isotherms have been obtained on the starting and modified silicalite-1 at 77 K (LN$_2$ temperature). The room temperature isotherms do not present any significant result being the adsorbed amounts very small and not valuable.

In figure 4.3 the PcT isotherms of the different samples obtained up to 80 bar and LN$_2$ temperature are shown.
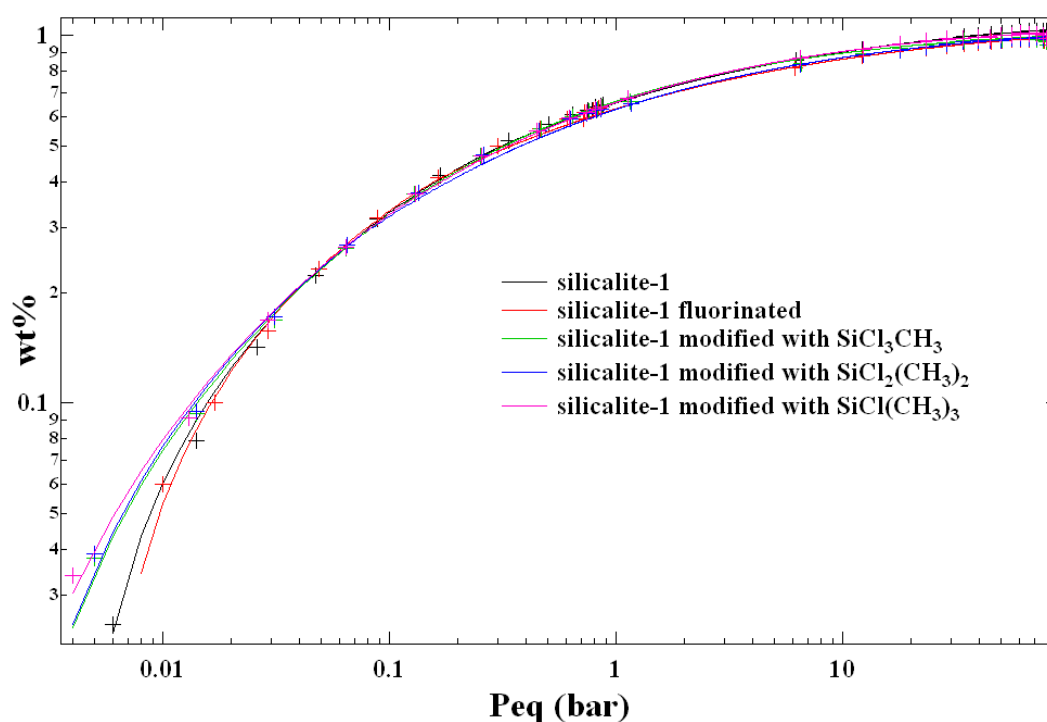
Figure 4.3: *PcT isotherms of the different samples obtained at 77 K in the pressure range (0-80) bar. The crosses represent the experimental data while the curves the fitting results obtained by the Tóth model (see table 4.1).*

In figure 4.3, PcT isotherms at 77 K of the different samples in the range (0 − 1) bar, and (0 − 80) bar are plotted in the same graph. The continuity of the curves accounts on the reliability of the system to get measurements in different pressure ranges. In addition the plot is presented in logarithmic scales to enhance the differences on the adsorption properties of the different samples.

The similar asymptotic capacity of the samples at high pressure is significant because it means the modification does not change the silicalite-1 adsorption properties. In view of application[22] this is extremely important because the silicalite-1 can be bound to polymer composite by organosilane molecules with no changes in its hydrogen adsorption properties.

When one monolayer (ML) of hydrogen molecules is adsorbed in the sample surface, an upper limit of (7-8) molecules per nm^2 is expected. As it was previously pointed out,[23] a good estimation of the coverage in terms of molecules per nm^2 can be calculated combining the values of the wt% adsorption capacity with the surface specific area (SSA) of the samples. Taking into account the results of figure 4.3 and by assuming a SSA=425 m^2/g[24] for all the samples, it is demonstrated that the unmodified and modified silicalite-1 adsorb only one or less monolayer of hydrogen molecule. All the examined samples show a H_2 coverage of 0.6 ML at 1 bar.

Considering figure 4.3, larger differences in the adsorption are present in the low pressure range. In fact, below 100 mbar the unmodified and fluorinated silicalite-1 present a lower H_2 coverage while in the remaining part of the pressure range a very similar behavior is observed. The observed differences can be adduced to different properties of the sample:

1) different homogeneity/dishomogeneity of the samples adsorption properties;
2) different kinetics of the gas;
3) different adsorption sites accessible at lower pressure values

An investigation in this sense can be performed by comparing the data with selected models for adsorption in high SSA media. The isotherms do not present any big differences in the line shape but significant changes are observed in the (0 – 1) bar range.

The experimental data in this range (see table 4.2) have been fitted with a Langmuir type equation (see formula 1.10, in section 1.2.1 of Fundamentals).

The value of the constant c in the adopted model is equal to 1 for physisorption processes and, thus, this value is expected for the present case.

The results obtained by fitting the data with relation (1.10) are shown in table 4.2.

Sample	Wt_{max} (%)	b (bar^{-1})	C
Silicalite-1	0.78 ± 0.02	7.3 ± 0.5	0.86 ± 0.03
silicalite-1 fluorinated	0.74 ± 0.02	7.7 ± 0.6	0.91 ± 0.03
silicalite -1 modified with $SiCl_3CH_3$	0.78 ± 0.01	6.63 ± 0.3	0.83 ± 0.02
silicalite -1 modified with $SiCl_2(CH3)_2$	0.79 ± 0.02	6.2 ± 0.4	0.79 ± 0.02
silicalite -1 modified with $SiCl(CH3)_3$	0.82 ± 0.01	6.3 ± 0.3	0.79 ± 0.02

Table 4.2: *Fitting results of PcT isotherms of figure 4.3 by Langmuir type equation.*

The variation of c-value from the unit is due to the inadequacy of the simple Langmuir model to describe the hydrogen adsorption into the silicalite-1 samples. In fact, the main approximation of the model is the equivalence of the material surface sites with respect to hydrogen molecules adsorption.

Actually, the pores morphology of silicalite-1 is complex which reflects on different adsorption sites and therefore on heterogeneous adsorption properties.

A typical equation which takes into account the adsorption heterogeneity of the sample surface is the Tóth equation[25,26] , derived from a modified Langmuir model (see section 1.2.2 of Fundamentals).

The fitting procedure was performed separately for different pressure ranges (namely 0 – 1 bar and 1 – 80 bar) in order to keep track of the changes from low (below 0.5 ML) to high coverage. As described above, the two data sets were collected in different runs. The fitting parameters on the (1 – 80) bar range have been obtained by leaving all them free, while it was fixed the maximum adsorption percentage to obtain the fitting parameters in the (0 – 1) bar range.

Sample		Wt% max	K	t
Silicalite-1	0 – 80 bar	1.17 ± 0.01	44 ± 11	0.37 ± 0.02
	0 – 1 bar		44 ± 12	0.40 ± 0.02
Silicalite-1 fluorinated	0 – 80 bar	1.13 ± 0.01	60 ± 14	0.36 ± 0.02
	0 – 1 bar		64 ± 18	0.39 ± 0.01
Silicalite-1 modified with SiCl$_3$CH$_3$	0 – 80 bar	1.07 ± 0.02	17 ± 8	0.47 ± 0.05
	0 – 1 bar		24 ± 4	0.46 ± 0.01
Silicalite-1 modified with SiCl$_2$(CH3)$_2$	0 – 80 bar	1.11 ± 0.02	30 ± 10	0.40 ± 0.02
	0 – 1 bar		28 ± 6	0.43 ± 0.01
Silicalite-1 modified with SiCl(CH3)$_3$	0 – 80 bar	1.11 ± 0.01	21 ± 6	0.44 ± 0.03
	0 – 1 bar		24 ± 4	0.44 ± 0.01

Table 4.3: *Fitting results of Tóth equation parameters. The values have been obtained fitting the experimental data of figure 4.3 in the pressure regions (0-1) bar and (1-80) bar.*

The fitting results obtained on the t-parameter in the two pressure ranges are similar, as it is expected. However the equilibrium constant K assumes different values depending on the pressure ranges. In particular the unmodified and fluorinated silicalite-1 present smaller K-value at lower pressure which increase at higher pressure range. In the remaining samples this behavior is reversed. On the

other hand the changes in K-values reflect the isotherms curvature variations which are visible in figure 4.4. If we take into account the IUPAC classification, we should attribute those changes to the different porosity of the samples from macro to micro scale length. But the SEM and XRD measurements does not show any difference after the silicalite-1 modifications. Therefore the difference in curvature could be attributed to the slower kinetic in the unmodified and fluorinated silicalite-1.

The results obtained by the analysis of the adsorption isotherms can be combined with the study of the dynamical features obtained from the analysis of the pressure transient status following an abrupt increase of P in the sample holder volume.[23] At first glance, the pressure decrease can be modeled with a negative exponential function whose time constant τ is related to the diffusion of the hydrogen molecules through the silicalite-1 channels and their adsorption on the zeolite walls. However considering the Fick equation on spherical shaped zeolite and taking into account the fraction of hydrogen adsorbed Λ,[27,28,29] the transient behavior of the total amount of the diffusing gas is represented from the formula 1.16 (see section 1.4 in Fundamentals).

The graph of typical fitting results is reported in figure 4.7. In that graph, the cross represents the calculated pressure step due to the expansion of the gas between the reservoir and the sample holder volume. The a-length considers an average size of the zeolite channel, therefore the fitted parameter is D/a^2, as it is reported in the literature.[28]
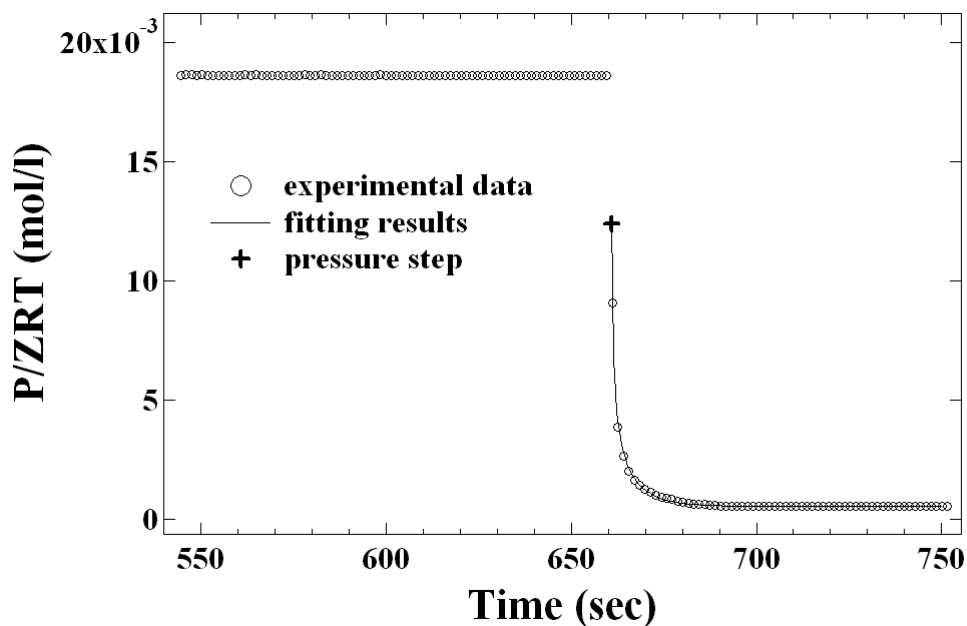
Figure 4.4: *PcT experimental data fitted by decaying function versus of hydrogen time diffusion/adsorption.*

In figure 4.5 it is reported the diffusion coefficient versus hydrogen coverage (θ) obtained for the different samples.
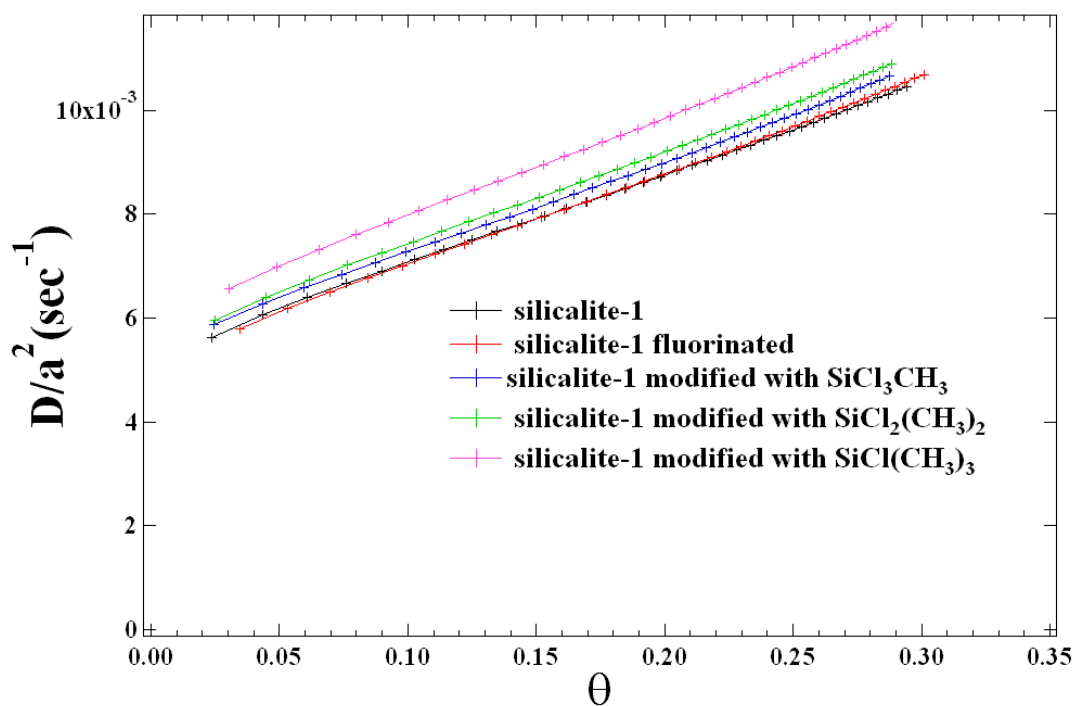
Figure 4.5: *D fitting results of the different materials as a function of the hydrogen coverage ϑ. The diffusion coefficient error is 3-5%.*

The D versus θ dependence is related to the 'Darken correction' $D=D_0[d\ln P/d\ln C]$ and considering the Tóth equation (1.12) we obtain

$$D = \frac{D_0}{(1-\theta^t)}$$

(4.1)

The silicalite-1 modified by organosilane molecules ended with methyl group present higher D/a^2 values, which means, roughly, faster kinetic. In this way the observed differences at lower pressures on the PcT isotherm of figure 4.3 could be related to the different H_2 kinetics into the modified zeolites. In fact the valve between the sample holder and the reservoir volumes has been opened for 30 seconds. Because of D/a^2 represents the inverse of the typical diffusion time of the gas molecules τ, in the present case it belongs, at lower pressure values, to the range (150 – 170) sec. Therefore the differences in H_2 storage observed in figure 4.3 can be adducted to the different kinetics into the modified silicalite-1.

4.3.3 TDS analysis

In order to investigate more accurately the modification induced by the functionalization processes discussed above, we performed a hydrogen desorption study by means of TDS. The samples were uploaded with H_2 at 25 K and warmed up with three heating rates (namely 0.1 K/s, 0.03 K/s and 0.001 K/s). A typical result obtained on $ClSi(CH_3)_3$:Silicalite 1 is shown in figure 4.6.
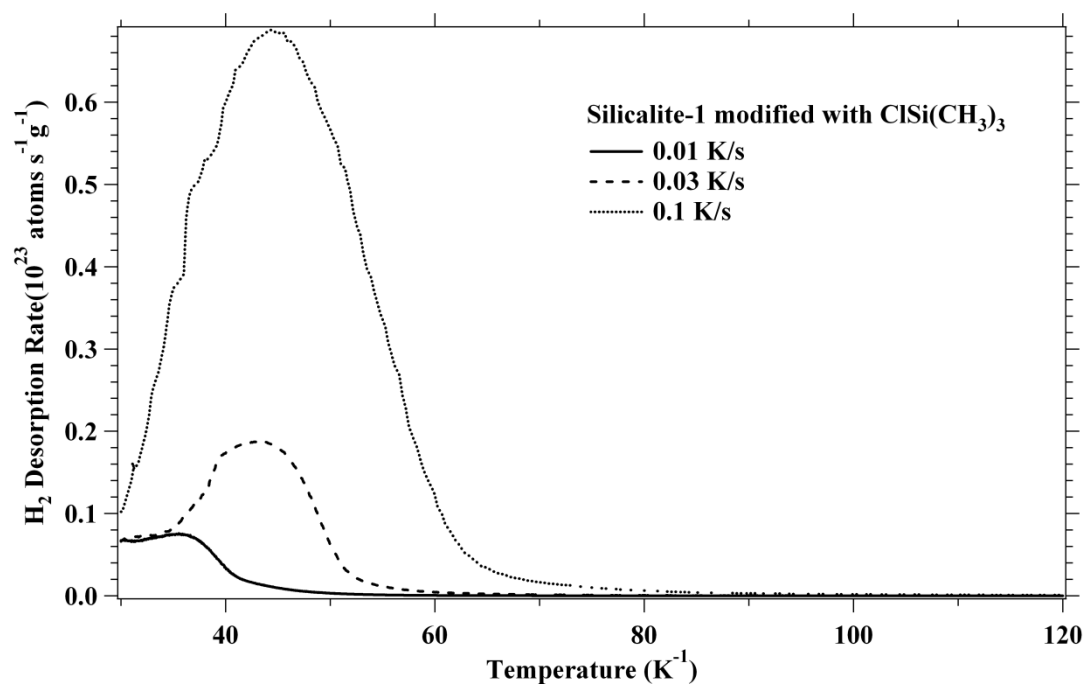
Figure 4.6: *TDS spectra in three different heating rates for the Silicalite-1 modified with SiCl(CH₃)₃.*

The analysis carried out at low different heating rates enhances the TDS sensitivity allowing the observation of the induced changes on the adsorption site by modification of the silicalite-1 surface.

In figure 4.7, the TDS spectra of all the samples acquired with the lowest desorption rate are shown.

As first evidence, in the TDS spectrum of unmodified silicalite-1, we find a desorption peak at 46 K which is not observed on the modified samples. This could be attributed to the adsorption of hydrogen molecules on the outer surface of the grains. In fact, on the external surface of unmodified silicalite-1, a high amount of silanol groups are present to which a higher desorption temperature is associated, considering the stronger interactions between the polar O–H bonds and hydrogen molecules. The lack of that peak on the others samples can be due to the modification by organosilane molecules, which replaces O–H bonds on the external silicalite-1 surface.[30]

The peaks at lower desorption temperature, in all the TDS spectra of figure 4.7, account for weaker adsorption sites. During the condensation process at the lowest temperature, the hydrogen molecules bind to lower energy binding sites around pre-adsorbed H_2 in the pores of silicalite-1, somewhat away from the surface.[31] The structured desorption feature at low temperature is slightly changed upon modification and, thus, they could be assigned to the H_2 adsorption in the sites inside the pore network. This assumption is corroborated by the observation that the PcT isotherms does not show any difference in the maximum storage capacity for the investigated samples (see figure 4.3) and, thus, the active surface remain essentially unaffected while the modification occurs on the external surface of the silicalite-1 grains. A further proof is given by the evaluation of the TDS calculated areas for the adsorption process which are very similar in all the investigated samples. The different intensity of the features in low temperature broad peak (dashed lines are centred to the features relative to the main adsorption sites in figure 4.7) could be due to a variation of the desorption kinetics of the hydrogen molecules on the adsorption sites on the pore walls.
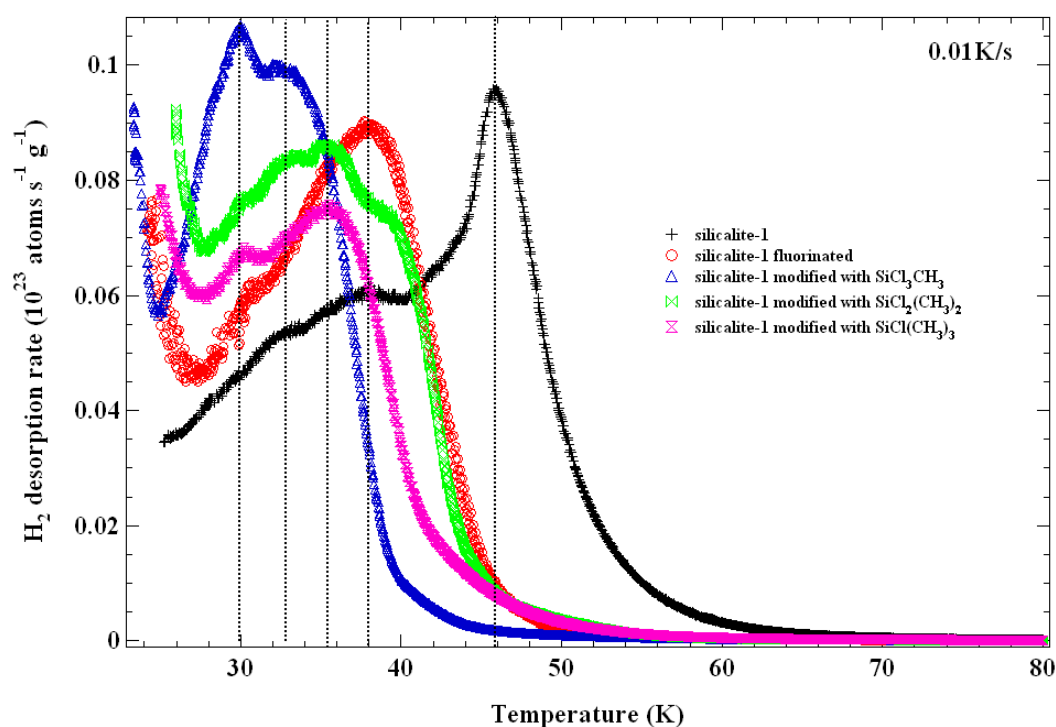
Figure 4.7: *TDS spectra of the different sample at heating rate of 0.01K/s.*

The TDS spectra acquired at higher desorption rates will result in a more intense signal but less structured, i.e. the fine structure given by the single adsorption sites is lost. In this condition, it is possible to observe the differences of overall dynamical desorption properties of the samples due to the diffusion of the desorbed gas into its porous structure. As an example, the TDS spectra acquired with desorption rate of 0.03 K/s are compared in figure 4.8. All the samples spectra present one main broad structure whose centroid position in temperature is shifted. In particular the unmodified silicalite-1 and the fluorinated sample have very similar centroid position, while in the other curves the centroid is downshifted.

This variation can be explained from the different desorption/diffusion kinetics of the samples at lower pressure values. By assuming that the diffusion is the rate-limiting step for our microporous materials[32] we can evaluate the diffusion coefficient D by relating it to the diffusion time τ by the relation

$$D = l^2/6\tau \tag{4.2}$$

where l is the typical dimension of the pores. According to the result of figure 4.7, $\tau \sim 40$ sec in unmodified silicalite-1.

Because of diffusion coefficient is temperature dependent,[28,33,34] and considering relation (4.2) we obtain the formula

$$\tau = \tau_0 \exp(E_a/kT) \tag{4.3}$$

where E_a is the barrier energy[33,34] that the hydrogen molecules meets on the samples surface in order to diffuse inside the porous material. Therefore

$$\Delta\tau = \tau_{43} - \tau_{47} = \tau_{47} e^{-\frac{E_a}{k \cdot 77}} \left(e^{\frac{E_a}{k \cdot 43}} - e^{\frac{E_a}{k \cdot 47}} \right) \tag{4.4}$$

In this way the temperature shifts observed in figure 4.8 can be attributed to the different diffusion characteristics for hydrogen molecules in the samples internal pores. For instance, if thermal shift of ~4 K is considered between the unmodified and modified silicalite-1 with $SiCl(CH_3)_3$ (see figure 4.8), the delay introduced from the different diffusion of H_2 trough their external surfaces is 133 sec. On the other hand if relation (4.4) is utilized, considering barrier energy of E_a~2 kJ/mol for silicalite-1,[33] the energy barrier $E_a' = E_a + \Delta E$ of modified silicalite-1 can be calculated, obtaining $\Delta E = -45$ J/mol. Therefore, according to the diffusion analysis of figure 4.5, the external modification of silicalite-1 introduces quicker kinetics of the hydrogen molecules.

It seems that a sort of a "stopper" on the pore mouth is keeping the H_2 molecules inside the pore network, and this "stopper" is mostly effective in the non-modified silicalite-1, where surface oxygens are bound to H atoms, with an effectiveness decreasing in the order $OH>SiCH_2CH_2Rf>SiMe_3$~$SiMe_2>SiMe$, where Me represent the methyl groups and $SiCH_2CH_2Rf$ the fluorinated molecule. Therefore we can argue that strongly adsorbed hydrogen molecules on the outer silanols of unmodified silicalite-1, close to the pore mouth, effectively hinder the hydrogen desorption from the internal pores. The reduction in the number of the surface silanols caused by the bonding of the chlorosilanes strongly reduces the number of silanols groups of the silicalite-1 and the amount of adsorbed hydrogen, and therefore the maxima of the correspondent TDS spectra are shifted at lower temperatures. Bulky linear fluorinated alkyl chains are known to self-assemble, and therefore it is no wonder if MFI crystals modified with this moiety yield the second slowest desorption rate. If the other modifications introduced on the surface of the MFI crystals are considered, it seems that after modification, the size of the group bound to the outer surface of the zeolite governs the desorption rate of H_2 and therefore the dynamical desorption properties of modified silicalite-1.

If these experimental evidences are compared with the diffusion coefficients during sorption (figure 4.5), a fair agreement is found. In fact, the slowest sorption is shown again for the non modified MFI and the MFI modified with the fluorinated chains.
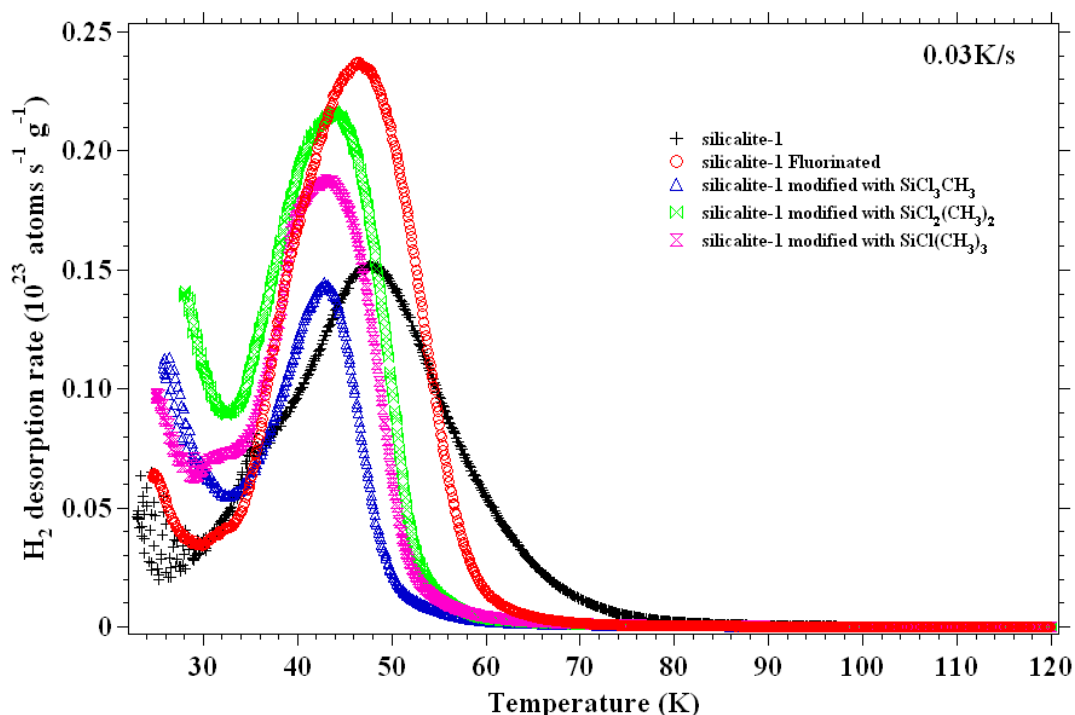
Figure 4.8: *TDS spectra of the different sample at heating rate of 0.03 K/s.*

4.4 Conclusions

The external surface of silicalite-1 (MFI) crystals has been modified with four different chlorosilanes. The surface modifications do not change the hydrogen adsorption capacity at 80 bar, since the specific surface areas are very similar. On the other hand TDS spectra acquired with desorption rate of 0.01 K/s show the same adsorption sites, except of stronger-bound H_2 Adsorption sites due to the sylanol group present in the external surface of silicalite-1 which are removed in the modified samples after the functionalization. Small changes on the adsorption properties of H_2 are observed at lower pressure values by PcT isotherm curve. Considering the diffusion analysis, those differences can be attributed to the changes of the dynamical properties of modified siliclaite-1. The different dynamical properties observed between the modified and unmodified siliclaite-1 is confirmed from the TDS spectra acquired at 0.03 K/s which show a thermal shift due to the different kinetics between the modified and unmodified sioliclaite-1. This difference

is related to the different rate of desorption of H_2 molecules from the different silicalite-1 samples; the surface of the pristine crystals is the most effective in creating a barrier for desorption of hydrogen. This difference could be the effect of strongly adsorbed hydrogen on surface silanols close to the pore entrance.

Bibliography Chapter 4

(1) Caro, J., Noack, M., Kolsch, P. *et al. Microporous and Mesoporous Materials*, **2000**, *38*, 3-24.

(2) Scholes, C.; Kentish, S.; Stevens, G. *Separation and Purification Reviews*, **2009**, *38*, DOI 10.1080/15422110802411442|PII 908455701.

(3) Lu, G. Q., da Costa, J. C. D., Duke, M. *et al. Journal of Colloid and Interface Science*, **2007**, *314*, 589-603.

(4) Chung, T. S., Jiang, L. Y., Li, Y. *et al. Progress in Polymer Science*, **2007**, *32*, 483-507.

(5) Mahajan, R.; Koros, W. J. *Industrial & Engineering Chemistry Research*, **2000**, *39*, 2692-2696.

(6) Davis, M. E. *Nature*, **2002**, *417*, 813-821.

(7) Diaz, U.; Vidal-Moya, J. A.; Corma, A. *Microporous and Mesoporous Materials*, **2006**, *93*, 180-189.

(8) Jones, C. W.; Tsuji, K.; Davis, M. E. *Nature*, **1998**, *393*, 52-54.

(9) Gu, X. H.; Tang, Z.; Dong, J. H. *Microporous and Mesoporous Materials*, **2008**, *111*, 441-448.

(10) Zimmerman, C. M.; Singh, A.; Koros, W. J. *Journal of Membrane Science*, **1997**, *137*, 145-154.

(11) Weber, R. W., Moller, K. P., Unger, M. *et al. Microporous and Mesoporous Materials*, **1998**, *23*, 179-187.

(12) Zhang, H. Y.; Kim, Y.; Dutta, P. K. *Microporous and Mesoporous Materials*, **2006**, *88*, 312-318.

(13) Kawai, T.; Tsutsumi, K. *Colloid and Polymer Science*, **1998**, *276*, 992-998.

(14) Han, A. J., Guo, J. G., Yu, H. *et al. Chemphyschem*, **2006**, *7*, 607-613.

(15) Zapilko, C., Widenmeyer, M., Nagl, I. *et al. Journal of the American Chemical Society*, **2006**, *128*, 16266-16276.

(16) Dong, J. X., Wang, X. Y., Xu, H. *et al. International Journal of Hydrogen Energy*, **2007**, *32*, 4998-5004.

(17) van Koningsveld, H.; Jansen, J.C.; van Bekkum, H. *Zeolite*, **1990**, *10*, 235-242.

(18) Cheng, C. H., Bae, T. H., McCool, B. A. *et al. Journal of Physical Chemistry C*, **2008**, *112*, 3543-3551.

(19) Shin, Y., Zemanian, T. S., Fryxell, G. E. *et al. Microporous and Mesoporous Materials*, **2000**, *37*, 49-56.

(20) Palmer, D. C.; Finger, L. W. *American Mineralogist*, **1994**, *79*, 1-8.

(21) Kox, M. H. F., Stavifski, E., Groen, J. C. *et al. Chemistry-A European Journal*, **2008**, *14*, 1718-1725.

(22) Moore, T. T., Mahajan, R., Vu, D. Q. *et al. Aiche Journal*, **2004**, *50*, 311-321.

(23) Maccallini, E., Policicchio, A., Kalantzopoulos, G. *et al. in preparation*, **2009**.

(24) Jhung, S. H., Yoon, J. W., Lee, S. *et al. Chemistry-A European Journal*, **2007**, *13*, 6502-6507.

(25) Toth, J. *Journal of Colloid and Interface Science*, **1997**, *185*, 228-235.

(26) Toth, J. *Advances in Colloid and Interface Science*, **1995**, *55*, 1-239.

(27) Crank, J. *The Mathematics of Diffusion*, 2nd ed., Oxford University Press, New York, **1975**.

(28) Karger, J; Ruthven, D.M. *Diffusion in zeolites and other microporous solids*, 1rst ed., John Wiley & Sons, **1992**. p.605.

(29) Sircar, S.; Hufton, J. R. *Adsorption-Journal of the International Adsorption Society*, **2000**, *6*, 137-147.

(30) Vuong, G. T.; Do, T. O. *Journal of the American Chemical Society*, **2007**, *129*, 3810-+.

(31) Song, M. K.; No, K. T. *International Journal of Hydrogen Energy*, **2009**, *34*, 2325-2328.

(32) Ulbricht H., Kriebel J., Moos G. *et al. Chemical Physics Letters*, **2002**, *363*, 262 - 260.

(33) Bouchaud, J.P.; Cohen de Lara, E.; Kahn, R. *Europhysics Letters*, **1992**, *17*, 583-587.

(34) van den Berg, A. W. C., Bromley, S. T., Flikkema, E. *et al. Journal of Chemical Physics*, **2004**, *120*, 10285-10289.

5.   Conclusions

In the present experimental work, a systematic characterization of adsorption properties in periodic nanoporous organo-silica (PNOs) materials and modified and unmodified silicalite-1 by organosilane molecules has been obtained by novel and home-made volumetric PcT apparatus. The experimental setup has been developed by considering the main guidelines of the European Union and the Department of Energy (DOE) of US concerning the adsorption mechanism during gas expansion. In particular that system minimizes all the error sources due to the experimental measurements of the main variables involved during adsorption processes (pressure, temperature and volume) and considering all the required approximations in the calculation of the adsorbed moles in order to exploit gas species adsorption in a wide range of temperature ((77÷400) K) and pressure ((0÷8) MPa). The PcT apparatus allows the determination of either the static adsorption properties by isotherm curves analysis either the dynamical adsorption mechanism by analysing the pressure vs time graphs in correspondence of the gas adsorption or desorption processes.

PNOs were investigated by changing the starting raw material, varying the length of used surfactant, altering aromaticity, making cations substitution in the structure, insertion of Alkali and by studying the variation of all the above parameters by having acid or basic synthesis conditions. A further substitution of the precursor with phenyl triethoxy silane was carried out under acid conditions, too.

According to the reported analysis, we are going to compare and discuss the adsorption properties for the samples synthesized in both the acid and the basic conditions.

First of all we can compare the effect on the adsorption properties due to the variation of the surfactant chain length. In the case of the samples synthesized under basic conditions, the adsorption properties and the number of hydrogen molecules adsorbed per nm^2 increase reversely to the chain length. Instead, in the case of the samples synthesized in acid conditions, the adsorption properties do not depend on the surfactant chain length but to a complex combination of all the sample

properties as pore size, pore arrangement ordering and SSA. In particular the best hydrogen storage capacity has been observed on the sample BA_C16Py_100 which presents the higher SSA, the smaller pore size and a disordered pore arrangement.

In the case of Si substitution with BTB in samples synthesized in basic conditions, the hydrogen storage capacity improves at a peculiar concentration of the two precursors. In the case of samples synthesized in acid condition, there is no improvement on the adsorption properties. The pore arrangement is disordered hexagonal and disordered cubic in the case of "basic" and "acid" samples, respectively. Thus, it could be excluded that the pore arrangement has an influence on the adsorption properties. On the other hand, by changing the synthesis conditions, different parts of the precursor material can be driven to face the surfactant agglomerates. Then, the pore wall can have a different composition even though we start with the same mixture of precursor materials leading to a different behavior towards adsorption. In the present case, the BTB can be driven to the interface during the synthesis in basic condition while it is pushed away from it in the acid one.

The same behavior has been observed on other substitutional precursor. In particular, the Al^{+3} insertion into the PNO walls for the "basic" sample enhances the hydrogen storage capacity, while the insertion of phenyl groups does not improve the adsorption properties for the "acid" samples. Altering the initial material with the admixture of the double phenyl ring is enhancing the adsorption properties for the "basic" samples but does not induce the same variation for the "acid" ones.

A difficult modification by Li^+ doping has also been attempted. The only case where the lithium atoms insertion has been successful was performed on samples synthesized in the acid conditions. In fact, in the case of the sample with hexagonal pores arrangement (basic conditions) the Li atoms insertion failed for two main problems: 1) the Li atoms get rapidly oxidized and 2) the Li atoms are not inserted into the pore samples blocking the pore access. The former case could be due to the fact that the synthesis is carried out in basic condition in a solution with NaOH (see synthesis section above). Therefore the OH^- radicals present in the solution react with the Li atoms creating lithium hydroxide. The same oxidation process has not

been obtained into the samples synthesized in acid conditions because the synthesis has been carried out in a solution with HCl.

Summarizing the previous results, for the first time in the literature, a systematic characterization of the adsorption properties of porous materials has been obtained by considering different synthesis procedures in order to change the sample porosity (pore size and pore arrangement), the sample crystallinity, the sample SSA and adsorption sites composition. The morphological, structural and H_2 adsorption characterizations indicate that the key parameters influencing the adsorption properties of PNOs are the pore size (by changing the main chain length of the surfactants), the SSA extension and the utilization of a mixed composition of the precursor materials for the samples synthesis. However, the successful improvement of the PNOs adsorption properties depends dramatically on the synthesis condition being fundamental to operate in basic conditions and on the surfactant specie utilized (see synthesis section). Finally the insertion of "point charge" into the samples pore, like Li^+, is an additional strategy that can be used in order to enhance the physical interaction between the pore walls and the H_2 molecules. However, in the future, the introduction of lithium atoms into the porous samples has to be improved.

To conclude, the PNOs samples show quite high hydrogen storage capacity at 77 K compared to the other investigated porous sample. In particular:

1) compared to the metal hydrides, PNOs store reversibly the hydrogen molecules, too, but with an increased kinetics and reducing the heat transfer problems;

2) compared to the metal organic frameworks (MOFs), they are stable at high pressure value (do not collapse) and in normal environmental conditions;

3) compared to the zeolite, PNOs have higher SSA and are lighter permitting to get higher wt% of stored hydrogen;

4) in general, compared to the other porous materials, there are several synthesis parameters that can be easily changed in order to tune the adsorption properties.

All the results are corroborated, for the first time, from a new analysis which takes into consideration the number of adsorbed H_2 molecules per nm^2. In fact, this

analysis considers the adsorption of hydrogen molecules per surface unit in order to verify if the hydrogen storage capacity, obtained by PcT isotherm curves, is mainly due to either the SSA value or the physical interaction between the adsorbent and the adsorbate.

The outlook of this thesis is the combination of all those results in order to synthesize the best sample with the higher adsorption properties which could reach the 6 wt% DOE target for hydrogen storage.

In the future, the external surface of the PNOs samples could be functionalized in order to tune the dynamical diffusion of the different gas species into the pores. This kind of work could be interesting in the application of mixed matrix membrane (MMMs) constituted from polymer composite and PNOs samples. In order to explore this subject, we utilized well known system for the diffusion processes: the silicalite-1 zeolite. In particular the external surface of silicalite-1 was modified by different organosilane molecules. The characterization carried out on these samples showed that external surface modification does not alter the adsorption properties of the inner pores.